ATTENUATION OF ULTRAVIOLET LIGHT BY THE LOWER ATMOSPHERE

Thesis by

William Alvin Baum

In Partial Fulfillment of the Requirements

For the Degree of

Doctor of Philosophy

California Institute of Technology

Pasadena, California

1950

ACKNOWLEDGMENTS

It is a pleasure to acknowledge the helpful guidance of Professor W. R. Smythe at the California Institute of Technology and Dr. Richard Tousey at the Naval Research Laboratory, who took active interest in this research.

I am especially indebted to the Optics Division of N.R.L., headed by Dr. J. A. Sanderson, for the extensive use of equipment and facilities not available at C.I.T. Special thanks are also due Dr. Oliver R. Wulf of the United States Weather Bureau for the use of his objective quartz spectrograph.

The collaboration in certain phases of this work by Mr. Lawrence Dunkelman of N.R.L. and the help of Mr. Robert Serviss of C.I.T. have been sincerely appreciated.

The advice and assistance of Dr. Wolfgang Finkelnburg at Fort Belvoir, Virginia, in connection with ultraviolet sources were extremely valuable.

I wish also to thank Dr. E. O. Hulburt, Director of Research at N.R.L., for his personal interest in this investigation, which is so closely related to his own research.

ABSTRACT

The attenuation of ultraviolet radiation by air near the ground was measured as a function of wavelength under a wide variety of meteorological conditions. These measurements were made over the tops of buildings at the California Institute of Technology on 125 nights between March 1949 and March 1950. Attenuation coefficients in km^{-1} have been plotted against wavelengths in Angstroms for 78 representative nights.

The primary data were obtained from four independent experiments, two which yielded coefficients as a continuous function of wavelength from 2300A to 4600A, and two which monitored coefficients at 2537A and at 5500A. The first method employed photographic spectrophotometry to compare the light transmitted through two paths differing in length by 680 meters. The second method was similar but utilized other apparatus and a path difference of 340 meters. The third method involved mercury lamps and cadmium photocells, and the fourth method consisted of visual observations with a Loofah hazemeter.

Except for the Herzberg O_2 bands in the neighborhood of 2500A, the attenuation coefficient was found to vary smoothly (though differently) with wavelength on all nights analyzed, including many when smog was present in noticeable concentrations. Attenuation data for unpolluted air were successfully fitted by a simple empirical formula involving wavelength and visibility range as parameters.

TABLE OF CONTENTS

I. INTRODUCTION

A ray of light, passing through air, is attenuated both by scattering and by absorption. The fraction of its energy which is transmitted through x kilometers of homogeneous air is given simply by $e^{-\sigma x}$, where the coefficient σ represents the total attenuation and is a function of wavelength λ only. Therefore the attenuation of light by a particular sample of air can conveniently be described by plotting σ against λ for the spectral region of interest.

Air is so common a medium that one would suppose its attenuation coefficients to be well known for every part of the optical spectrum and for almost any air condition near the ground. However, such is not the case. One reason for the lack of usable attenuation data is that no two samples of air behave exactly alike, and the range of possible variation is extremely large. Values of σ at the same wavelength for two samples of air can easily differ by a hundred to one. An even more troublesome fact is that two samples of air having the same σ at one wavelength may have quite different values at another.

One can speculate on applications to which reliable atmospheric attenuation coefficients could be put. Presumably they would be useful in measuring the intense optical radiation from an atomic explosion, especially in the ultraviolet where the high attenuation critically influences the result. Other possible applications concern such matters as visibility range, optical signaling (infrared and ultraviolet as well as visual), spectroscopic detection of industrial air pollutants (smog), and the measurement of variable natural constituents such as ozone and water vapor.

Previous measures of atmospheric attenuation as a function of wavelength have been made by several investigators for various segments of the optical

spectrum. For the most part, however, their considerations have been confined to exceptionally clear air or to a few particular samples of haze, sometimes with low resolution (i.e., using filters). Since attenuation coefficients depend critically upon variable conditions, it was felt in the present case that much could be gained by more extensive sampling with good resolution. Moreover, the practical value of an atmospheric attenuation study will be enhanced if the results of many observations can be systematized to provide means for estimating σ_λ whenever such information is desired.

Before details of the present investigation are discussed, it will be worthwhile here to outline briefly some of the work which has preceded it.*

Except for the vertical transmission of sunlight, there was relatively little known about the spectral transparency of air, particularly for layers near the ground, until after World War I.

In 1922 Schaeffer[1] used a cadmium spark and an objective spectrograph to compare measured ultraviolet attenuation between 2600A and 3300A with that predicted by theory. He concluded that molecular scattering would not account for his results and he believed that the discrepancy might be due to absorption by oxygen and ionized air but not by ozone.

In 1929 Dawson, Granath, and Hulburt[2] used a mercury lamp and quartz spectrograph at distances of 400 meters and less to obtain coefficients down to 2050A; their data above 2600A did not agree too closely with Schaeffer's. With different apparatus, Granath and Hulburt[3] also measured the absorption by fog of visible and near infrared light out to 3μ.

---

* This outline does NOT constitute a complete bibliography on atmospheric attenuation of optical radiation. Researches which are not sufficiently related to the present experiment (particularly those in the infrared) have been omitted.

In 1930 Link and Hugon[4] employed blue, green, and red filters to observe attenuation of visible light over a path 29.9 kilometers long at an average elevation of 2830 meters. Their coefficients, which implied a maximum transparency approaching the limit imposed by Rayleigh scattering, are probably not valid, because the clearest air ever observed by anyone else has had roughly twice that opacity.

In the same year Buisson, Jausseran, and Rouard[5] used line sources and a spectrograph to determine coefficients at 18 wavelengths between 2482A and 5780A for exceptionally clear air, and in 1934 they extended their measurements down to 1855A.

Meanwhile, in 1933 Gotz and Maier-Leibnitz[6] conducted a similar experiment for the region from 2300A to 3900A; they were primarily interested in detecting ozone.

By photographing the contrast of a distant object against the sky through each of seven color filters, Duclaux[7] computed visible attenuation coefficients for 27 samples of relatively clear air observed between 1928 and 1933. His results were more reasonable than those of Link and Hugon.

In 1935 Middleton published his book[8] entitled "Visibility in Meteorology", which included an empirical formula for σ in the visible region as a function of visibility range. A report by Stiles, Bennett, and Green[9] in 1937 contained similar information, but Hulburt[10] has found that Middleton's values are in better agreement with the data of other observers.

M. and Mme. Vassy[11] obtained attenuation coefficients for the lower air on nine relatively clear nights in 1937. Their measurements were made spectrographically over paths from 5 to 15 kilometers long and covered the region from 2700A to 8200A. By using sources of spectrally continuous

radiation instead of line sources as others had done before, they achieved a great improvement in resolution. Probably the best existing ultraviolet data for exceptionally clear air are those given by Mme. Vassy in her 1941 thesis[12].

Using filters to select eight "colors" between 2700A and 7800A, Koch[13] measured the transmission of paths varying in length from 170 meters to 7.5 kilometers during the winter of 1942-43. His source was a modulated high-pressure mercury lamp, and instead of a photographic plate he employed Cs, Na, and Cd photocells with amplifiers.

One of the most recent determinations of coefficients for the visible was made in 1944 by Dessens[14] who photographed distant targets in two planes of polarization and in nine colors. He sought to interpret his results for thirty air samples in terms of the average size and number of fog particles per unit volume.

Several investigations of atmospheric attenuation for air near the ground are currently in progress. The infrared work of Professor Strong at Johns Hopkins University under contract with the Office of Naval Research has been described in a preliminary report[15]. Meanwhile a renewed attack on the visible region is underway at the Chesapeake Bay Annex of the Naval Research Laboratory[16]. A current investigation of the ultraviolet is described in this thesis.

It should be emphasized that all researches cited in the foregoing outline are concerned only with the lower atmosphere. Data for the total atmosphere (i.e., along a vertical path extending into outer space) will be found in the Smithsonian Physical Tables[17] and the International Critical Tables[18].

The subject matter of the present study is concisely set forth in the

Abstract and need not be repeated here. Nevertheless, a few explanatory remarks will clarify the general plan of the experiment.

Ultraviolet attenuation measurements should begin at a wavelength long enough to join or overlap the visible blue data of others such as Middleton[8], so that they can be correlated with visual observations. The short wavelength limit is dependent upon path length, because it is merely the result of increasing attenuation. Hence, in order to cover as much of the ultraviolet as possible, it is evident that we should choose as short a path as is compatible with measurable attenuation near the blue. The appropriate path turns out to be in the neighborhood of several hundred meters and the corresponding wavelength region extends from about 2300A to 4500A. Since the attenuation rises so sharply with decreasing wavelength around 2300A, there is very little to gain by making additional measurements over shorter "outdoor" paths; the region from 2300A down to the "air cut-off" around 1850A can conveniently be studied inside the laboratory. Moreover, this region is not especially influenced by meteorological conditions, because the variations in σ due to haze are dwarfed by the high constant attenuation due to oxygen; consequently, the present investigation was confined to wavelengths longer than 2300A.

It was felt that the spectral resolution of the apparatus should be high enough to reveal any absorption lines or bands which might appear in some of the air samples measured. In this connection Vassy[12] has emphasized the advantage of using a spectrally-continuous source and a spectrograph instead of a line source and/or filters as most investigators have done. The present experiment, in which sources of both kinds were tried, verified the correctness of Vassy's contention. More important than the simple matter of relative convenience is the question of correctness: line

radiation which happens to coincide with molecular band structure in the absorption spectrum is certain to yield unreliable data.

The definite need for more extensive sampling, which is fairly apparent from the outline of previous studies, was met in the present experiment by measuring ultraviolet attenuation on 125 different nights for visibility conditions varying from less than 1 kilometer to over 100 kilometers and including all sorts of weather with both polluted and unpolluted air. Data for 78 of these nights were reduced to final σ values. Since so many measurements were involved, strict uniformity of procedure was adopted in every step of the work; not only did this policy help to avoid confusion, but it was also conducive to consistency in the results.

During the time that attenuation of a particular air sample is being measured, atmospheric conditions are likely to be changing, and it is common knowledge that noticeable changes can sometimes occur in a matter of minutes. In order to avoid the influence of such variations, an exceedingly fast optical system was devised to permit short spectrographic exposures. The standard sequence for most of the spectrograms consisted of seven 10-second exposures made in rapid succession.

II. THEORY

The purpose of the present investigation was to obtain an empirical answer to a practical question. Since there was no intent to establish or verify any particular theory, the following discussion is presented merely to aid our understanding of the quantities being measured.

If we have a source of power output Q surrounded by an attenuating medium which is homogeneous and isotropic, the intensity of unscattered radiation received at a distance x from the source is

$$I = Q e^{-\sigma x}, \qquad (1)$$

provided the physical size of the source is small compared to x. The attenuation coefficient σ defined by equation (1) is the sum of all losses due to scattering and absorption.

The total intensity of radiation from the source Q incident upon a surface at distance x is greater than I given by equation (1), because part of the scattered radiation also falls upon the same surface. A familiar example from everyday experience is atmospheric scattering of sunlight, which causes a substantial fraction of daylight to come from the sky instead of all coming directly from the sun. In clear weather, this scattering selectively favors short wavelengths, thereby making the sky bright blue.

It is evident that light scattered by the air surrounding a terrestrial source must be excluded from intensity measurements upon which σ's are based; Middleton[19] has recently found that very large errors arise if this condition is not met. He has shown theoretically that these errors depend both on the angular aperture of the telephotometer (receiver) and on the cone of air illuminated by the source. Let us consider a physically reasonable example: suppose that the telephotometer has a 2° field of view and that the source at a distance of one kilometer radiates in all directions

with spherical symmetry; it is then found from theory that 100 fog nucleii per cm^3, each with a diameter of about 2.5 microns, will cause the telephotometer reading for visible light to be <u>double</u> the correct value. These conditions correspond to a thin fog for which the daytime visibility range is roughly 1 kilometer. An experimental check of the foregoing theoretical conclusion shows that the actual errors in practice are even larger than calculated.

Generally it is quite difficult to make the source cone and the field of view of the receiver small enough for Middleton's scattering effect to be negligible. However, in the present experiment, over 90% of the σ-vs.-λ data were obtained with apparatus for which the source cone was masked down to about 2 minutes of arc while the field of view of the objective spectrograph was a half degree or less, depending somewhat on interpretation. A rough guess based on Middleton's work implies that for any air condition except very dense fog the corresponding error in measured intensity must be less than 1%.

Because the air attenuates largely by scattering rather than by absorption, there is no optical system capable of isolating an outdoor path to prevent extraneous radiation from other sources "leaking" into the receiver. Such interference can be avoided in practice only (a) if we confine our attention to wavelengths absent from daylight, (b) if the source is modulated so that its radiation can be selectively received, or (c) if measurements are made at night. Since neither (a) nor (b) is compatible with the aims of the experiment, we resorted to (c). Actually an attempt was also made to supplement night data by using a University of California Type G ultraviolet filter for daytime measurements below 2900A, but the method was discontinued because spectra thus obtained were optically inferior.

Now that we have defined what we mean by the attenuation coefficient σ and have shown how certain restrictions are imposed on the experiment in order to measure it correctly, we next consider briefly the physical interpretation of σ.

When several factors contribute to attenuation, the coefficient for the total effect is merely the sum of the coefficients for individual contributors.

$$\sigma = \sigma_A + \sigma_B + \sigma_C + \sigma_D. \qquad (2)$$

In the case of air near the earth's surface, these factors include:

(A) Molecular diffusion.

(B) Scattering by air-borne particles and droplets.

(C) Absorption by air-borne particles and droplets.

(D) Absorption by gases.

Each of these will be considered in turn.

(A) MOLECULAR DIFFUSION. The molecular diffusion of light was first treated by Lord Rayleigh[20] in 1871. From simple dimensional analysis he showed that:

> "When light is scattered by particles which are very small compared with any of the wavelengths, the ratio of the amplitudes of the vibrations of the scattered and incident light varies inversely as the square of the wavelength, and the intensity of the lights themselves as the inverse fourth power."

In the same paper Rayleigh reported some experimental observations comparing sunlight to skylight at various wavelengths; intensity ratios thus obtained tended to support his inverse fourth-power theory but gave no absolute values.

King[21] suggested that the attenuation coefficient be expressed in the form,

$$\sigma = C_1 + C_2\lambda^{-4} \qquad (3)$$

The only justification for the constant term was that he could achieve a closer fit to Abbot's Smithsonian data[22] on vertical transparency of the total atmosphere.

Around 1908-10, Smoluchowski[23] and Einstein[24] explained Rayleigh scattering by molecules of a medium in terms of a density fluctuation theory. Their formulation included the refractive index, the isothermal compressibility, the absolute temperature, and the Boltzmann constant.

In 1929 Cabannes[25] extended previous molecular scattering theory to take into account the observed lack of complete polarization for light scattered at $\pi/2$ from the incident pencil[26]. His final equation for the attenuation coefficient rewritten in our notation is

$$\sigma_A = \frac{8\pi^3 (n^2 - 1)^2}{3 N \lambda^4} \cdot \frac{6 + 3\rho}{6 - 7\rho} \cdot 10^5 \ km^{-1} \qquad (4)$$

where λ is the wavelength in cm, n is the refractive index of air (function of λ), N is the number of gas molecules per cm^3, and ρ is the polarization defect for light scattered at $\pi/2$.

At 0° C and 760 mm pressure, N_o is $2.7 \cdot 10^{19}$ molecules per cm^3 (Loschmidt's number). According to Born[27], the polarization defect for air molecules is about 0.04 throughout the optical spectrum; note that it influences σ_A by only a few per cent. Approximating $(n_o^2 - 1)^2$ by $4(n_o - 1)^2$, we can reduce equation (4) to

$$\sigma_A = 1.28 \cdot \frac{(n_s - 1)^2}{\lambda^4} \cdot 10^{-12} \ km^{-1} \qquad (5)$$

for N.T.P. conditions.

A modification of Cabannes' result was discussed by Dawson and Hulburt[28] in 1941 and applied by Tousey and Hulburt[29] in 1947 in the form

$$\sigma_A = \frac{8\pi^3 \cdot (n - 1)^2}{3 N \lambda^4} \cdot \frac{6(1 + \rho)}{6 - 7\rho} \cdot \left[3 + \frac{1 - \rho}{1 + \rho}\right] \cdot 10^5 \ km^{-1} \qquad (6)$$

where the symbols carry the same meaning as before.

Molecular diffusion depends somewhat on temperature and pressure because both n and N are affected. At 0° C, the variation of pressure with altitude gives

$$\log\left(\frac{p}{p_o}\right) = \log\left(\frac{n-1}{n_o-1}\right) = \log\left(\frac{N}{N_o}\right) = -0.054\ h \qquad (7)$$

for h in kilometers. Equation (7) applies fairly well throughout the lower atmosphere. At 760 mm pressure, the dependence on temperature is simply

$$\frac{n-1}{n_o-1} = \frac{N}{N_o} = \frac{T_o}{T} \qquad (8)$$

where T_o is 273° K. Equations (7) and (8) may be combined for air near the ground to give

$$\log\left(\frac{n-1}{n_o-1}\cdot\frac{T}{T_o}\right) = \log\left(\frac{N}{N_o}\cdot\frac{T}{T_o}\right) = -0.054\ h \qquad (9)$$

Since the present experiment was carried out at an elevation of 246.5 meters and at temperatures in the vicinity of 20° C (293° K), we find that

$$\begin{aligned} n-1 &\approx 0.9\,(n_o-1) \\ N &\approx 0.9\,N_o \end{aligned} \qquad (10)$$

As a result, the contribution of molecular diffusion in this case is about 90% of σ_A calculated from equation (5).

A few numerical values of σ_A are given in Table I, the last column of which has been plotted in figure 82.

Table I

Wavelength in Angstroms	σ_A for N.T.P. by Cabannes (km^{-1})	σ_A for N.T.P. by Tousey & Hulburt (km^{-1})	σ_A for present experiment (km^{-1})
2000	.973	.967	.873
2500	.341	.339	.306
3000	.153	.152	.137
4000	.046	.045	.041
5000	.018	.018	.016
6000	.009	.009	.008
8000	.003	.003	.002

(B) SCATTERING BY AIR-BORNE PARTICLES AND DROPLETS. Molecular

diffusion alone falls far short of accounting for the total attenuation of light by the lower atmosphere, even in relatively clear weather. In regions of the spectrum where gas absorptions play no role, the attenuation due to scattering by air-borne particles and droplets generally predominates. Extensive theoretical and experimental studies of haze, fog, dust, bacteria, salt crystals, and smoke in the air have been made by many observers, and it is beyond the scope of the present discussion to treat these in detail.

Sometimes dust, bacteria, salt crystals, and smoke are important light scatterers by themselves, especially around industrial cities, but often their main function is to provide nuclei for the condensation of water (haze or fog). Apparently the abundance and size distribution of water droplets depend not only on the usual meteorological variables (temperature, pressure, and humidity) but also upon the abundance and nature of potential nuclei . It also seems reasonable that preceding conditions as well as the instantaneous displacement from equilibrium should influence the formation or dissipation of droplets. It is therefore not surprising that haze or fog droplets occur in all sorts of populations and size distributions, and that it is nearly impossible to correlate their properties with other variables.

One of the most fascinating studies of water droplets and their formation has been made by Dessens[30], who used a spider web for collecting droplets and observed them in a controlled environment under the microscope. His attempt[14] to interpret spectral scattering in terms of the size and number of particles or droplets per cm^3 has already been cited in the preceding section.

Empirical studies of spectral scattering by artificial fogs were made by Houghton[31] in 1931 and by Nukiyama and Kobayasi[32] in 1932. In both

experiments the σ-vs-λ curve was found to have humps instead of following the form of λ^{-n}.

Theoretical investigations of spectral scattering by small particles were conducted by Mie[33] in 1908, by Stratton and Houghton[34] in 1931, by van de Hulst[35] in 1946, and by Houghton and Chalker[36] in 1949. The work of Stratton and Houghton, based on the theory of Mie[33], showed that the dependence of the attenuation coefficient σ on wavelength λ is not necessarily a monotonically decreasing function; thus the humps observed experimentally by Houghton for artificial fogs could be interpreted theoretically.

Natural hazes and fogs, however, appear to have smoother σ-vs-λ curves, perhaps because the particle size distribution is more heterogeneous. For meteorological purposes Middleton[8] has adopted the simple Linke-Borne formula[37],

$$\sigma = A\lambda^{-B} \qquad (11)$$

which, of course, cannot accommodate humps. The exponent B has been determined empirically as a function of the σ value at 5500A, and the coefficient A is accordingly adjusted so as to normalize σ at that wavelength. It will be appropriate to postpone further discussion of equation (11) until visibility range has been introduced.

Any experiment with natural fog automatically involves measuring the total attenuation σ for the air rather than the separate contribution σ_B due to particle scattering; however, in the visible region the importance of other contributions is known to be quite small for clean air.

(C) ABSORPTION BY AIR-BORNE PARTICLES AND DROPLETS. For air which is relatively free of dust and smoke, the direct absorption of radiant energy by suspended particles is exceedingly small. Vassy[12] believed that the

discrepancy between Rayleigh scattering and her data for exceptionally clear air should be ascribed to neutral absorption by dust; her value for σ_c was about 0.016 km^{-1}. It seems probable that her discrepancy was actually caused mainly by particle scattering, i.e., by σ_B instead of σ_c.

When absorbing particles are present in sufficient quantity to introduce appreciable attenuation, their effect should ordinarily have little dependence on wavelength. Dry smoke, whose gray appearance indicates that absorption predominates over scattering, behaves as a more or less neutral filter.

The only way that σ_c can be determined is by subtracting separate measurements of scattering $(\sigma_A + \sigma_B)$ from total attenuation σ for a spectral region where gas absorption is absent.

(D) ABSORPTION BY GASES. The absorption of radiation by gas molecules is more commonly associated with the infrared than with the visible or ultraviolet. The only prominent absorptions by natural gases of the air falling within the spectral region covered by the present experiment are those due to oxygen and ozone. Certain pollutants also have absorption bands in this region, but their detection by this method does not afford a satisfactory basis for smog analysis.

The absorption of ultraviolet sunlight by oxygen and ozone is associated with a continuous photochemical cycle, which was studied in 1935 by Wulf[38] and later by Wulf and Deming[39]. This process results in the maintenance of 2 or 3 mm pressure of ozone in the atmosphere. Nearly all of it is found between 15 and 40 km altitude, although a little finds its way into the lower air.

A good bibliography on ozone up until 1938 has been given by Gotz[40]. More recent summaries of the general subject will be found in the report of

the Tharandt conference of 1944[41] and also in a 1947 article by Hulburt[42] pertaining to the upper atmosphere of the earth.

The small quantity of ozone carried into the lower air has been the topic of several investigations. In 1931 Fabry and Buisson[43] estimated about 2 parts per 10^8 from attenuation measurements of very clear air. The results of Gotz and Ladenburg[44] were similar. In 1933 Gotz and Maier-Leibnitz[6] reported ozone concentrations for seven nights ranging from 0.9 to 3.5 parts per 10^8. In 1935 Gotz, Schein, and Stoll[45] found only about one-tenth as much ozone in city air as elsewhere. Other studies of ozone in the lower air include the work of D. Chalonge and E. Vassy[46], R. Auer[47], and A. Vassy[12].

The absorption due to ozone is a broad bumpy continuum extending from roughly 2000A to 3000A with its maximum around 2550A. The best coefficients for ozone itself are those of Ny Tsi-Ze and Choong Shin-Piaw[48]. Using these, we find that 1 part per 10^8 is equivalent to a maximum σ_D (around 2550A) of 0.145 km^{-1}, which may reasonably be observed for very clear air but which would be smothered by other attenuations in ordinary hazy atmospheres.

The classic method for determining ozone from attenuation data is to plot $\sigma - (\sigma_A + \sigma_C)$ against ozone coefficients, letting the wavelength be an idle parameter[43]. If only ozone absorption, Rayleigh scattering, and neutral absorption were actually involved, this plot would be a straight line whose slope is a measure of ozone concentration. In practice the plot is far from straight, and previous investigators have used only the initial slope associated with data above 2600A. Their procedure is not too well justified, because it substitutes a constant σ_C in place of a wavelength-dependent σ_B, resulting in ozone concentration values which are too large.

A more logical procedure, although it hinges partly on intuition, would be to sketch in whatever smooth gradual curve (instead of theoretical σ_A plus a constant) must be subtracted from σ to produce a straight line when the difference is plotted against ozone coefficients.

Atmospheric oxygen is responsible for the rapidly rising continuous absorption which sets the lower limit of the present experiment around 2300A. Below that wavelength this absorption continues to rise until it renders the air almost totally opaque around 1850A for paths longer than a few millimeters. Coefficients for part of that region have been given by Granath[49].

Oxygen is also responsible for a weak system of ultraviolet bands commencing abruptly at 2420A and petering out around 2700A for ordinary pressures. They represent forbidden transitions between the ground state and certain vibration levels in the O_2 molecule. These bands, which have been noted by various observers in the laboratory since 1886, have come to be associated with the name of Herzberg[50], who reported them again in 1932. A bibliography to previous work was given in 1928 by Wulf[51], who called them the Ciechomski bands. In 1934 D. Chalonge and E. Vassy[52] found them in outdoor air while using a 1.55 km path. They appeared again in the present experiment (see figures 64 and 81) and will be discussed in a later section.

Various other bands due to oxygen appear at elevated pressures[53], but they do not interest us in the present connection. Other gases possessing molecular absorptions in the ultraviolet and visible regions are either extremely rare in the lower air or occur only as pollutants. When humps are found in σ-vs-λ curves, there arises the question as to whether these humps represent natural spectral scattering of the type described by

Houghton[31] and others, or whether they are gas absorptions. It is not possible to answer this question with certainty, but one can make guesses by comparing the observed humps to known gas absorption spectra treated in various texts[54][55][56] and in the literature[57][58][59]. Intermittent recurrence of the same hump is a fairly good clue that it is caused by a polluting gas. On the other hand, the absence of certain discrete lines or bands sometimes precludes the presence of a certain gas. In the air around an industrial city one might expect to find pollutants such as SO_2 and NO_2; these were looked for in the present experiment.

Now that the physical interpretations of the several factors comprising σ have been considered, we conclude this section with a few remarks on their combined effects.

If one assumes that particle scattering predominates, then equations can be derived for the angular distribution of atmospheric scattering as a function of particle radius and index. Part of this scattering is caused by refraction, part by reflection, and part by diffraction; van de Hulst[35] has treated them all. Experimental measurements, together with brief summaries of theory, were given by Hulburt[60] in 1941 and by Bullrich[61] in 1947. Figures 3 and 5 in Hulburt's paper[60] are especially informative; he has found that the angular distribution is more or less independent of the visibility and that it corresponds to theoretical scattering by spherical dielectric particles whose diameters are the same order of magnitude as the wavelength.

Assuming again that scattering predominates over absorption, but this time including both σ_A and σ_B, we can relate the brightness contrast of distant targets to atmospheric attenuation coefficients. Moreover, by taking into account the threshhold contrast for detection by the human eye,

we can also calculate visibility ranges.

Brief theoretical discussions of visibility have been given by Koschmieder[62], by Middleton[8], and by Hulburt[60]. The apparent brightness of a distant target is

$$B_x = B_t e^{-\bar{\sigma}x} + B_s(1 - e^{-\bar{\sigma}x}) \qquad (12)$$

where B_t is the inherent brightness at zero distance and B_s is the brightness of the sky background (interpreted here as a scattering air column of infinite length). The contrast of the target against its background will evidently be

$$C = \frac{B_s - B_x}{B_s} = 1 - \frac{B_x}{B_s} \qquad (13)$$

Combining equations (12) and (13) we get

$$C = e^{-\bar{\sigma}x}(1 - \frac{B_t}{B_s}) \qquad (14)$$

Equation (14) has been empirically verified by Koschnieder[62] and again recently by Coleman, Morris, and Rosenberger[63].

Since visibility range is defined as the maximum x for visual detection of a target, it is desirable to select as black a target as possible so that $B_t \ll B_s$. Equation (14) then becomes

$$x = \frac{1}{\bar{\sigma}} \cdot \ln \frac{1}{C} \qquad (15)$$

Middleton[64] found experimentally that the threshold of visual contrast is about 2% for angular transitions of brightness subtending 5 minutes of arc or less; for more diffuse boundaries, a somewhat greater contrast is required. If the boundary is sharp (i.e., if the 2% threshold applies), then the visibility range is

$$V = \text{maximum } x = \frac{1}{\bar{\sigma}} \cdot \ln \frac{1}{0.02} = \frac{3.912}{\bar{\sigma}} \qquad (16)$$

The coefficient $\bar{\sigma}$ is an effective average for the integrated visible spectrum; Hulburt[10] takes it to be equal to σ at 5500A.

It may clarify the preceding remarks to emphasize that nighttime

visibility of sources and daytime visibility of objects pertain to physically different situations. Nighttime visibility concerns merely the penetration of attenuating atmosphere by light; thus it depends upon the strength of the source, the attenuation coefficient, and the sensitivity of the eye or detector. On the other hand, daytime visibility range concerns the near-obscuration of a target by light scattered within an intervening air-column under daylight illumination; for a black target against the sky it depends only upon the attenuation coefficient.

Since daytime target contrast falls off rapidly for small increments in distance, the visibility range given by equation (16) is not sensitive to variations in contrast-threshold among different observers. By the same token, it is not especially important that the target be perfectly black. This notion of a sharply-defined visibility range is easily confirmed by recalling the familiar suddenness with which a receding object fades and disappears in a fog. Figure 1 relates visibility range (as defined for 2% contrast-threshold) to the attenuation coefficient; a line for 5% contrast is also shown in order to exhibit graphically the effect just described.

By international agreement, various weather designations are generally associated with the visibility ranges and attenuation coefficients given in Table II[60].

The practical limit for visibility range at altitudes near sea level is around 100 km, corresponding to $\bar{\sigma} = 0.04$ km^{-1}. Vassy's data for exceptionally clear air at higher altitudes implies a visibility range somewhere in the vicinity of 130 km. The theoretical limit for visibility range under N.T.P. is imposed by Rayleigh scattering, for which $\bar{\sigma}_A = 0.0126$ km^{-1}; corresponding to 310 km in range.

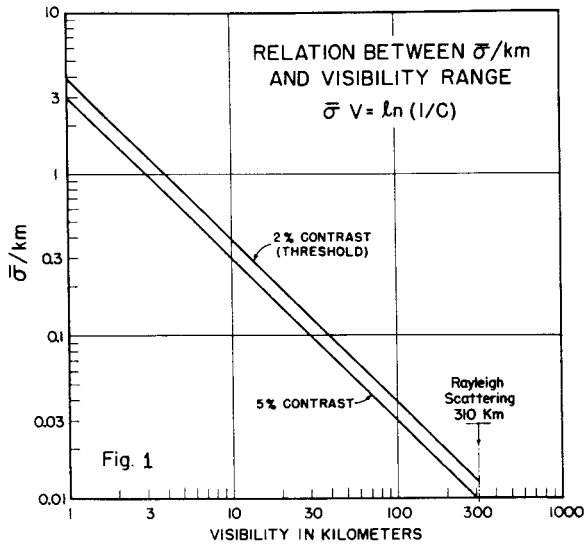

Fig. 1

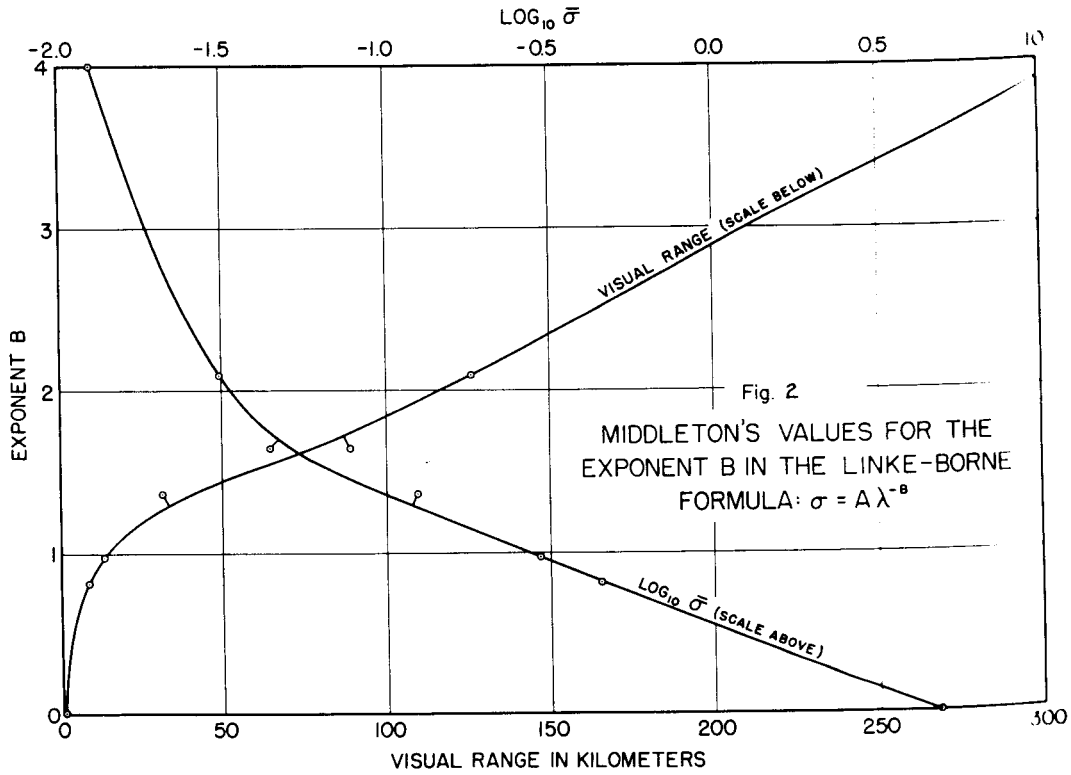

Fig. 2

MIDDLETON'S VALUES FOR THE EXPONENT B IN THE LINKE-BORNE FORMULA: $\sigma = A\lambda^{-B}$

Table II

Weather Designation	Daylight Visibility Range		Attenuation Coefficient in km^{-1} (base e)	
	from	to	from	to
Dense fog		50 m		86
Thick fog	50 m	200 m	86	21
Moderate fog	200 m	500 m	21	8.5
Light fog	500 m	1 km	8.5	4.3
Thin fog	1 km	2 km	4.3	2.1
Haze	2 km	4 km	2.1	1.1
Light haze	4 km	10 km	1.1	0.43
Clear	10 km	20 km	0.43	0.21
Very clear	20 km	50 km	0.21	0.07
Exceptionally clear	50 km		0.07	

The meaning of visibility range is often misinterpreted. It is merely another means of expressing the local visual attenuation coefficient; that is, it applies only to air in the immediate vicinity of the observer, because the atmosphere is not always homogeneous over long ranges. For example, when the visibility range is nominally 50 km according to the local $\bar{\sigma}$, one might actually see objects as far as 60 km in one direction but perhaps only 40 km in another.

Visibility ranges were useful to the present problem in that they provided a handy tag for labeling air samples whose ultraviolet σ-vs.-λ curves were being measured. When used in conjunction with the Linke-Borne formula,

$$\sigma = A\lambda^{-B}, \tag{11}$$

the visibility range also provided a σ-vs.-λ curve for the visible region which could be joined to the measured ultraviolet data. It was gratifying that the ordinates and the slopes of these two independently determined curves were both found to be in excellent agreement where they met in the blue. Subsequently in Section VII it will be seen how this congruence was utilized for monitoring "drift" of the ultraviolet equipment. Apparatus for measuring visibilities will be described in Section VI.

Middleton's[8] empirical values of B in equation (11) are plotted in figure 2 against visibility range and also against log $\bar{\sigma}$. The corresponding curves representing equation (11) itself are given in figure 3 for various values of $\bar{\sigma}$ from 0.05 to 2.00; they are also labeled with visibility ranges.

Extending the idea that the visibility range is just another way of writing $\bar{\sigma}$, Koch[13] has recently applied equation (16) to various σ_λ for eight segments of the spectrum between 2700A and 7800A. These spectral "visibility" ranges are not especially meaningful at short wavelengths where absorption is no longer negligible compared to scattering.

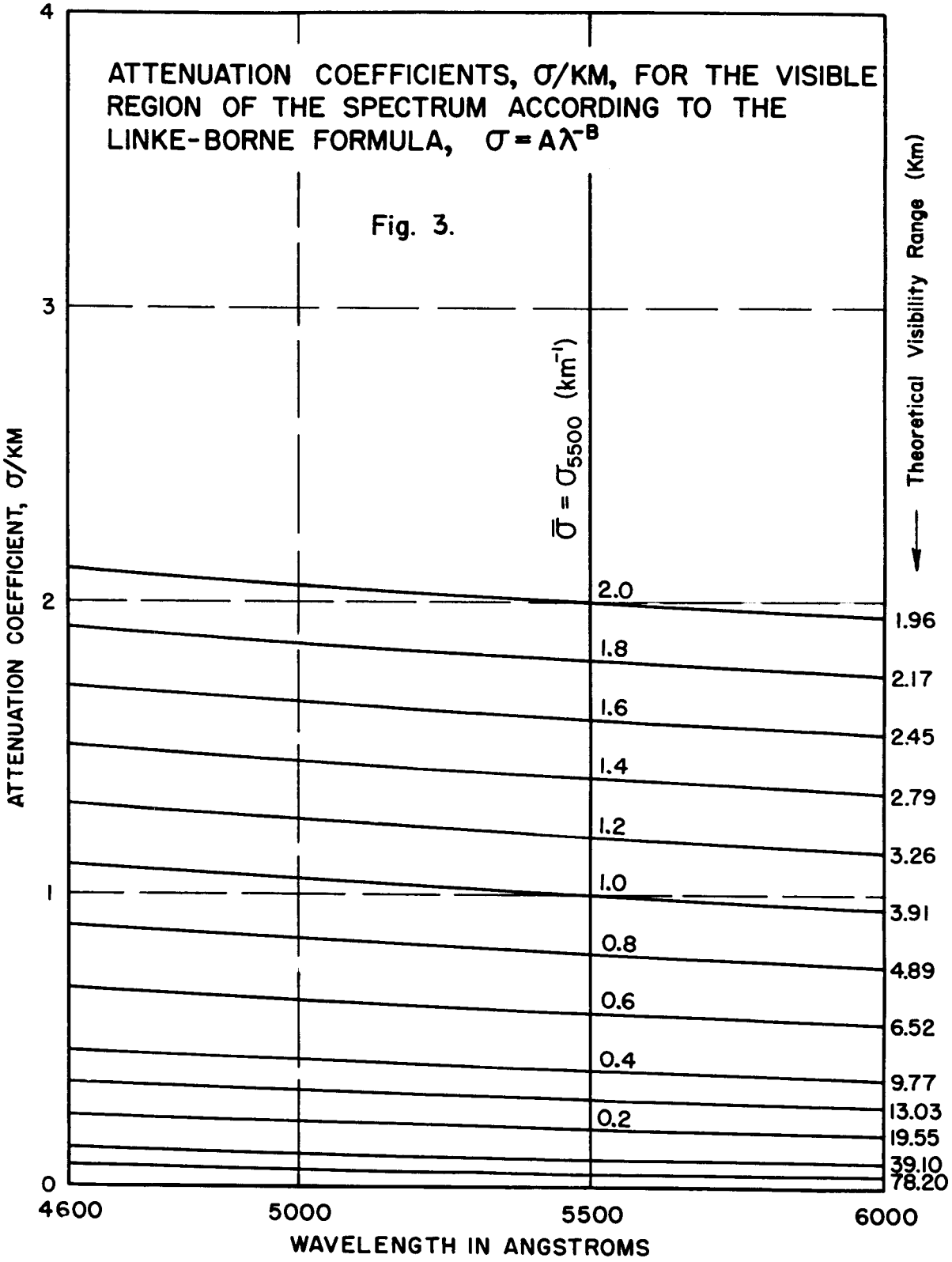
ATTENUATION COEFFICIENTS, σ/KM, FOR THE VISIBLE REGION OF THE SPECTRUM ACCORDING TO THE LINKE-BORNE FORMULA, σ = Aλ^-B
Fig. 3.
ATTENUATION COEFFICIENT, σ/KM
WAVELENGTH IN ANGSTROMS
σ̄ = σ5500 (km^-1)
Theoretical Visibility Range (Km)
4
3
2
1
0
4600
5000
5500
6000
2.0
1.8
1.6
1.4
1.2
1.0
0.8
0.6
0.4
0.2
1.96
2.17
2.45
2.79
3.26
3.91
4.89
6.52
9.77
13.03
19.55
39.10
78.20

III. PRELIMINARY EXPERIMENTS

In the preceding sections several factors are mentioned which influence the design and arrangement of apparatus for convenient and accurate spectral telephotometry. Among these we have stressed: (a) the desirability for extensive and regular sampling, (b) the advantages of detailed spectral resolution, (c) the selection of optimum path length for the spectral region involved, (d) the importance of minimizing exposure times so as to obviate effects due to changing meteorological conditions, and (e) the necessity for employing a narrow source beam and a narrow field of view at the receiver.

The first attempt in the present investigation to meet these criteria was carried out in 1948 using the equipment shown in figure 4, which is a composite of twelve views. This preliminary phase of the work served mainly as an opportunity to test various methods and ideas, thereby facilitating the development of the final apparatus.

The source was a conventional 60-inch 20-kilowatt General Electric searchlight shown in the first view. It was equipped with an automatic feed mechanism for manipulating the electrodes so as to maintain a fairly constant current, adjustable from 50 to 200 amperes at 110 volts d.c.

The searchlight beam was aimed at a 12-inch square front-surface plate-glass mirror mounted on the penthouse of West Bridge Laboratory; this unit can be seen in the second and third views.

From that location the beam was directed horizontally over the tops of campus buildings toward the Athenaeum, where part of it was intercepted and returned by a 6-inch square front-surface plate-glass mirror mounted on one of the cupolas as shown in the fourth and fifth views.

Another part of the outgoing beam was intercepted at shorter range

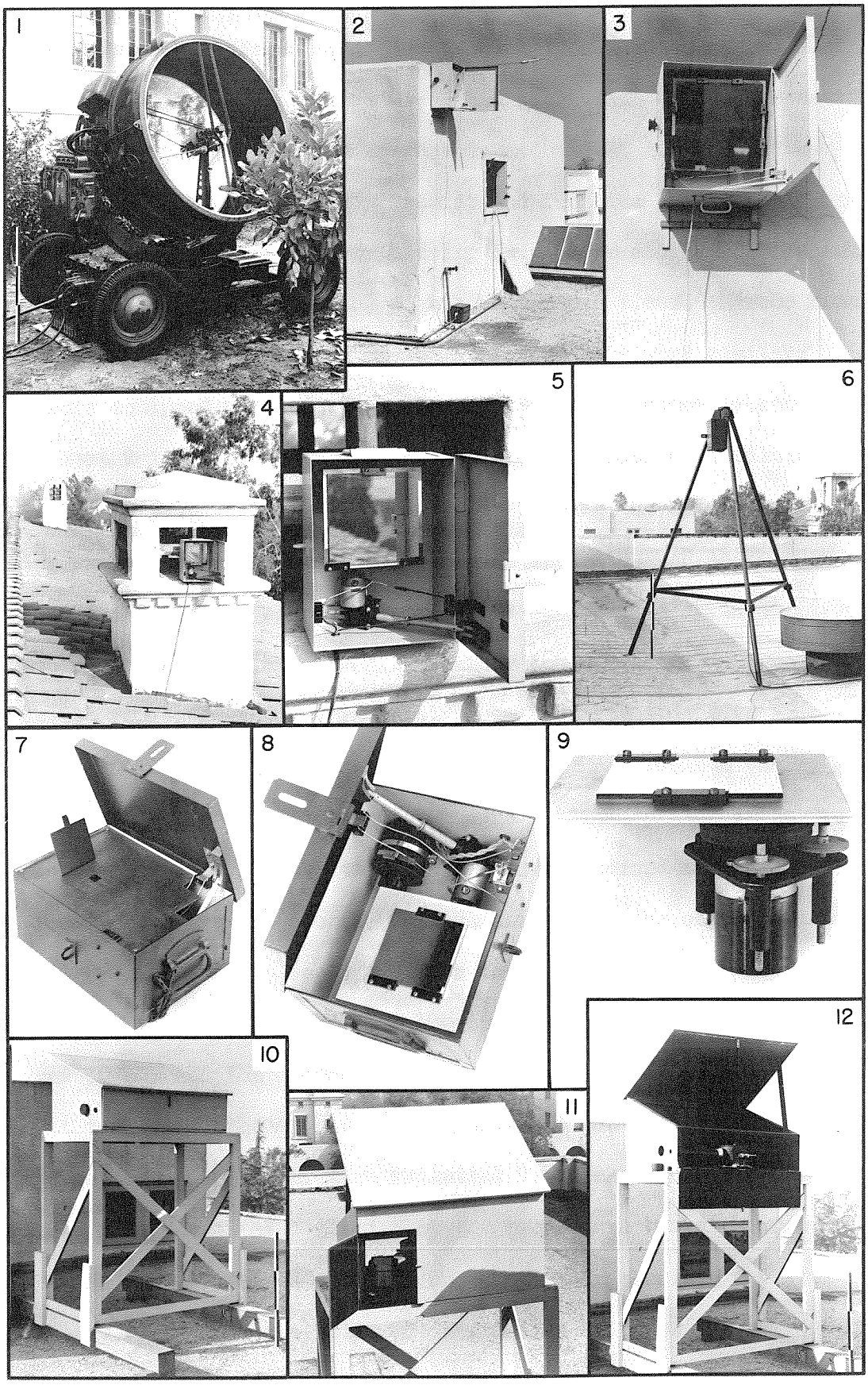

Fig. 4. APPARATUS FOR THE SEARCHLIGHT EXPERIMENT.

by a similar mirror attached to a high steel tripod located on the roof of the High Potential Research Laboratory; this short-path mirror was masked down to a small aperture so that comparable amounts of light would be received at East Bridge Laboratory from it and from the long-path Athenaeum mirror. The tripod and its mirror housing in various stages of disassembly can be seen in the sixth, seventh, eighth, and ninth views. Mirror housings on the West Bridge penthouse and at the Athenaeum were very similar; all of them were equipped with electrically operated doors remotely controlled from the East Bridge roof, and all of them were provided with tilting screws to facilitate aiming. The reason for folding the optical path and providing remote controls was that the entire apparatus had to be operated by one person; extensive sampling with a less centralized arrangement would have required more assistance than the author could reasonably expect.

The two reflected beams were received by a quartz objective spectrograph shown in its housing in the tenth, eleventh, and twelfth views. The spectrograph aperture was located in the same vertical plane as the two path-folding mirrors, so that its field of view contained two bright images, one just above the other. Optical details of the objective spectrograph will be discussed in Section V; for the present it will suffice to state that the area of the receiving aperture was about 1 in^2, the focal length was 50 cm, and the dispersion was 43 A/mm at 3000A.

Light traversing the Athenaeum path traveled 680 meters farther than light reflected from atop the High Potential Research Laboratory; hence, differences in spectral distribution of the two return beams provided a measure of relative spectral attenuation. To obtain absolute coefficients, it was necessary to know the ratio of intensities which would be received at the spectrograph if attenuation were absent. The run-of-the-mill

quality of the various mirrors (including the searchlight reflector) did not permit computing this ratio geometrically. Instead, it was determined indirectly by estimating the approximate visibility range.

Spectra obtained with the apparatus of figure 4 had more than adequate density for exposures of only a few seconds. However, the line spectrum emitted by ordinary commercial "white-flame" arc electrodes made spectral attenuation measurements more difficult than had been anticipated. So-called pure carbon electrodes did not perform much better. Several tricks were tried in an effort to remedy the situation, the first attempt being to produce a searchlight spectrum having so many lines that it could be blended into a pseudo-continuum. Figure 5 shows how cores of iron were inserted into carbon anodes. The resulting iron arc spectrum exhibited in figure 6 was magnificent, but the success of this artifice was offset by ensuing complications when attempts were made to blend or smear the lines. Defocusing the spectrograph was precluded by the fact that the only setting yielding equally diffuse spectra for the two paths fell midway between the two positions of individually sharp focus, and the spectra were not sufficiently out-of-focus in that position to blend properly. The only possible hope for achieving satisfactory results was to move or vibrate the plate during exposure. The electric plate vibrator shown in figure 48b was designed to provide damped sinusoidal oscillation with an initial amplitude of a few tenths of a millimeter; although it functioned as expected, the resulting spectra still left much to be desired.

The approximate ultraviolet attenuation curve sketched in figure 7 was computed from a sequence of vibrated spectra. Since the "scatter" of experimental points was rather bad, it was apparent that the accuracy of this apparatus was unsatisfactory and that there was no hope of resolving

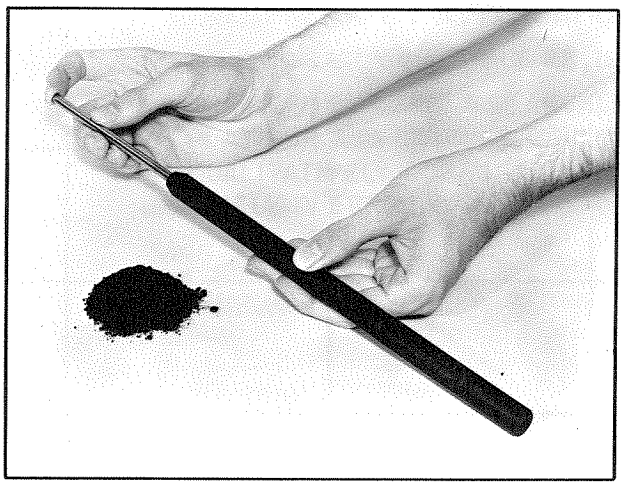

Fig. 5. METHOD FOR OBTAINING AN INTENSE IRON ARC FROM A CONVENTIONAL SEARCHLIGHT.

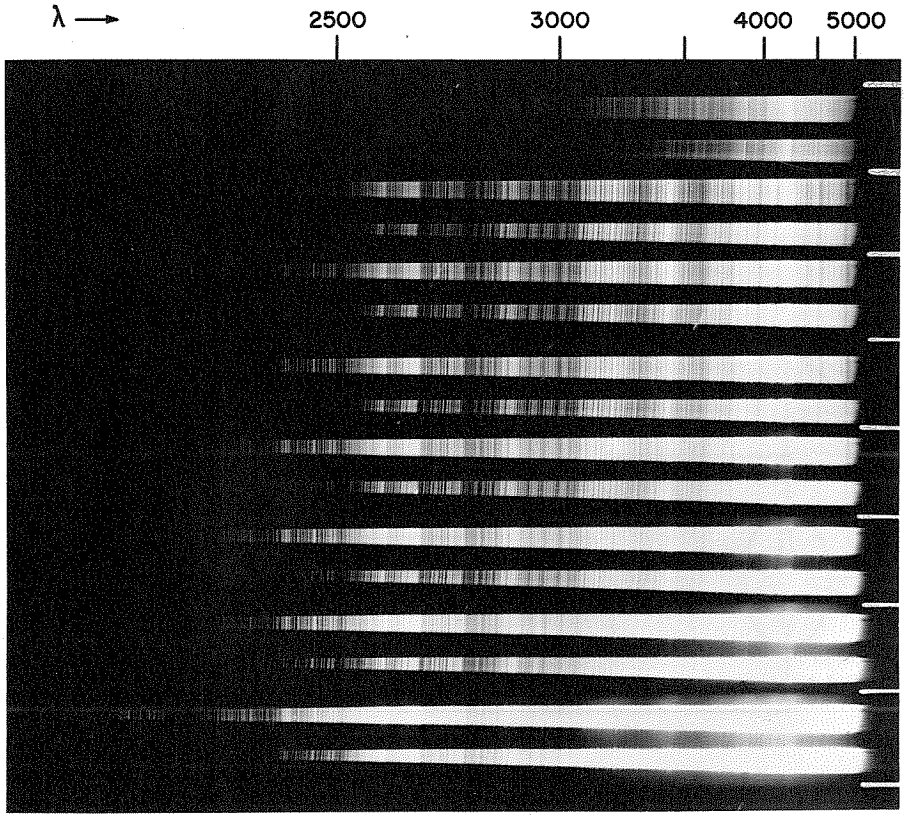

Fig. 6. IRON-CORED SEARCHLIGHT CARBONS WERE USED IN CONJUNCTION WITH APPARATUS IN Fig. 4 TO PRODUCE THIS SEQUENCE OF SPECTRA.

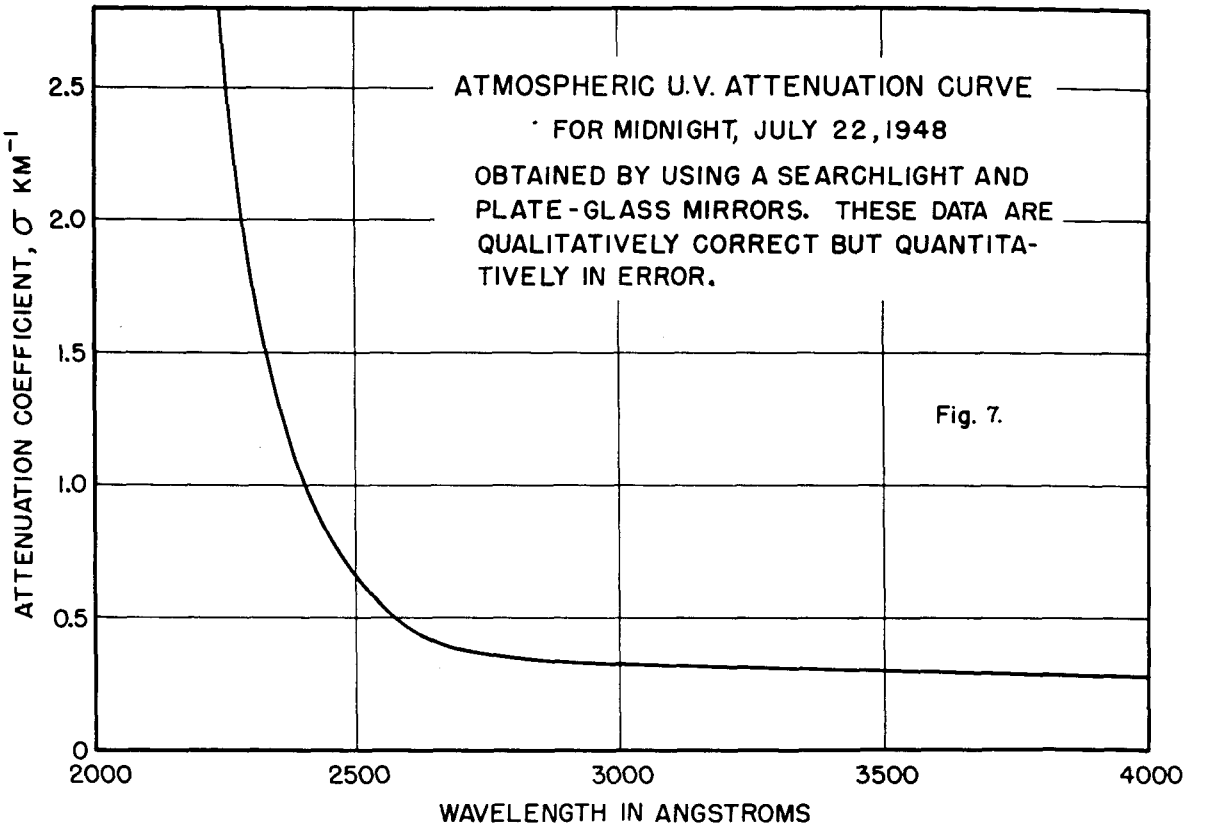

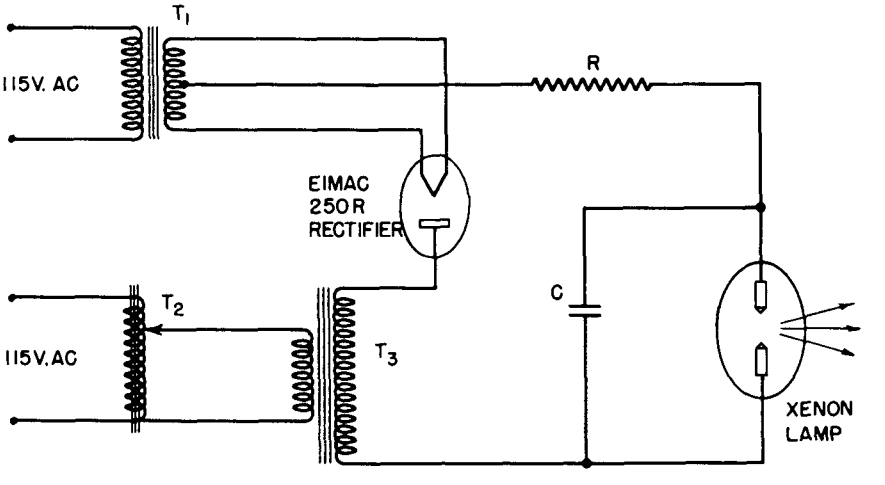

Fig. 8.

CIRCUIT FOR XENON FLASH LAMP

desired detail in the absorption spectrum unless a suitable spectrally-continuous source could be found. Consequently, the searchlight arc-flame was abandoned and attention was immediately directed toward the relative merits of other ultraviolet sources.

The next source to be tried was a xenon flash lamp of the type shown in figure 9; it was patterned in some respects after General Electric's FT230. The electrodes were turned out of molybdenum and were nickel-welded to tungsten rods; this welding was done by induction-heating in a hydrogen atmosphere. Quartz was used for the central portion of the envelope so that it would transmit the ultraviolet, and conventional graded seals were used to join this quartz section to lime-glass ends which supported the electrodes. The lamp was pumped out, flushed, filled with 1.5 atmospheres xenon, and sealed with an ordinary copper housekeeper seal.

Figure 8 is a diagram of the circuit used for operating this xenon flash lamp. T_1 = 50-watt filament transformer with high voltage insulation of the secondary, T_2 = G.R. variac, T_3 = 25,000-volt transformer rated at 1 kva, R = 10,000 ohms at 160 watts, and C = 12 microfarads rated at 10,000-volts maximum. Starting at zero charge, about 2 seconds were required for the potential on C to climb up to 9000 volts, at which point the condenser discharged through the lamp with a sudden flash. The cycle then repeated itself, resulting in one flash every two seconds. The duration of each flash was a few microseconds, during which time about 500 joules of energy were released. Effective color temperatures of flash lamps are generally estimated at more than 10,000 ^{o}K; consequently, they are exceedingly rich sources of ultraviolet.

Figure 10 shows the ultraviolet spectrum of the flash lamp just described. It was encouraging to find that line radiation was rather weak

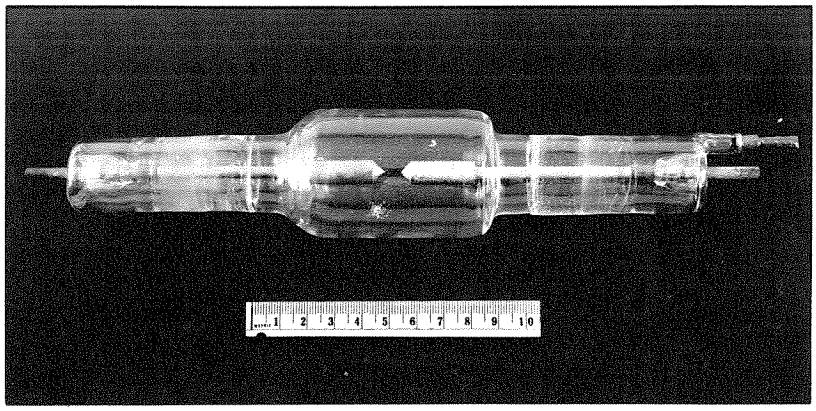

Fig. 9. HOME-MADE XENON FLASH LAMP WITH QUARTZ ENVELOPE. PRESSURE IS ABOUT 1.5 ATMOSPHERES.

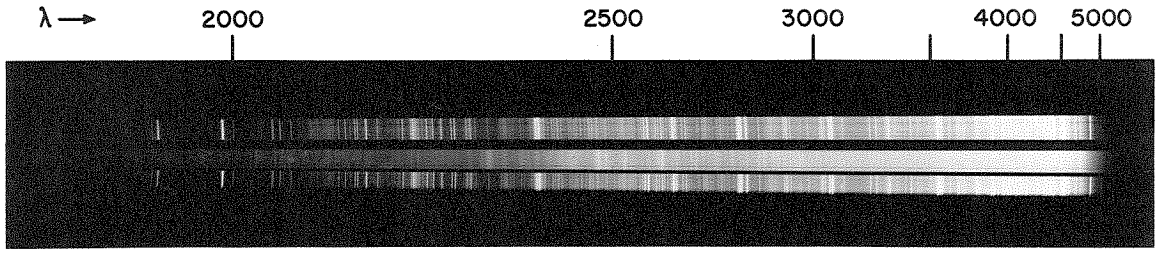

Fig. 10. SPECTRAL COMPARISON OF THE XENON FLASH LAMP (CENTER) TO AN ALUMINUM SPARK. HILGER E31 SPECTROGRAPH WAS USED.

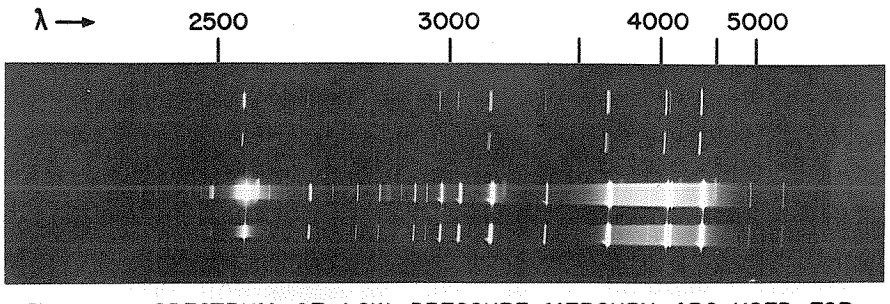

Fig. 11. SPECTRUM OF LOW PRESSURE MERCURY ARC USED FOR λ-CALIBRATION OF THE OBJECTIVE SPECTROGRAPH.

compared to the strong continuum. However, when used in place of the searchlight for attenuation measurements, the flash lamp appeared to be much less efficient photographically than had been expected, even when reciprocity failure of the emulsion[65] was taken into account. This inefficiency was likely caused by the Clayden effect[66][67], which is a sort of latent image paralysis produced by exceptionally short intense exposures.

In order to determine whether any sort of high-voltage spark in air could be induced to yield a satisfactory continuum in addition to its lines, the apparatus in figure 12 was constructed. Electrodes of various metals were inserted, and a blast of air was arranged to blow ions from the gap so that the spark would not degenerate into an arc. A few sample spark spectra photographed at a distance of 30 meters with the objective quartz spectrograph are exhibited in figure 13. Note especially the short-wavelength continuum emitted by the magnesium spark.

While both the xenon flash-lamp and the high-voltage magnesium spark were spectrally more satisfactory than the searchlight arc-flame, their intensities were somewhat lower than wished; consequently, they were set aside in favor of investigating still other sources. Actually the high voltage spark, particularly with aluminum electrodes, continued throughout the experiment to be quite useful for wavelength calibration of the objective spectrograph. Another source found convenient for wavelength calibration above 2500A was a low-pressure mercury arc, whose spectrum is shown in figure 11.

The source finally adopted for over 90% of the attenuation measurements was a high-pressure xenon arc lamp which is separately described in considerable detail in the following section; it provided both the extraor-

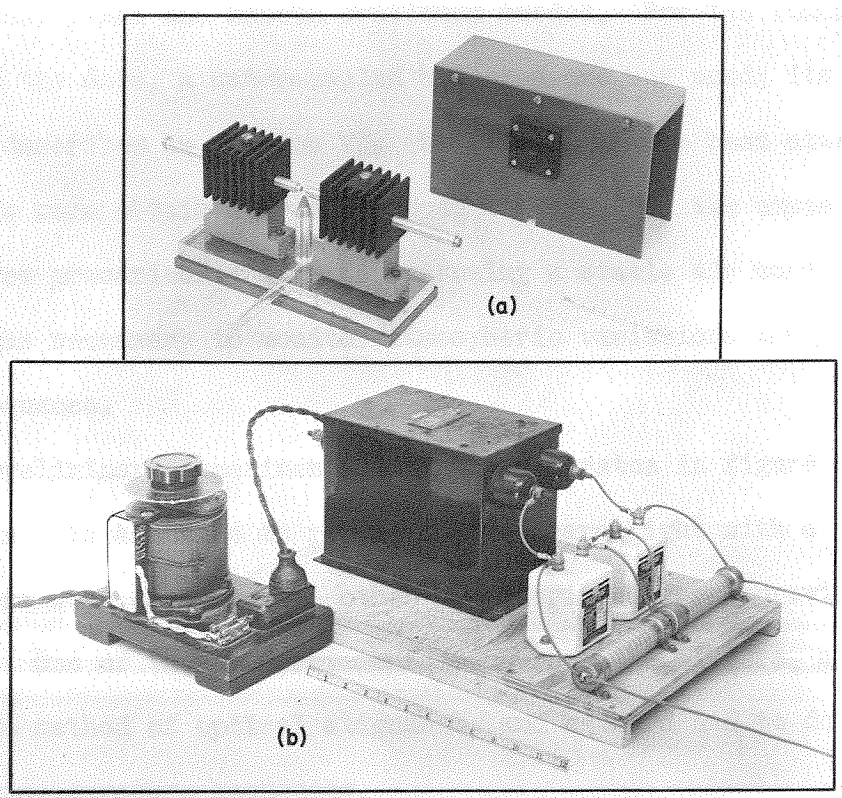

Fig. 12. (a) 20-KILOVOLT SPARK and (b) POWER SUPPLY

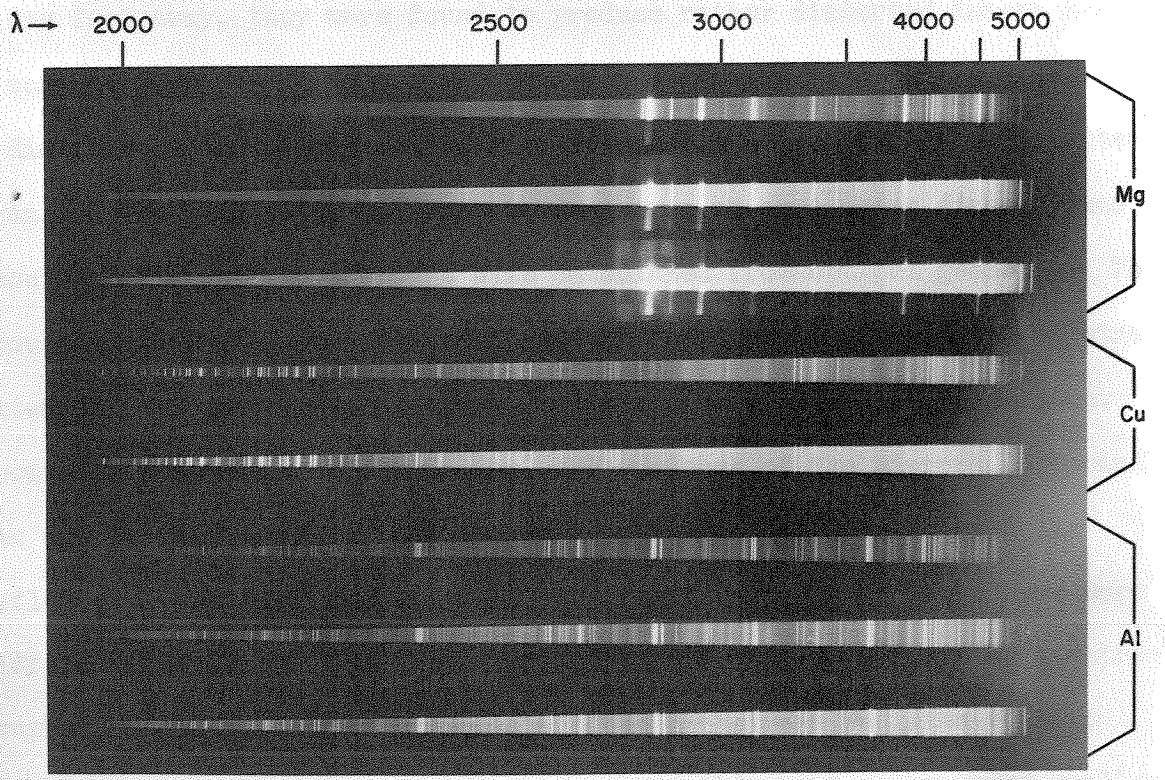

Fig. 13. SAMPLE SPARK SPECTRA MADE WITH THE OBJECTIVE SPECTROGRAPH

dinary intensity and the smooth continuum needed. For the remaining fraction of the data, a water-cooled hydrogen arc was used; its characteristics are described in Section VI. While some of the best attenuation coefficients were obtained from hydrogen arc spectra, the exposure times required were precariously long for assuming a stable air condition; hence, it was necessary to monitor atmospheric variations throughout the exposure sequence.

From preliminary experiments with the apparatus in figure 4, it was apparent that, in addition to replacing the searchlight with a better source, there were also several other opportunities for improving the experiment. One of these improvements concerned the mirrors, another involved the method of optical alignment, and a third had to do with producing precise exposure sequences.

Although the front-surface plate-glass mirrors looked very good from a few feet away, they were found to produce rather distorted images from a somewhat greater distance, indicating that they were slightly wavy. At a distance of 380 meters (Athenaeum mirror to spectrograph) the reflected beam was found to be spread out unevenly over an area whose diameter was about 1 meter greater than the size calculated from optical geometry. The resulting loss of light was not in itself detrimental to relative spectral attenuation measurements, because it introduced no spectral dispersion. However, in a much more subtle way, the waviness of the mirrors, especially the one at the Athenaeum, <u>did</u> introduce spectral differences into the reflected beams; this came about because various <u>parts</u> of the source were differently emphasized in the distorted mirror images seen by the spectrograph. For example, the hot nucleus of an arc stream radiates quite a different spectrum than its cooler edges; if this nucleus appeared swollen

in one of the distorted reflections but appeared shrunk in the other, the spectrograph would receive two light fluxes having inherent differences in spectral character in addition to the differences introduced by path attenuations. The only remedy for this difficulty was to replace the path-folding mirrors with aluminized optical flats of very high quality.

Since the use of these flats made coherent optical imaging possible for long paths, it was necessary also to provide a more precise and stable method for aligning them, especially the Athenaeum mirror for which the angular tolerance on orientation became 10 seconds of arc. A mechanism described in Section V proved more than satisfactory for this purpose.

As outlined in Section VII, accurate photographic spectrophotometry requires a sequence of graduated exposures which simultaneously provide emulsion characteristics and attenuation data on the same plate. Unfortunately, graduated exposures cannot be properly obtained by varying the duration of exposure, because reciprocity failure of the emulsion[66] introduces sizable errors. Two methods for producing graduated exposures of equal duration are considered to be correct: one involves direct variation of the intensity by filters or suitably located diaphragms, while the other employs rapid chopping with sector disks of different percentage aperture. The latter method was adopted, and details of the mechanism are described in Section V.

IV. THE HIGH PRESSURE XENON ARC[68]

The search for a source emitting an intense continuous spectrum in the ultraviolet led to an investigation of the high pressure xenon arc lamps described by Schulz[69][70][71]. Two of these lamps are shown in figure 14, and the ultraviolet spectrum of the larger one is exhibited in figure 15. The envelopes are fused quartz and the electrodes are tungsten. Thin molybdenum strips, sealed directly into the quartz, serve as leads. A third electrode located on one side of the lamp introduces a high voltage spark for initial striking of the arc. The general characteristics of these lamps as given by Schulz are summarized in Table III.

Table III

	Small Lamp	Large Lamp
Xenon pressure during operation (atmospheres)	40	40
Maximum current (amperes)	8	30
Terminal voltage	30	30
Average brightness (candles per mm^2)	100	230
Luminous area (mm^2)	3	8
Wavelength of peak output (Angstroms)	5500	5500
Approximate color temperature (degrees Kelvin)	5200	5200

Ultraviolet characteristics of only the large lamp will be described; those of the small one appeared to be similar except for differences associated with size.

The arc was operated for periods varying from a few minutes to several hours at a time. When the lamp was new, it was possible to maintain a stable arc at a current of 30 amperes. As the lamp aged in use, it became

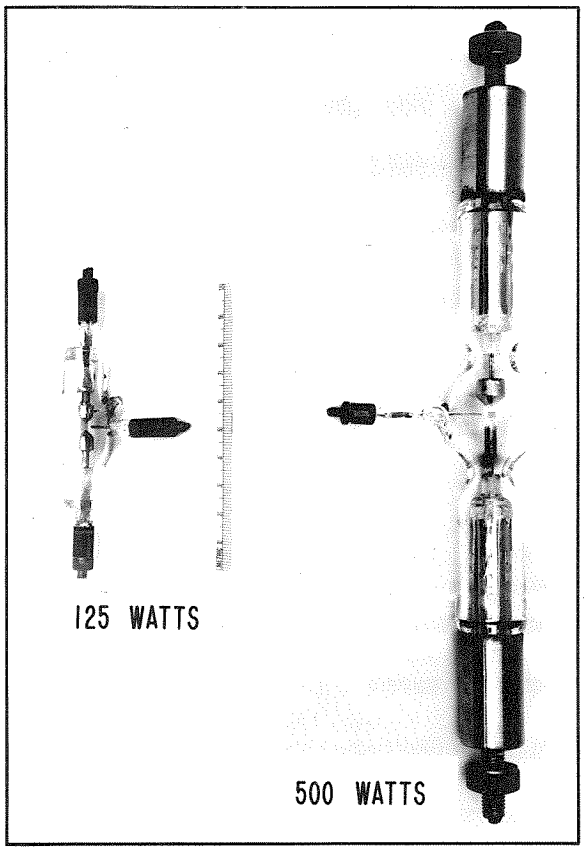

Fig. 14. HIGH-PRESSURE XENON ARC LAMPS

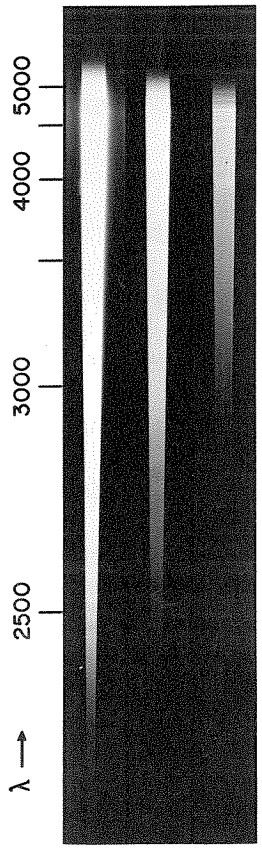

Fig. 15.
U.V. SPECTRUM

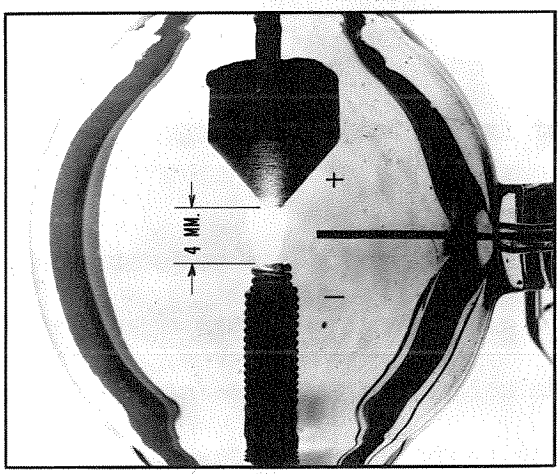

Fig. 16. ELECTRODES AND ARC STREAM
OF 500-WATT XENON LAMP

necessary to operate with less and less current; after a total of 75 hours, the maximum current for a stable arc was 15 amperes. No blackening of the lamp interior was observed, but a white coating has formed around portions of the envelope where the electrodes are supported.

The exact pressure of xenon in this particular lamp was unknown. However, using a relation between pressure and terminal voltage given by Schulz (see figure 17), one can estimate the pressure to be nearer 20 than 40 atmospheres, because the potential drop across the terminals during operation was 19 volts instead of 30 volts as reported by Schulz.

Figure 16 is a double-exposure photograph of the electrodes and arc stream under operating conditions. It was often necessary when starting the lamp to strike the arc several times before it became stable. Once a stable arc formed, it maintained itself indefinitely. The lamp was operated with natural ventilation only; forced cooling was unnecessary. Power was supplied by a 110-volt d.c. generator in series with a conventional ballast of tungsten lamps.

It can be seen from figure 18 that ten minutes was ample time for the lamp to reach equilibrium; thereafter no changes in radiant output were observed within the accuracy of measurement (about 1%).

As one might expect, radiation from the lamp was found to be symmetric in a plane passing through the arc and normal to the electrode axis.

The spectrum of the xenon arc was compared by photographic spectrophotometry to the spectrum of a carbon arc crater in order to determine the absolute spectral radiant intensity distribution of the xenon arc. A small Hilger ultraviolet quartz spectrograph, whose dispersion curve is given in figure 20, was used in conjunction with calibrated wire-mesh

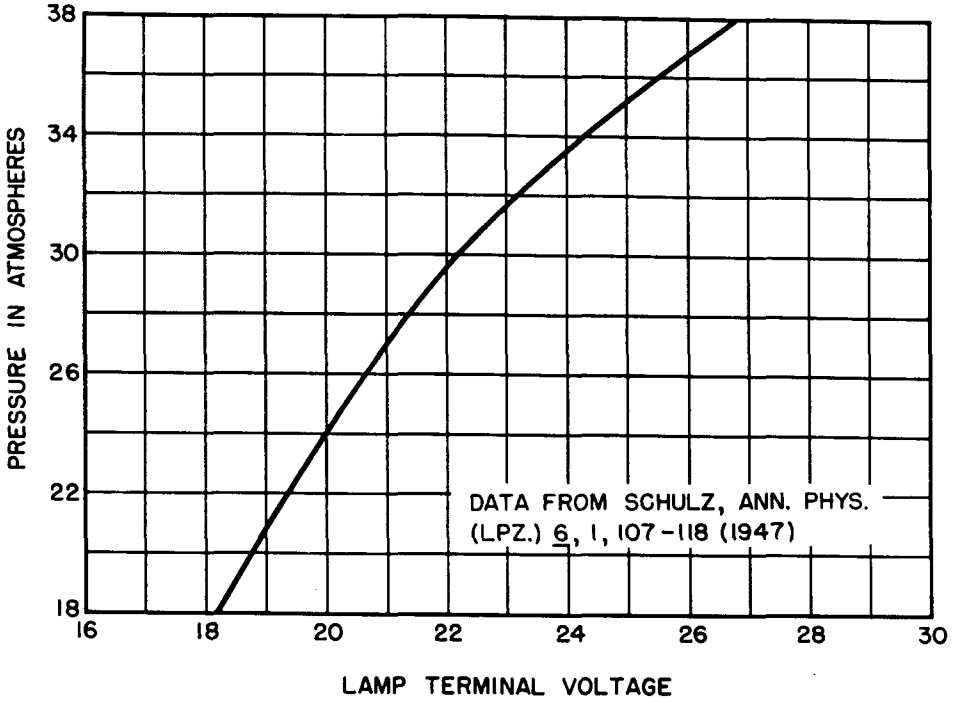

Fig. 17. RELATION BETWEEN XENON PRESSURE AND LAMP TERMINAL VOLTAGE AT EQUILIBRIUM.

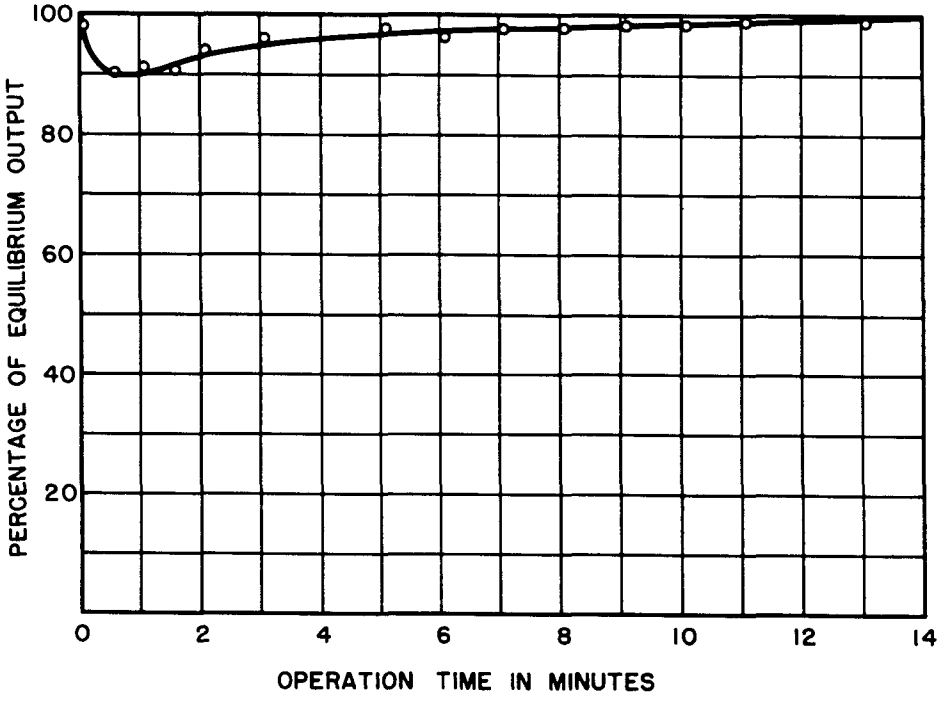

Fig. 18. RADIANT INTENSITY AT 2900A DURING WARM-UP.

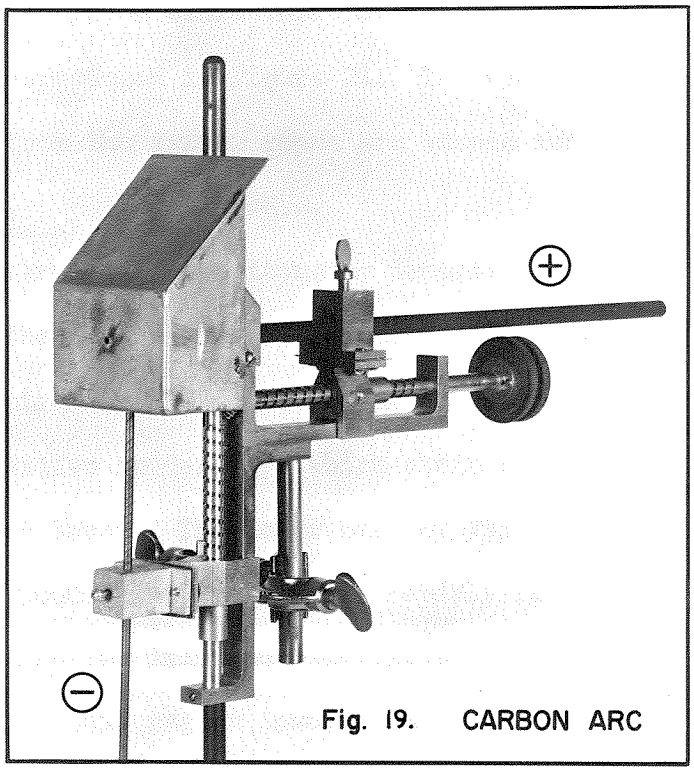

Fig. 19. CARBON ARC

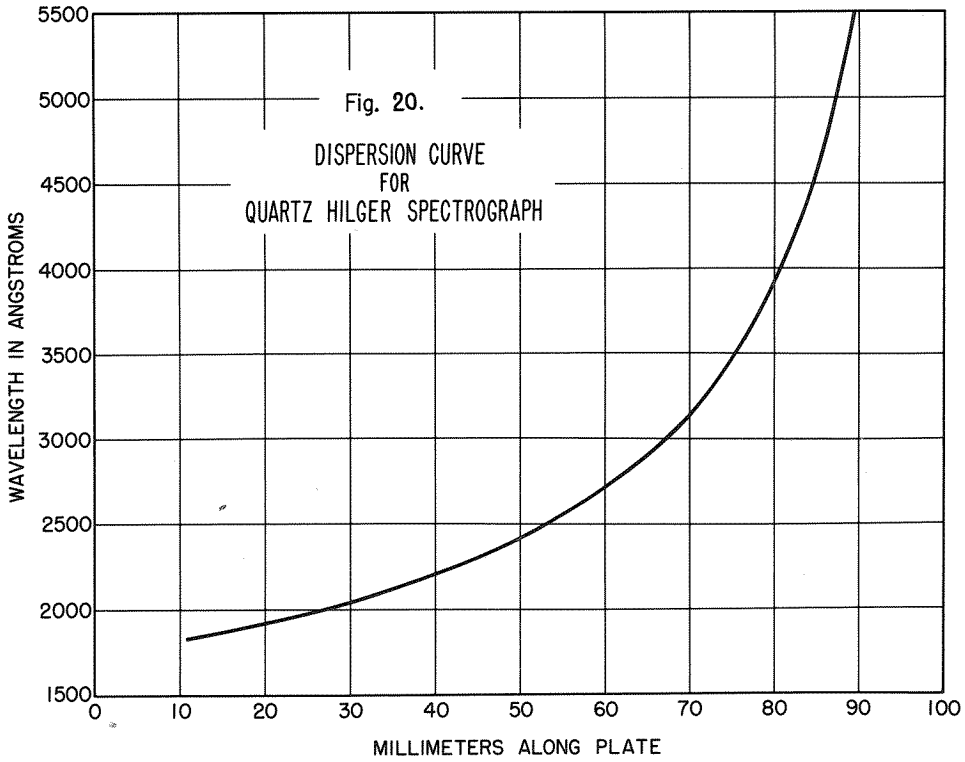

Fig. 20.

DISPERSION CURVE
FOR
QUARTZ HILGER SPECTROGRAPH

filters[72] and Eastman 103-O ultraviolet sensitive film to photograph the sequence of spectra reproduced in figure 21. The spectrograph was arranged to accept radiation from the entire xenon arc stream and from a known area of the carbon crater.

A Leeds and Northrup microdensitometer described in Section VII was employed to analyze the spectrogram. The upper half of figure 23 is a trace of the arc spectrum from 2200A to 3800A; the two abrupt breaks are changes in scale (additive in density) which avoid crowding the high density portion of the trace. The lower half of figure 23 includes the region from 3800A to 5000A; the trace falls rapidly for wavelengths longer than 4500A due to decreasing film sensitivity, but the arc output is actually rising through this region toward a maximum in the green. It is apparent from these traces that the xenon arc radiates a smooth continuum in the ultraviolet, and that several weak lines are superimposed on the continuum in the blue region (note also figure 22). Schulz reported that the spectral continuum extends through the visible region with an energy distribution quite similar to that of sunlight. In the infrared, however, he found that most of the radiation is contributed by lines.

In order to use the carbon arc as a reference standard, it was set up as shown in figure 19 and operated as prescribed by MacPherson[73]; his data for the absolute spectral radiance were used. The anode was a 5/16 inch spectroscopically-pure carbon rod viewed end-on through a small aperture in a metal crater shield. The cathode was a 1/8 inch pure graphite rod placed at right angles to the anode. By a manual feed mechanism, the arc was operated in such a way as to avoid hissing, and its current was maintained as close to 12 amperes as possible.

The spectral distribution of radiant intensity in milliwatts per 100

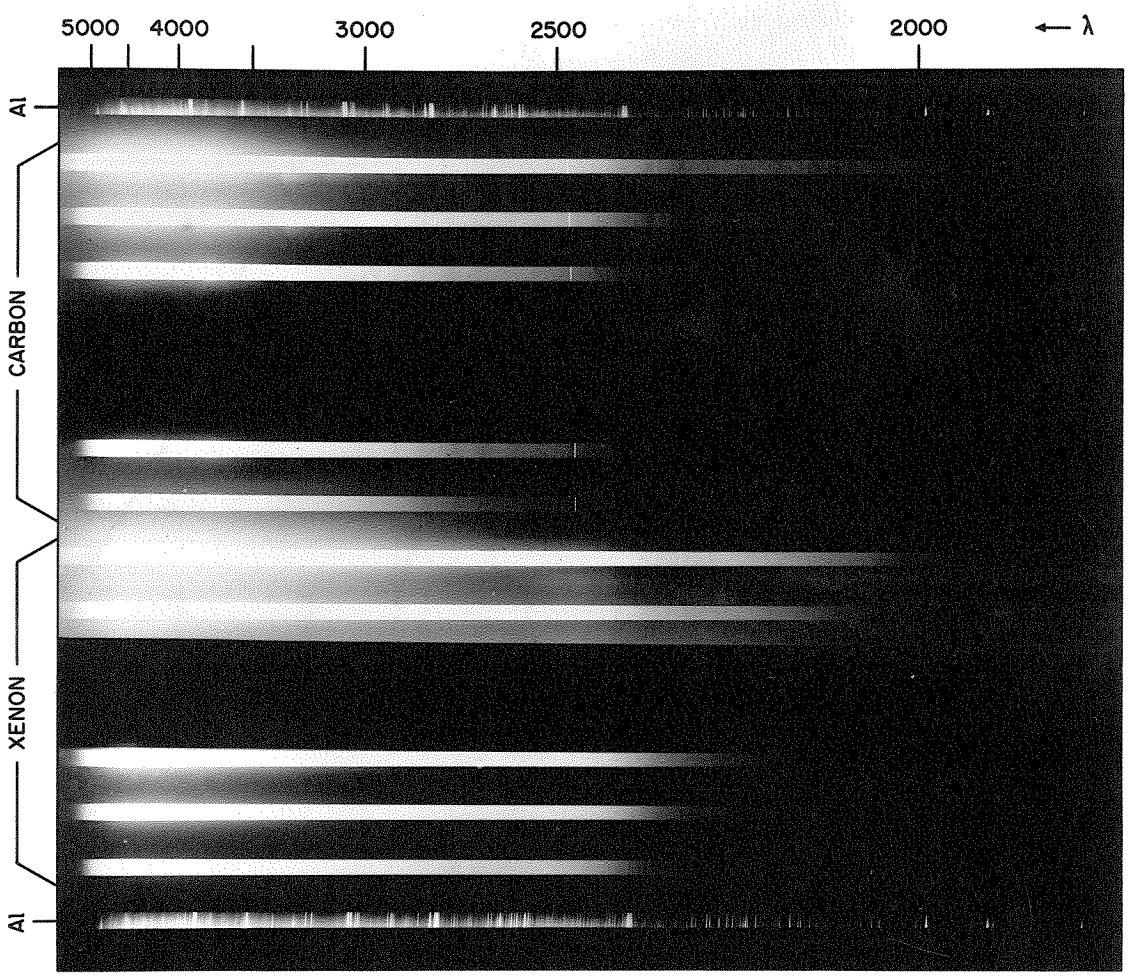

Fig. 21. SPECTROGRAPHIC COMPARISON OF THE HIGH PRESSURE XENON ARC TO THE CARBON ARC CRATER. THIS FIGURE IS ABOUT DOUBLE SIZE. (HILGER E31)

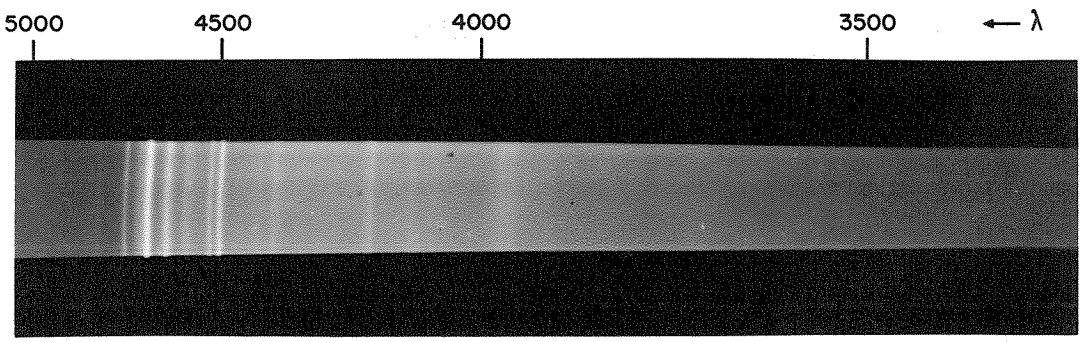

Fig. 22. BLUE REGION OF THE XENON ARC SPECTRUM ENLARGED ABOUT TEN TIMES. (OBJECTIVE SPECTROGRAPH)

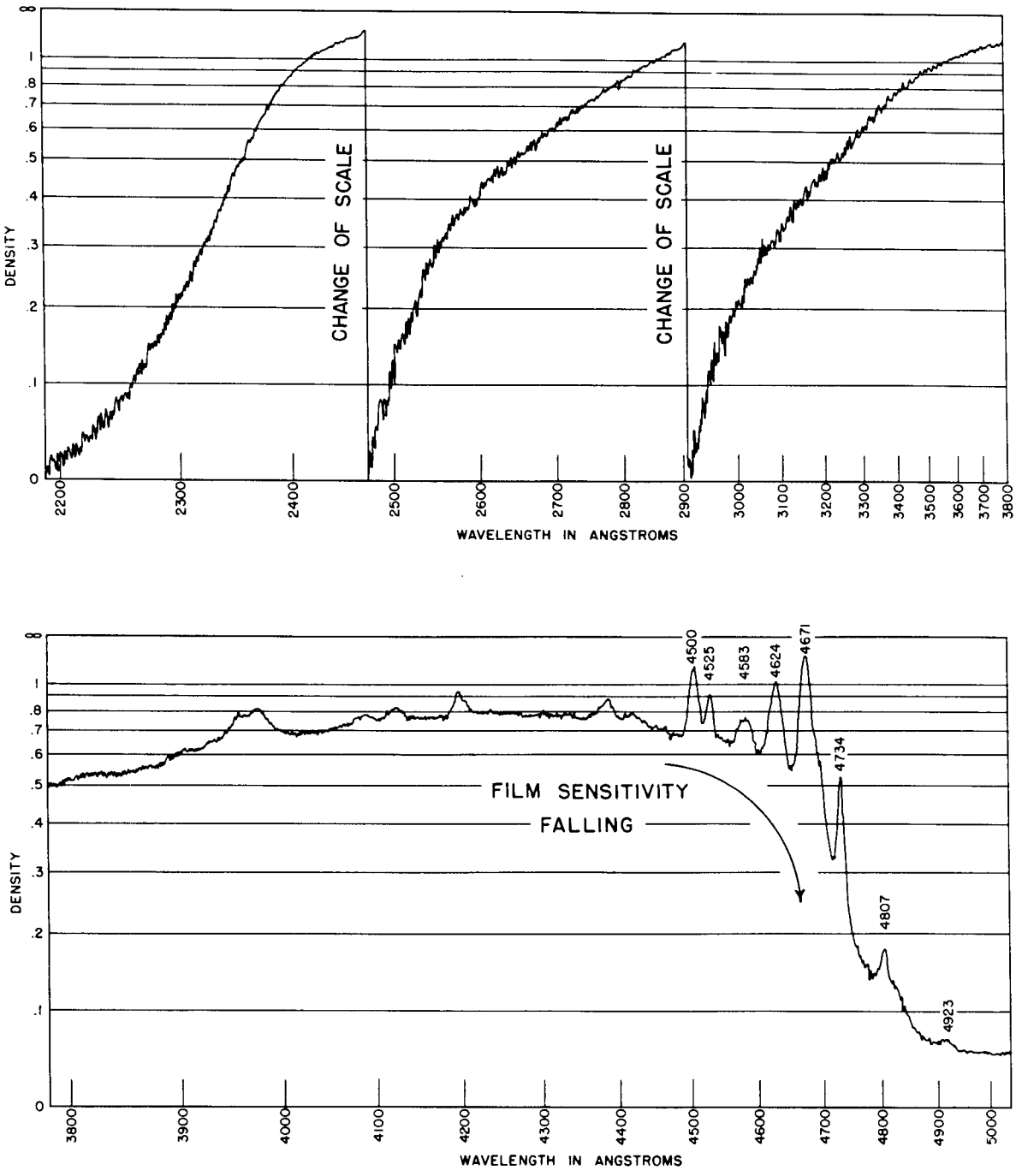

Fig. 23. DENSITOMETER TRACES OF THE XENON ARC SPECTRUM.

Angstroms per steradian for the whole xenon arc operating at 22.8 amperes is given in figure 24. Since the xenon arc stream spreads over roughly 10 mm^2, the same area of carbon crater was selected for comparison. To obtain the distribution below 2230A, it was necessary to extrapolate MacPherson's data. If the extrapolation is valid, then the radiant intensity of the xenon lamp falls off rapidly below that wavelength, due perhaps to attenuation by the quartz envelope.

For spectroscopic purposes and other applications where the light source is imaged on a slit or limiting aperture, the brightness or radiance of the emitting surface is of more interest than the total output or radiant intensity of the whole source. Since the radiance of the xenon arc was not uniform, its distribution over the arc stream was measured. Figure 26 is an isoradiance map of the arc for about 3300A. This map and those in figure 27 were obtained from densitometer measurements of arc stream photographs made with an ordinary camera. The three wavelength regions were isolated by appropriate films and filters, whose response curves appear in figure 25. The most intense part of the arc was assigned a radiance value of 100% in each case, so that the isoradiance contours shown represent percentages of these maxima. By measuring the areas enclosed within the contours, one can compute relative contributions of various zones of the arc, as shown for the ultraviolet in figure 28. The same information is plotted against zone area in figure 29. Areas enclosed by contours of the three maps in figure 27 are compared in figure 30. It can be seen that these areas are nearly identical for the ultraviolet and green maps. This was taken to indicate that the radiance distribution probably has little wavelength dependence in the ultraviolet.

Using this information, we can convert our ultraviolet spectral radiant

Fig. 24.

SPECTRAL RADIANT INTENSITY OF THE XENON ARC

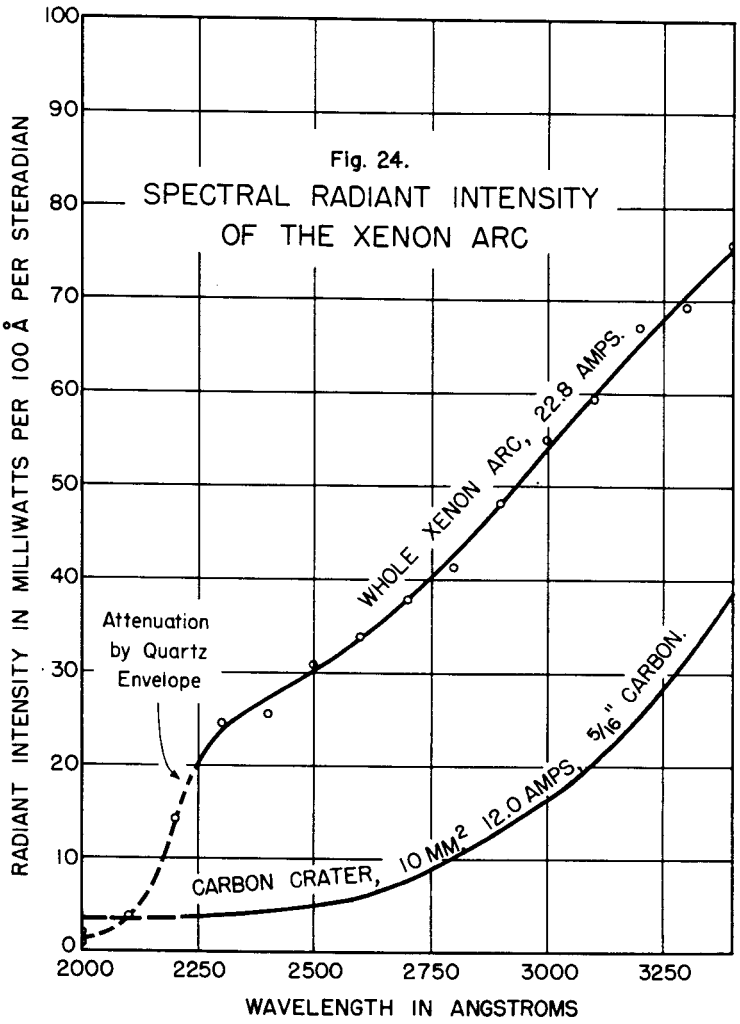

Fig. 25.

EXPERIMENTAL H & D CURVES FOR MAPPING THE XENON ARC

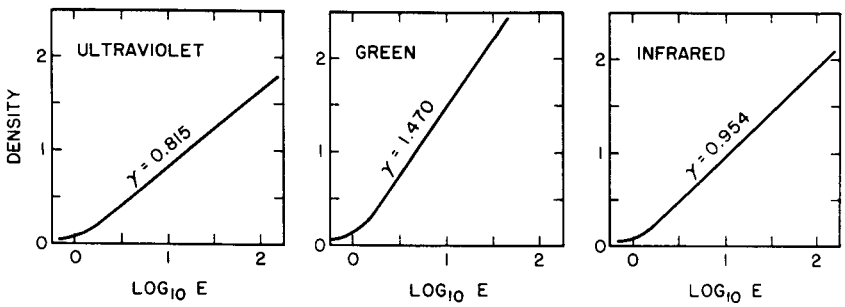

KODAK COMMERCIAL FILM
U. OF C. TYPE G FILTER

DEFENDER FINE-GRAIN PAN
WRATTEN NO. 61 FILTER

KODAK INFRARED FILM
WRATTEN NO. 87 FILTER

ALL FILMS WERE DEVELOPED IN D-19 AT 68°F. FOR 2.0 MINUTES.

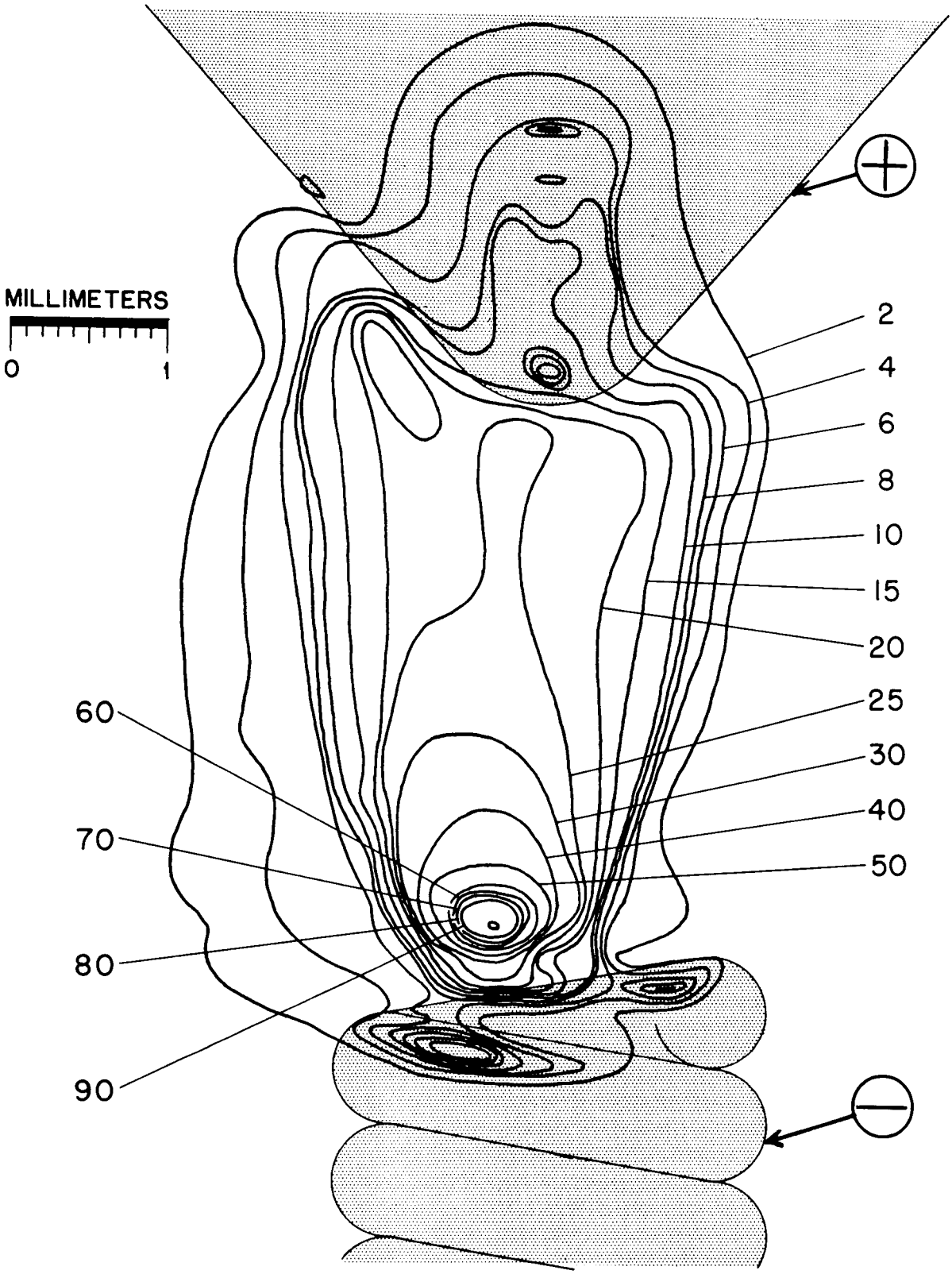

Fig. 26. ULTRAVIOLET MAP OF THE XENON ARC STREAM SHOWING ISORADIANCE CONTOURS AT 3300A.

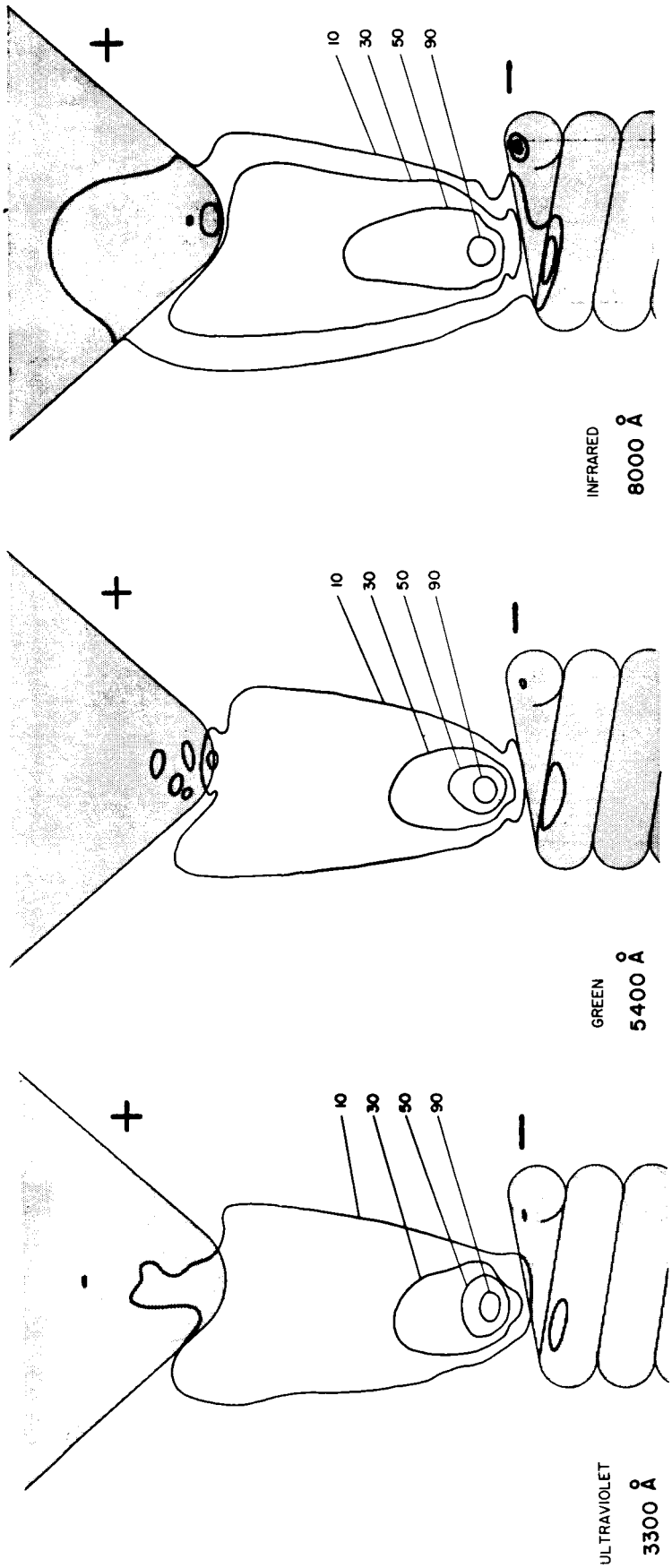

Fig. 27. XENON ARC MAPS FOR THREE SPECTRAL REGIONS.

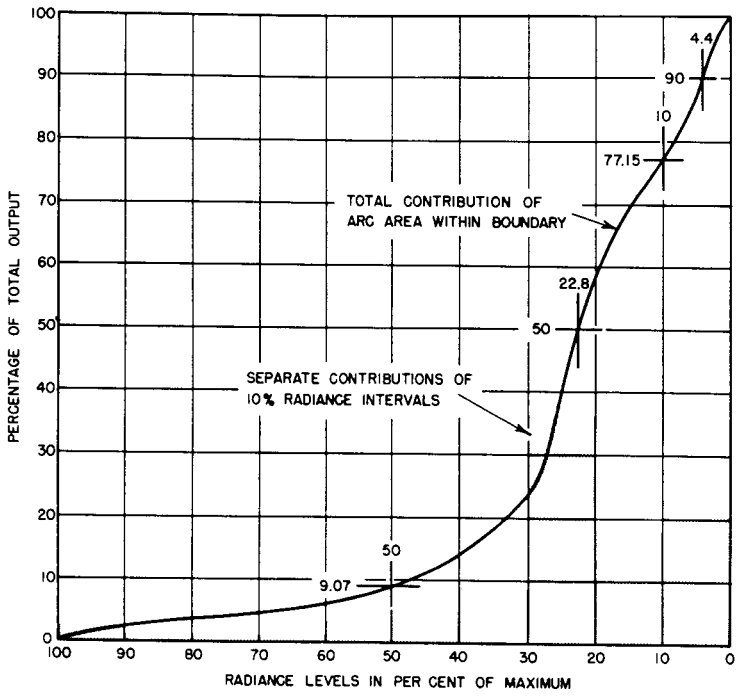

Fig. 28. RELATIVE CONTRIBUTIONS OF ZONES IN THE ULTRAVIOLET MAP (FIGURE 26).

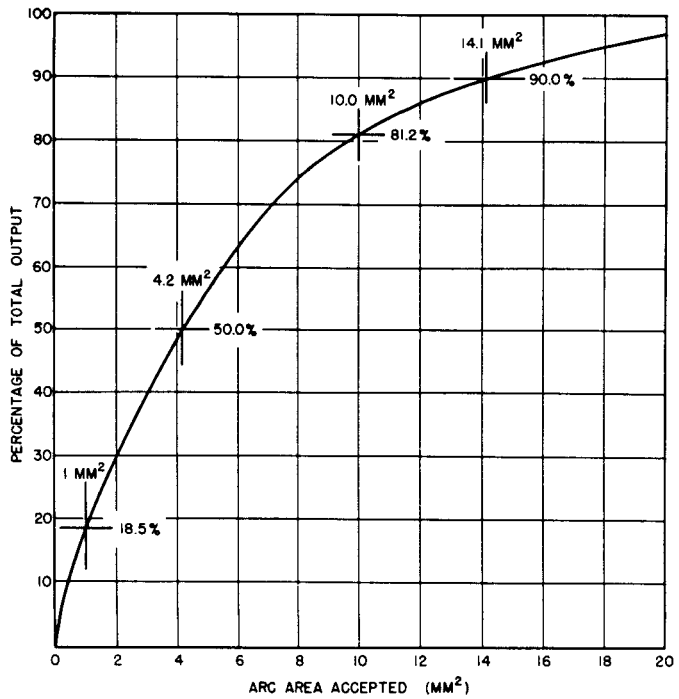

Fig. 29. HOW THE ARC STREAM SPREADS OUT (ULTRAVIOLET)

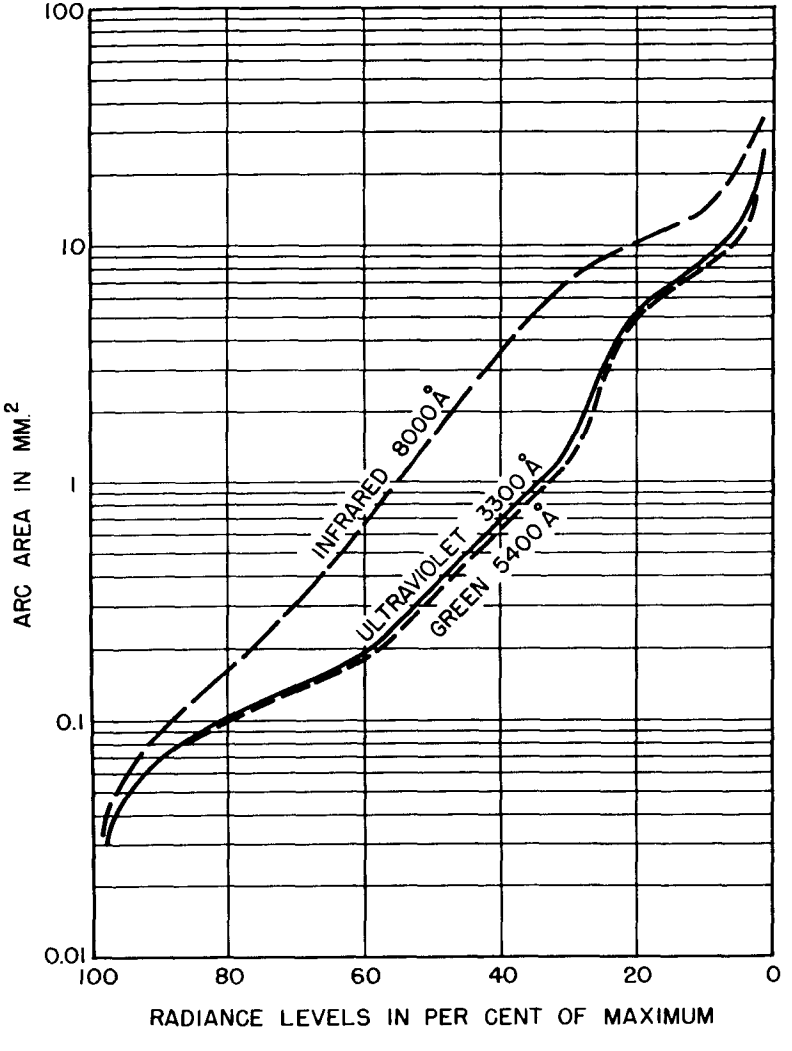

Fig. 30. AREAS ENCLOSED BY ISORADIANCE CONTOURS.

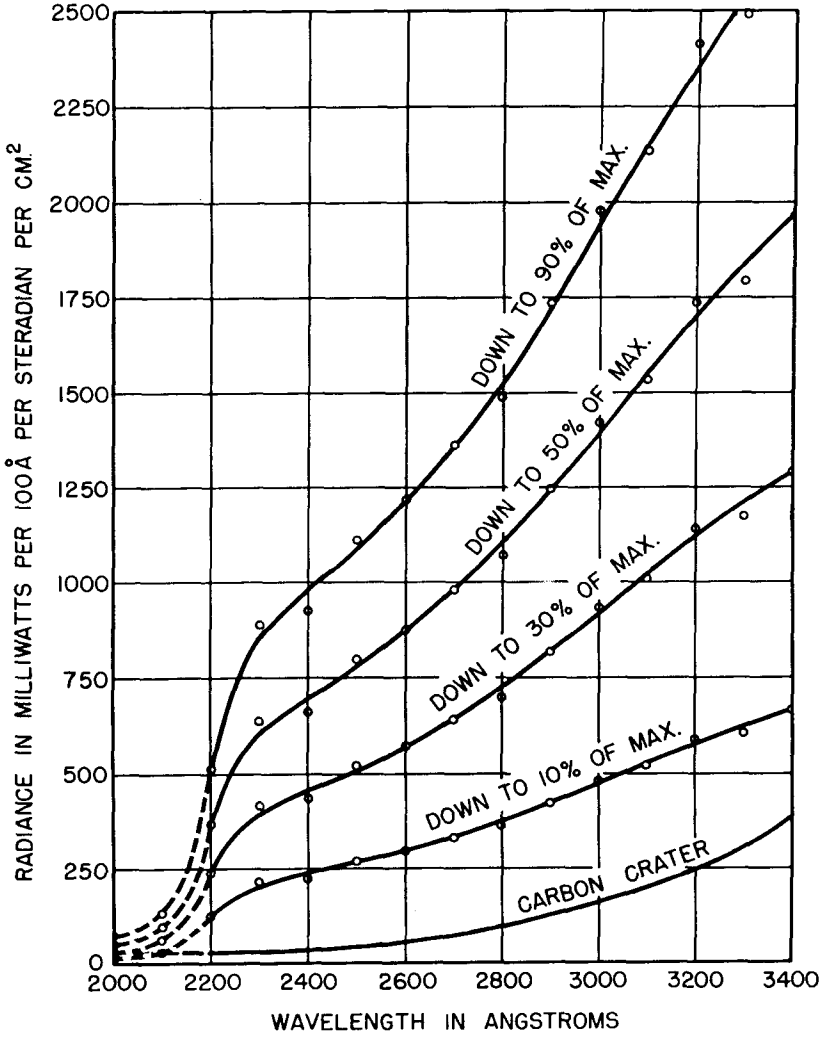

Fig. 31. AVERAGE SPECTRAL RADIANCE OF THE XENON ARC.

intensity distribution for the whole arc (figure 24) to absolute spectral radiance values for various parts of the arc stream; that is, from milliwatts per 100 Angstroms per steradian to milliwatts per 100 Angstroms per steradian per square centimeter of arc area. This amounts simply to replacing percentage labels on the ultraviolet map contours (figure 26) by a set of absolute radiance values for each wavelength.

Instead of plotting a spectral radiance distribution for each of the individual zones, one can compute average or effective spectral radiance curves for the arc when masked down to certain isoradiance boundaries. This is more informative because, when imaging the arc on a slit or aperture, one usually selects the brightest portion of the arc stream; hence, the average radiance over that portion is the significant quantity. Figure 31 is a family of average spectral radiance curves for imaginary masks of optimum shape placed in succession at 10%, 30%, 50%, and 90% boundaries. Obviously the average radiance diminishes as more of the arc is included. The spectral radiance of the carbon crater is shown for comparison.

Spectral radiance values in figure 32 were obtained by considering only the most intense part of the arc stream; that is, by closing down the mask to a pin-hole or short slit. The carbon crater is again shown for comparison. Both plots are fitted with theoretical gray-body curves. Appropriate distribution temperatures for the continuum of the xenon arc vary from 6600°K for this spectral region to Schulz' value of 5200°K for visible green. MacPherson's value of 3840°K was used for fitting the carbon arc data.

Figure 33 gives the ratio of the radiance of the most intense part of the xenon arc to the radiance of the carbon crater; this is simply the ratio of the two empirical curves in figure 32.

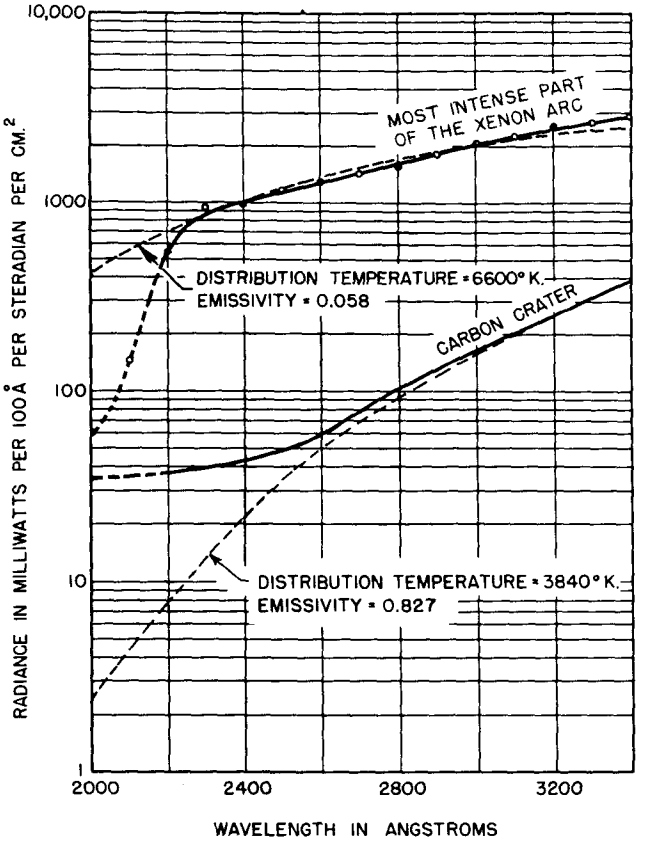

Fig. 32. COMPARISON WITH GRAY-BODY DATA.

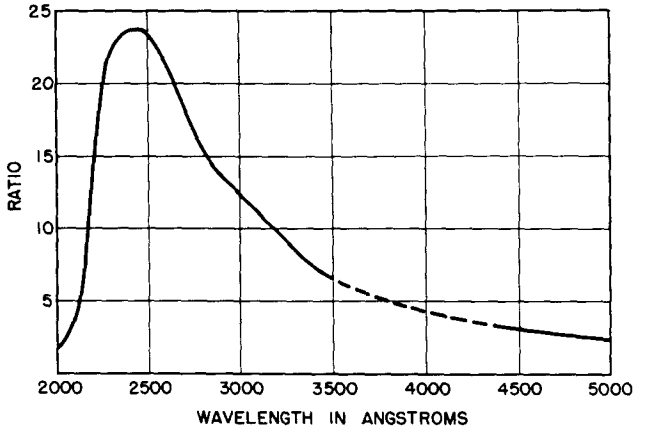

Fig. 33. SPECTRAL RADIANCE OF THE XENON ARC NUCLEUS DIVIDED BY THE SPECTRAL RADIANCE OF THE POSITIVE CARBON CRATER.

The spectral radiance of the most intense part of the xenon arc is compared with several well known ultraviolet sources in figure 34. Three hydrogen arcs are shown: one made by Hanovia, another described by Allen and Franklin[74] and made by Nestor, and a third made by the National Technical Laboratories. Two mercury arcs are also shown: the H-4 with glass envelope removed, and the H-6. The curves for the hydrogen arcs and for the H-4 mercury lamp were based on spectral radiance values reported by Matz and Merrill[75]. Data for the H-6 mercury lamp were computed from spectral irradiation measurements made by the General Electric Company Lamp Department. In comparing hydrogen arcs with the xenon arc, we see, for example, that the radiance of the xenon arc at 2500A exceeds that of the Hanovia hydrogen arc by a factor of more than 10, the Nestor hydrogen arc by almost 100, and the National Technical Laboratories hydrogen arc by nearly 200. At 3000A there is an additional factor of 4 in each case in favor of the xenon arc. It is difficult to compare the smooth continuum of the xenon arc to the radiation from the mercury sources because of the pseudo-continuum of the H-6 and the line emission of the H-4; however, the xenon arc is apparently more intense in the ultraviolet than the H-4 lamp but less intense over most of the range than the H-6.

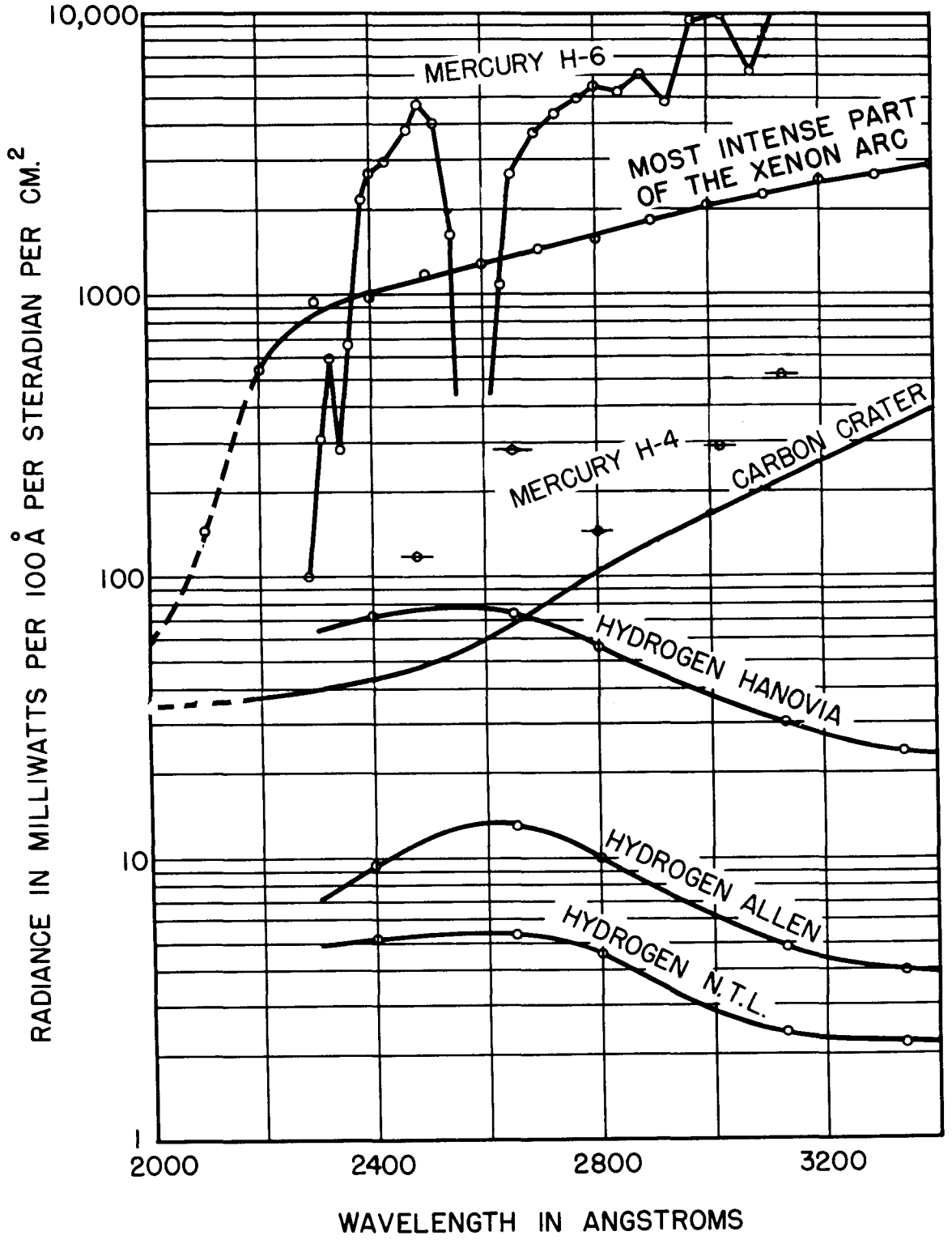

Fig. 34. COMPARISON OF ULTRAVIOLET SOURCES.

V. ATTENUATION MEASUREMENTS USING THE XENON ARC

More than 90% of the ultraviolet atmospheric attenuation measurements in the present investigation were made using the large high pressure xenon arc lamp described in the preceding section. The light-path was essentially the same as that employed for preliminary work, but the equipment itself was completely redesigned to incorporate the improvements outlined at the end of Section III.

Figure 35 is an aerial view of the California Institute of Technology campus showing the placement of apparatus. Figures 36 through 41 are photographs of equipment located at points A, B, and C. Station A housed both the xenon arc and the spectrograph; stations B and C housed path-folding mirrors. Controls for all stations were centralized at A as described in Section III, thus enabling one person to make attenuation measurements without assistance. Figure 44 is a diagram of one of the remote control circuits. Sound-powered telephones were also connected between the three stations to aid optical alignment and to facilitate trouble-shooting; owing to relatively trouble-free functioning of equipment throughout the investigation, these phones were rarely used except for special experiments (see Section VI).

Figure 42 is a schematic diagram of the optical system. Mirrors M_3 and M_4 were located at stations C and B, respectively, while the rest of the system was at A. Mirror M_1 was a 12-inch parabola (f/8) of astronomical quality; M_2 was a 4-inch optical flat; M_3 and M_4 were 8-inch optical flats formerly used as interferometer plates. All four mirror blanks were coated with aluminum by vacuum deposition and were then topped with a protective layer of silicon monoxide as prescribed by Hass and Scott[76]. This protective layer was supposedly identical on all four surfaces and

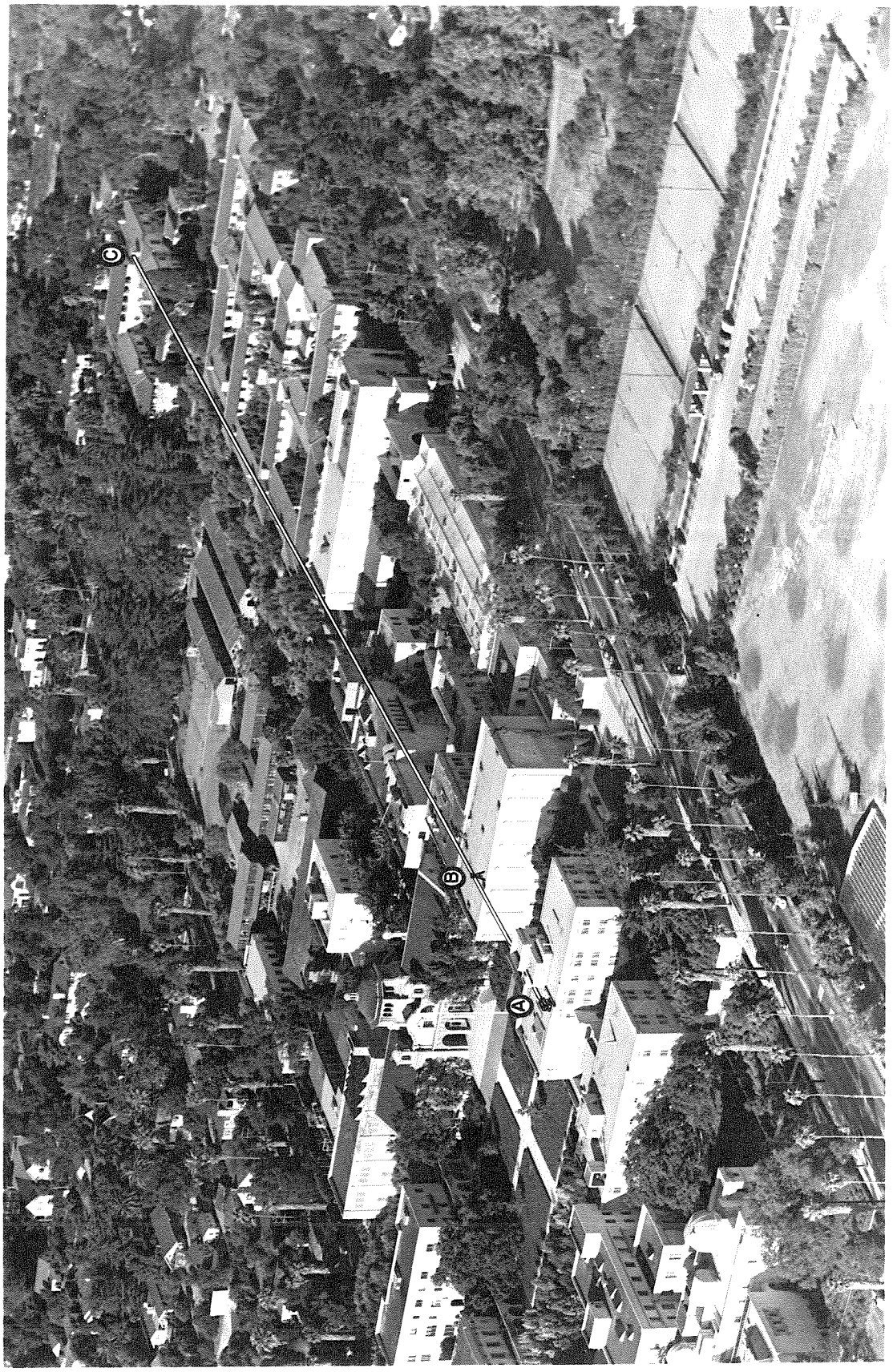

Fig. 35. AERIAL VIEW OF THE CALIFORNIA INSTITUTE OF TECHNOLOGY CAMPUS SHOWING THE PLACEMENT OF APPARATUS.

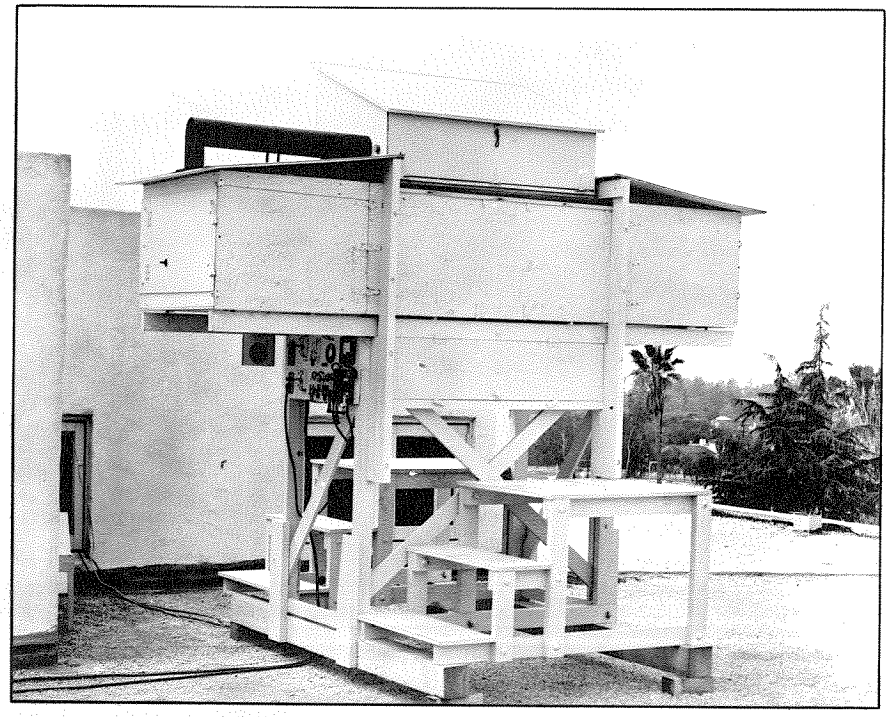

Fig. 36. STATION "A" AS IT NORMALLY APPEARS. HEIGHT ≈ 10 FT.

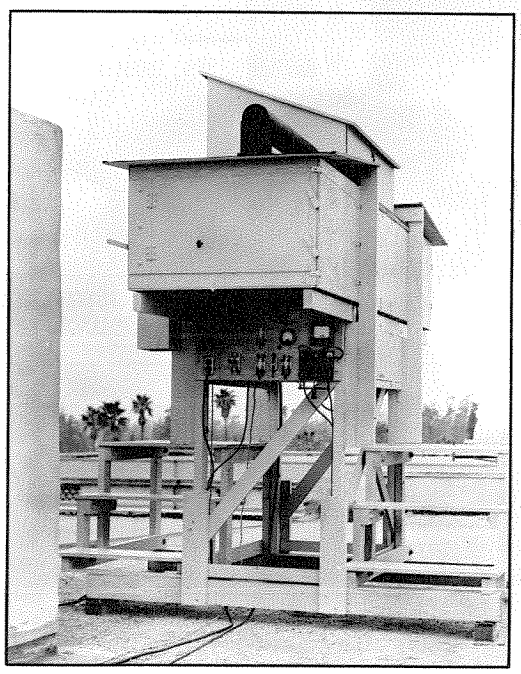

Fig. 37. FRONT VIEW. THE PANEL INCLUDES REMOTE CONTROLS FOR STATIONS "B" AND "C".

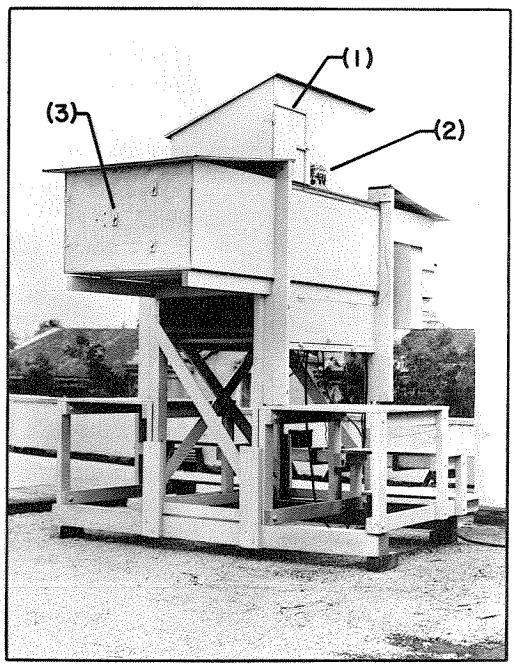

Fig. 38. REAR VIEW. (1) PORT FOR LOADING SPECTROGRAPH, (2) CONTROLS FOR SHUTTER AND SECTOR DISK, (3) ADJUSTMENTS FOR MIRRORS.

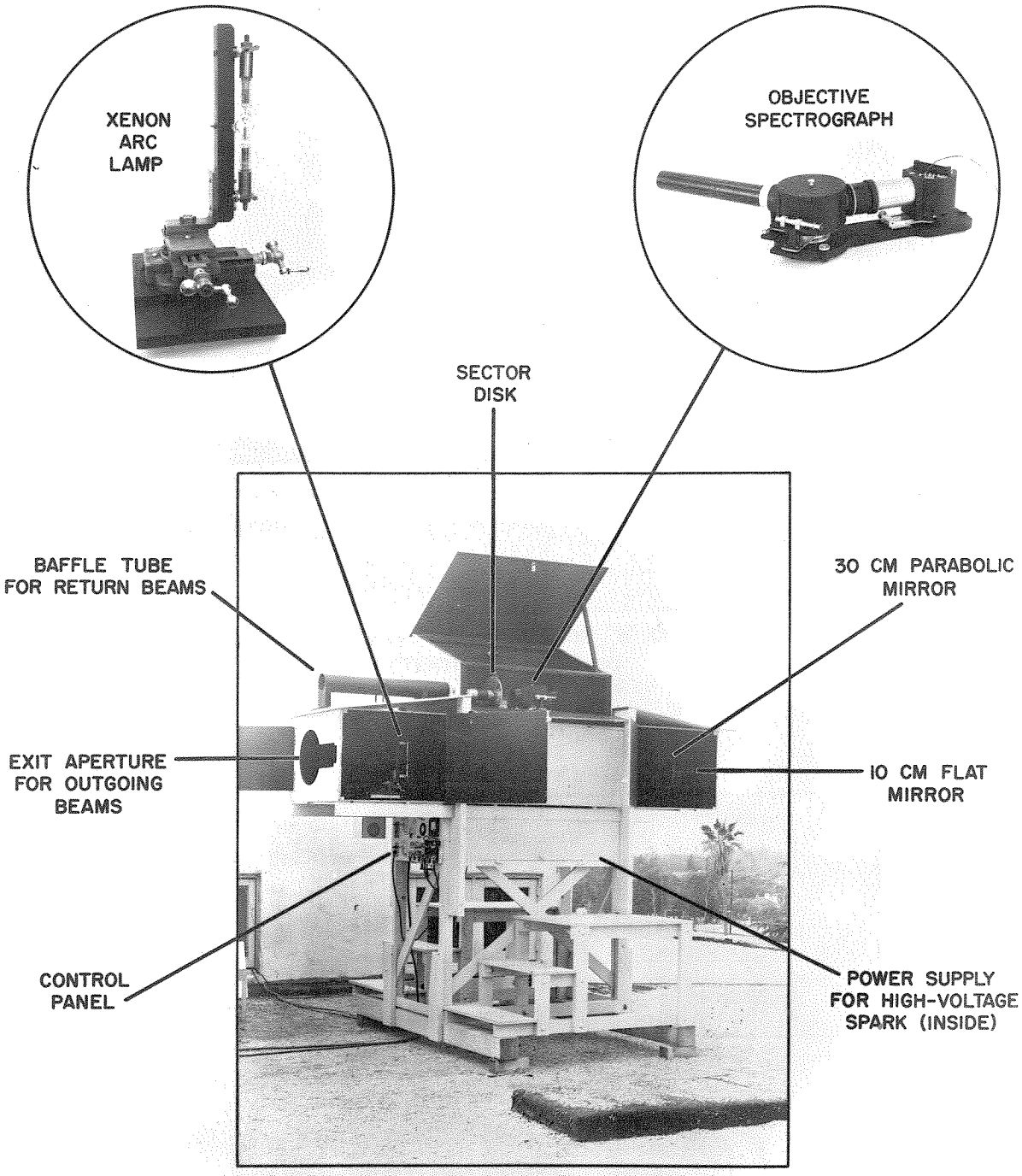

Fig. 39. APPARATUS AT STATION "A" (SEE Fig. 35.) ON TOP OF EAST BRIDGE LABORATORY.

Fig. 40. APPARATUS AT STATION "B" ON TOP OF THE HIGH-POTENTIAL LABORATORY.

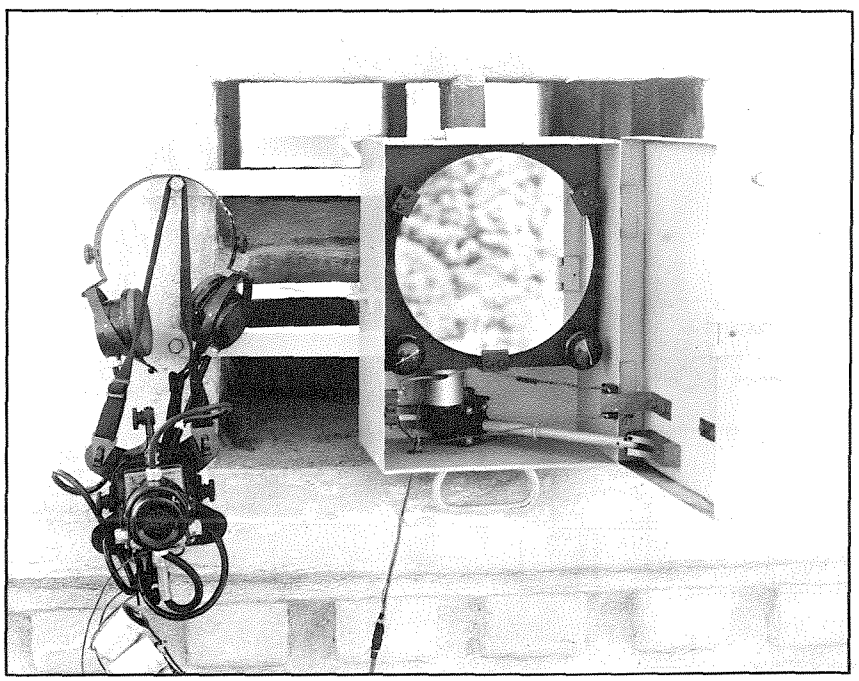

Fig. 41. APPARATUS AT STATION "C" ON ATHENAEUM CUPOLA.

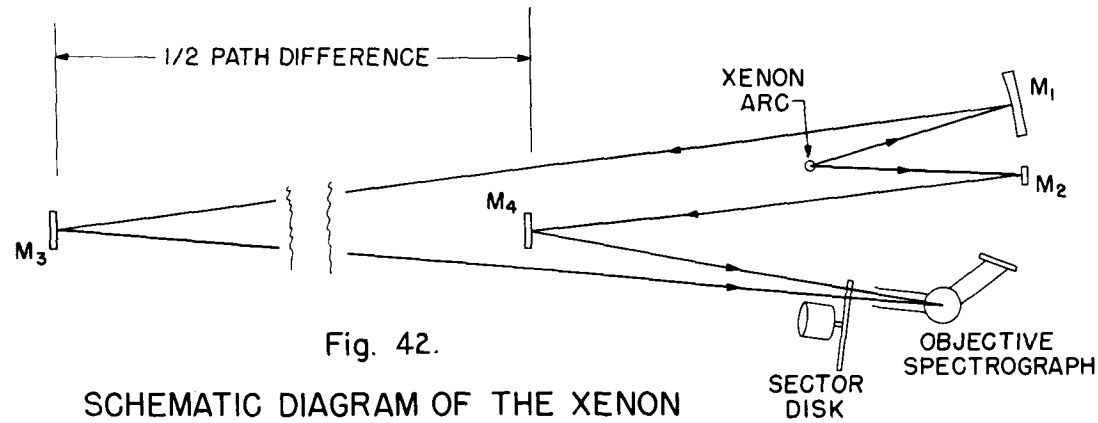

Fig. 42.

SCHEMATIC DIAGRAM OF THE XENON ARC SYSTEM FOR MEASURING ATMOSPHERIC U.V. ATTENUATION

(NOT TO SCALE)

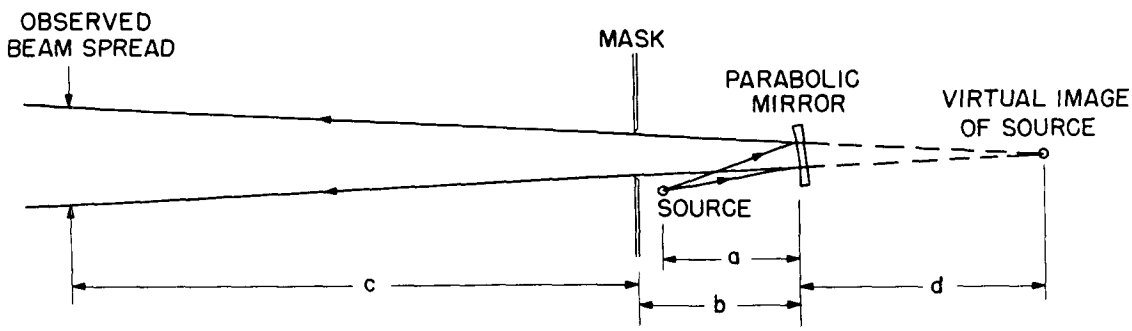

Fig. 43. MAGNIFICATION OF SOURCE IN PARABOLIC MIRROR

(NOT TO SCALE)

Fig. 44.

REMOTE CONTROL CIRCUIT FOR MIRROR BOXES

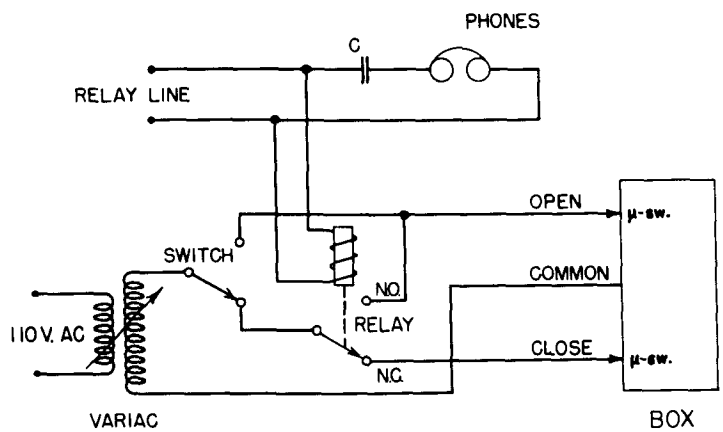

was made thinner than usual so as to avoid ultraviolet interference effects. Unfortunately, however, the mirrors were found to possess different spectral reflectances in the ultraviolet, and as a consequence it was necessary to apply spectrally dependent correction factors to the attenuation data.

When viewed from C, mirror M_1 formed a virtual image of the whole arc stream enlarged about 10 times; when viewed from B, mirror M_2 formed a virtual image of natural size. The lamp itself was obscured from direct view so that only these reflected images could be seen. Since the resulting ratio of virtual source diameters was roughly the same as the ratio of corresponding path lengths, the spectrograph received comparable amounts of light from the two paths. Figure 43 shows a simple geometrical method for determining the magnification due to M_1; it is valid because the size of the arc stream is small compared to other dimensions involved.

Path-folding mirrors M_3 and M_4 were actually in the same vertical plane as the spectrograph aperture, although to avoid confusion they are diagrammed differently in figure 42. Thus, the objective spectrograph simultaneously viewed two distant virtual "point sources", one about a half degree directly above the other, and each subtending 10 seconds of arc.

Neglecting back-scattering compared to forward-scattering, we may regard the apertures of the path-folding mirrors as source-cone diaphragms which prevent errors due to Middleton's scattering effect[19] discussed in Section II; for the long path (via M_3 at C) the source-cone was thus limited to less than 2 minutes of arc; for the short path (via M_4 at B) the distance was too small for scattering to be important.

As one might expect from geometry, the projected long-path source-cone attained a 16-inch diameter when it reached the spectrograph at A. The observed definiteness of the beam width was proof of the exceptional

flatness of M_3. Since centering this beam on the spectrograph aperture depended very critically upon the precision with which M_3 could be oriented, the adjustable support system for that mirror required kinematical design[77]. The glass disk was suitably mounted on a thick aluminum plate which was supported inside a steel housing at three widely spaced points, one being fixed and the other two being adjustable with micrometer screws. The fixed point was a ball-in-cone pivot, while the two micrometers pushed against retained steel balls, one of which rested in a groove and the other on a plane surface. The assembled mirror housing (see figure 41) was then clamped with heavy steel bars to the concrete Athenaeum cupola. With this rugged foundation and precise mechanism for adjusting M_3, the 16-inch disk of illumination at the spectrograph could be moved by distances as small as a half inch, corresponding to an orientation accuracy of 2 seconds of arc. Re-aiming of M_3 was required only after earthquake tremors.

Alignment of the other three mirrors was also important but much less critical than for M_3 at the Athenaeum. M_1 and M_2 were mounted on spring-loaded plates each held against three adjusting screws. The mounting base for M_4 was adapted from a small theodolite.

After passing through a long black baffle tube attached to the upper front of the structure at station A (see figures 36 and 37), the two return beams were chopped about 100 times per second just in front of the spectrograph. The chopper consisted of two identical 30% sector disks mounted face-to-face on the same shaft; by varying the angular phase of one relative to the other, openings of different sizes could be formed so as to produce a sequence of exposures. Dowel pins were inserted in the disks to permit accurately reproducible sector settings at 30%, 10%, 3%, and 1% openings. 100% was, of course, obtained with the sector disk stationary

and properly oriented. Two additional steps were added to the sequence by cutting the spectrograph aperture to 10% of its full width, and then repeating sector settings for 3% and 1%. Thus the complete sequence consisted of seven logarithmically distributed exposures starting at 100% and extending down to 0.1% in relative value. As already pointed out at the end of Section III, the foregoing method for varying exposures was correct, but changing the duration of exposures would not have been.

The objective quartz spectrograph and some of its parts are shown in figures 45 through 48. The instrument was constructed mostly of aluminum and was patterned somewhat after the one described by Chalonge and Vassy[78].

Figure 49 is a schematic diagram of the spectrograph optical system. Nearly parallel light from the two distant source images was incident upon a 60° quartz Cornu prism of 40 mm height. Just behind the prism was a plano-convex singlet quartz lens with a diameter of 50 mm and a nominal focal length of 500 mm. By orienting this lens as shown in the figure, one can introduce astigmatism so that the spectrum of a point source is not stigmatic. If the photographic plate or film is placed at the loci of primary astigmatic images for various wavelengths, the resulting spectrum has nearly the appearance of a spectrum formed by an ordinary slit spectrograph except that the height of the spectrum in this case is tapered (see figure 65). The dispersion curve is given in figure 50 and may be fitted algebraically by

$$X = K_1 \lambda^{-4} + K_2 \lambda^{-2} + K_3 \lambda^{0} + K_4 \lambda^{2} \qquad (17)$$

where $K_1 = -0.0243$
$K_2 = -2.56$
$K_3 = +45.35$
$K_4 = +5.1$

for λ in microns and X in millimeters.

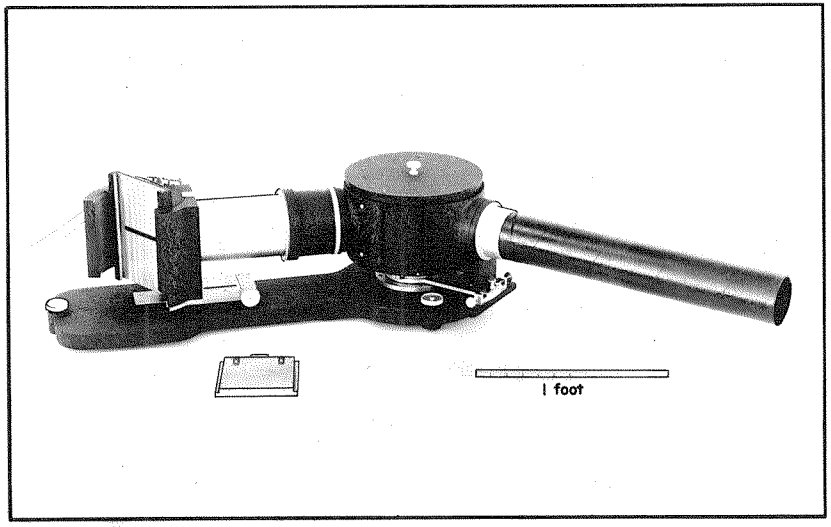

Fig. 45. QUARTZ OBJECTIVE SPECTROGRAPH.

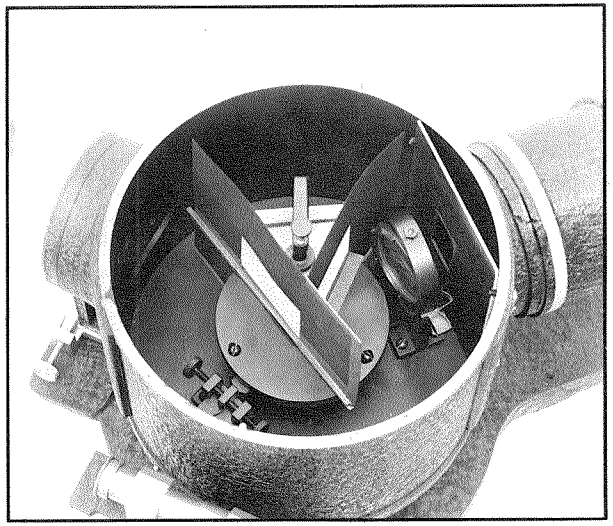

Fig. 46. QUARTZ PRISM AND LENS.

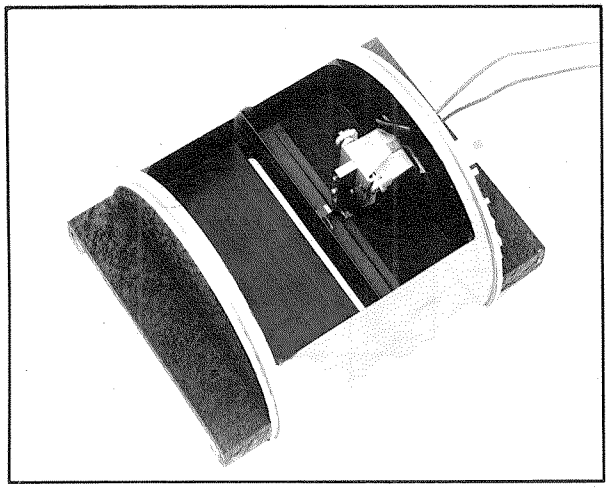

Fig. 47. ELECTRICALLY-OPERATED SHUTTER.

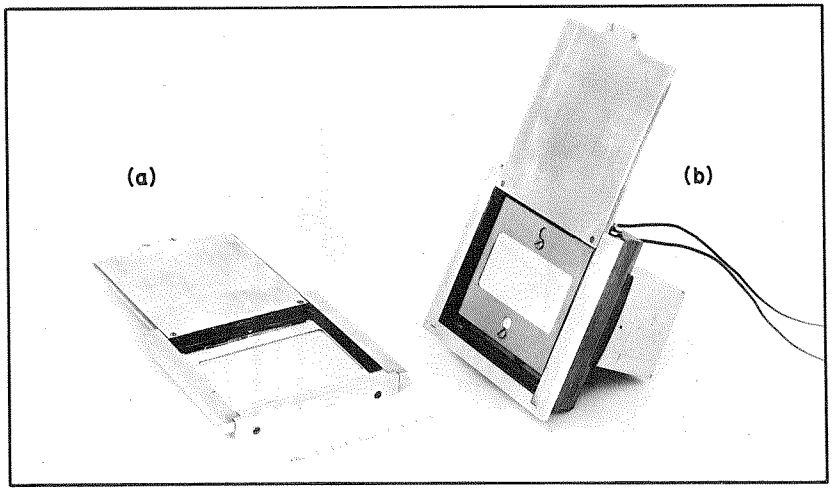

Fig. 48. FILM HOLDERS: (a) PLAIN, (b) VIBRATED.

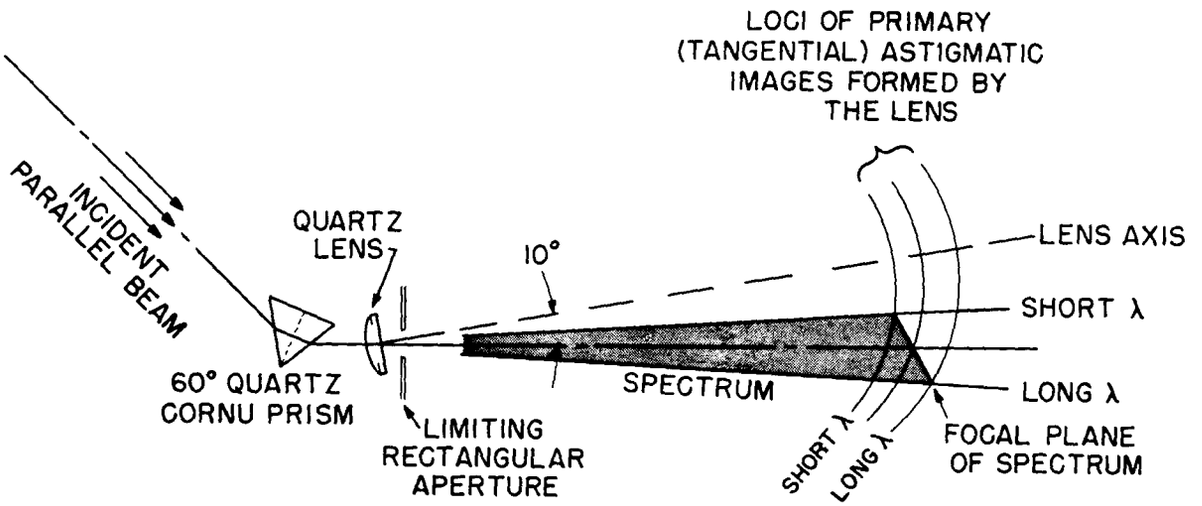

Fig. 49. OPTICS OF THE OBJECTIVE SPECTROGRAPH

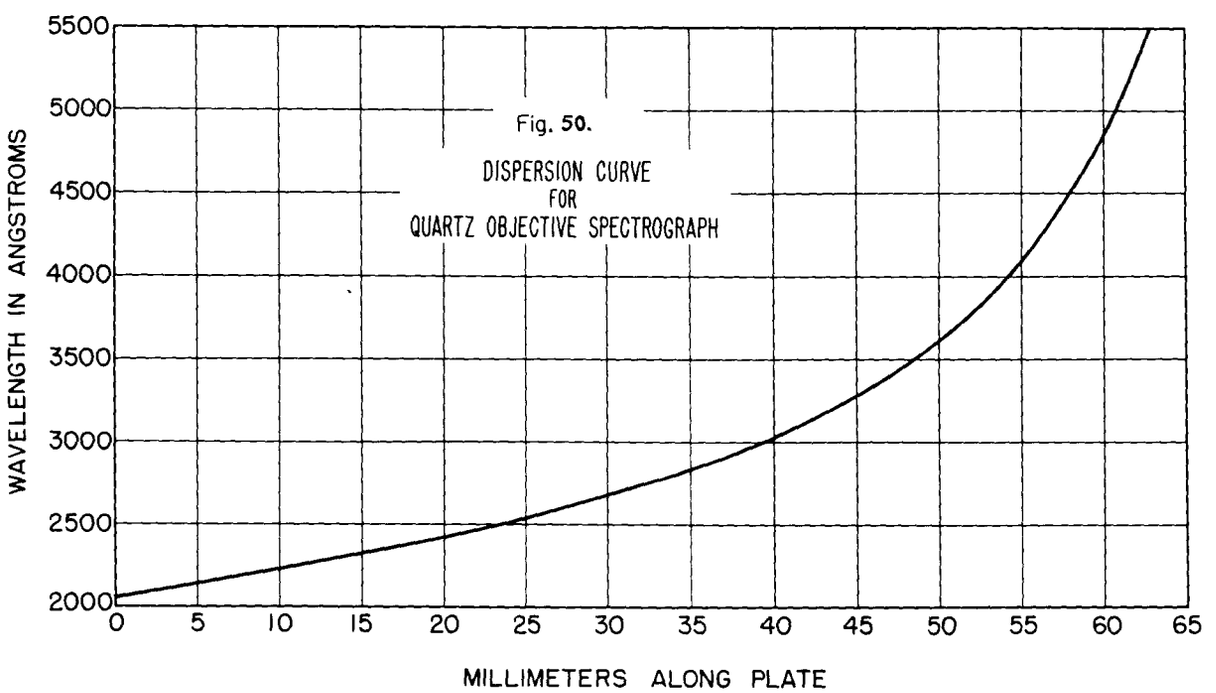

The limiting aperture of the spectrograph was a carefully machined stop, 20.30 mm wide by 32.85 mm high, located just behind the lens. Its rectangular shape resulted in approximately uniform density over the astigmatic height of the spectrum (see figure 66). For reducing the aperture to extend the exposure sequence, a sliding plate carrying a 2.03 mm slot was inserted into the aperture stop. By cutting the width but preserving the height of the aperture, one finds no change in the astigmatic spectrum except a uniform reduction of exposure. Since diffraction by the slot was scarcely detectable, its effect on attenuation data could safely be neglected. A ten-times reduction in exposure by insertion of the slot was found experimentally to agree well with a corresponding ten-times reduction by the sector disk.

Most of the atmospheric ultraviolet attenuation spectra were photographed on 3 1/4" x 4" pieces of Eastman 103-O film having a black anhalation backing and an ultraviolet-sensitive (fluorescent) front coating. For higher resolution, a few spectra were also photographed on 3 1/4" x 4" Eastman lantern slide plates.

Since it was found that a 100% exposure (i.e., unchopped) for 10 seconds on 103-O film produced spectra as dense as could comfortably be used, that amount of exposure was appropriate for the maximum of the sequence. Heavier exposures would have introduced excessive fogging, while lighter exposures (for 100%) would have lost some of the shorter wavelengths around 2300A. A sequence of seven 10-second exposures was ideally suited to the present experiment, because its duration was short enough to obviate difficulties due to variations in local meteorological conditions but also long enough to integrate variations due to atmospheric "boil"[79]. However, in order to time such short intervals (i.e., 10

seconds) with accuracy, it was necessary to equip the spectrograph with a rapid electric shutter (figure 47) operated in series with an electric timer; in this manner, timing errors were held to ±0.5%.

In order to promote consistency in the results and avoid mistakes, routine procedures were adopted for operating the arc, manipulating the remote controls, checking alignment of the optical system, making the sequence of exposures, and developing the negative under controlled conditions.

The darkroom for developing the spectrograms was equipped with a large Wratten Series 2 red safelight, an electric sweep-second clock with a red light on its face, and a pair of flashlights fitted with Wratten No. 25 red photographic filters; it was found that 103-O film could safely be handled under appreciable illumination from such sources. Small stainless-steel trays were provided for cyclohexane, developer, hypo, sodium sulfite, and wetting agent. The developer tray was mounted in a cooling tank fed by a flow of cold tap water (sometimes ice water in warm weather) regulated to maintain the developer at 68°F ± 0.5°F.

The procedure of development was as follows: first the negative was washed in cyclohexane to remove the fluorescent front-coating. After drying, it was rinsed in fresh cyclohexane and dried again. The negative was then clipped to a small lucite plaque and developed in D-19 for exactly 4.0 minutes, during which time a camels-hair brush was passed continuously over it to insure uniformity of development and to minimize the Eberhard effect[66]. Immediately at the end of development the negative was plunged into acid hypo which served both as short-stop and fixer. After ten minutes it was removed from the plaque, rinsed, and placed in a 10% solution of sodium sulfite for about a minute to loosen the black backing.

The negative was then washed thoroughly, inspected carefully for flaws, dipped in a wetting agent, and hung up to dry under 8 grams tension. The wetting agent was found to be more effective than distilled water for preventing the spotty deposition of water residue during drying.

The procedure for analyzing these spectrograms will be outlined in Section VII.

VI. AUXILIARY EXPERIMENTS

Three independent auxiliary experiments were conducted to corroborate ultraviolet attenuation data obtained from the xenon arc apparatus described in the preceding section. These were:

(A) Ultraviolet measurements using a portable hydrogen arc.

(B) Haze-meter readings at 5500A.

(C) Cadmium photocell data at 2537A.

The first of these yielded spectrally continuous attenuation data over the same region covered by the xenon arc system, while the other two each provided a single check-point at one wavelength.

(A) A PORTABLE HYDROGEN ARC and its power supply were used in conjunction with the objective quartz spectrograph and the light-chopper; sequences of spectra very similar to those produced by the xenon arc were obtained. In this case, however, the source was carried to two locations as shown in figure 51 so that the spectral reflectances of mirrors were not involved. From geometry alone, the photometric data could be reduced directly without correction to absolute attenuation coefficients. Because of this simplification of analysis as well as the associated improvement in accuracy, the portable-source method had much to recommend it. On the other hand, it required two or three persons instead of one to produce each spectrogram, and it also required stable air conditions to accommodate the much longer exposures involved. As a consequence, the hydrogen arc was used on only a few of the many nights when attenuation was measured. Moreover, each hydrogen arc spectrogram also included a routine sequence of xenon arc spectra, so that the desired spectral corrections for the xenon arc apparatus could be determined.

Hydrogen arc lamps of high output have been described by Lawrence and Edlefson[80] and by Kistiakowsky[81]. A more portable type having moderate

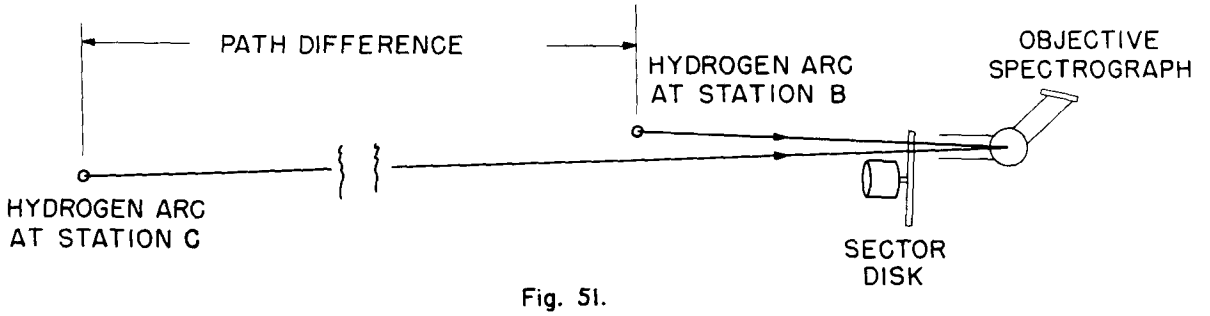

Fig. 51.

SCHEMATIC DIAGRAM OF THE HYDROGEN ARC SYSTEM FOR MEASURING ATMOSPHERIC U.V. ATTENUATION

(NOT TO SCALE)

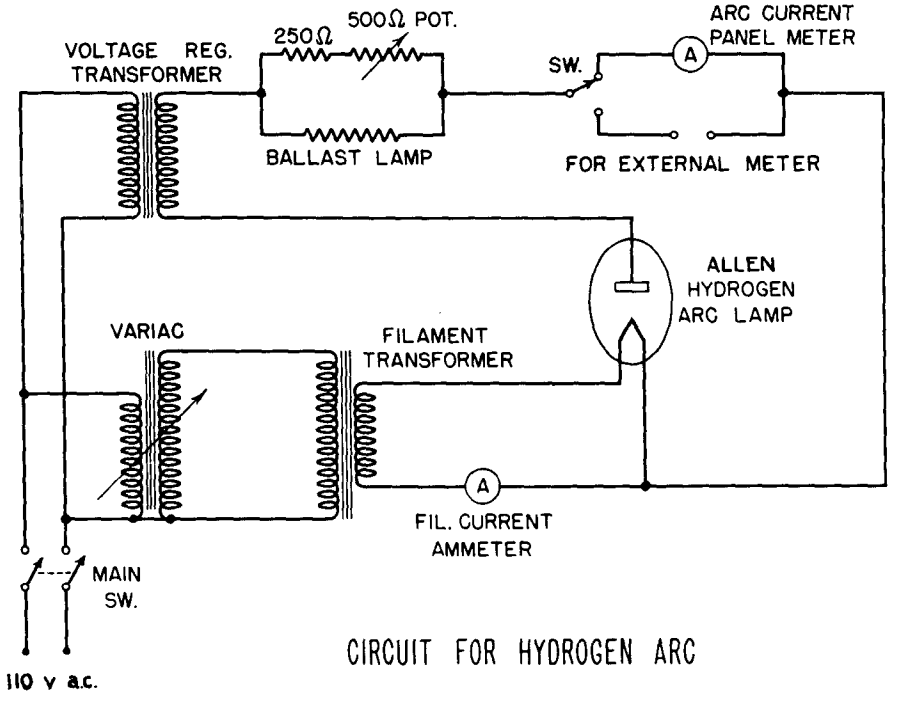

CIRCUIT FOR HYDROGEN ARC

Fig. 52.

output and operating on low voltage has been described by Allen and Franklin[74]. From its spectral radiance curve in figure 34 one can see that the Allen lamp is quite weak compared to the xenon arc. Nevertheless, its power requirements could be more easily provided in a portable system than could those of other ultraviolet continuum sources (especially the xenon arc); hence, it was selected for this experiment.

Figure 52 is a circuit diagram of the power supply for the Allen hydrogen lamp. A 12-ampere filament current at 3 volts was applied for about a minute to start the arc; this current was then turned off, and the arc maintained itself indefinitely on 110 volts a.c. in series with a ballast. The anode current, initially set at 1.25 amperes, was found to be exceptionally steady; a high-resistance rheostat in parallel with the main ballast easily compensated for any drift. The potential drop across the arc itself was 40 volts, implying a power input to the lamp of 50 watts.

Figure 53 is a photograph of the Allen lamp as mounted for this experiment. In use it was simply hung on the fronts of the mirror housings at stations B and C. The power supply shown in figure 54 was plugged into 110 volt a.c. lines already installed at those stations. A mere trickle of cooling water siphoned from glass jugs at the rate of four gallons per hour was found to be adequate.

Exposures of 1000 seconds each were required to produce usable densities on the spectrograms. Since only one hydrogen arc was used, the spectra had to be photographed individually rather than in simultaneous pairs. Sector percentages used for the abbreviated exposure sequence were: 0.3, 1, 3, and 10 for the short path; 30 and 100 for the long path. The 1% short path exposure was roughly comparable to the 100% long path exposure. Fogging of the film by scattered light was similar in extent

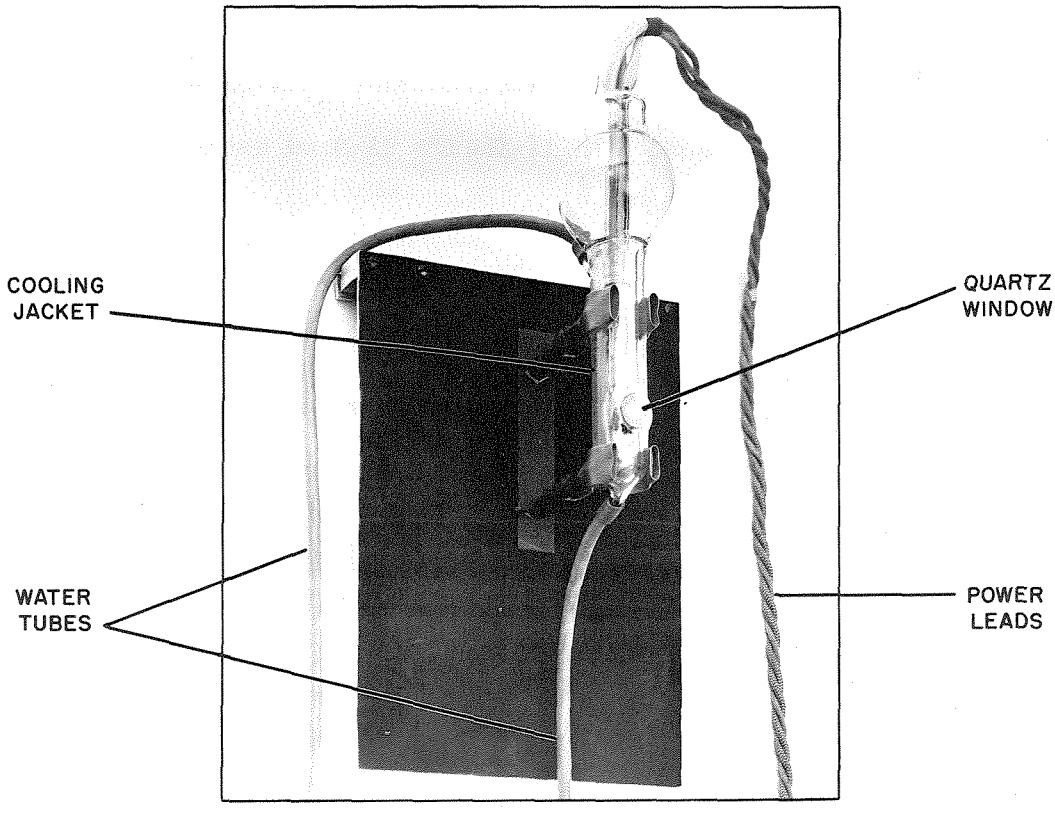

Fig. 53. THE ALLEN HYDROGEN ARC.

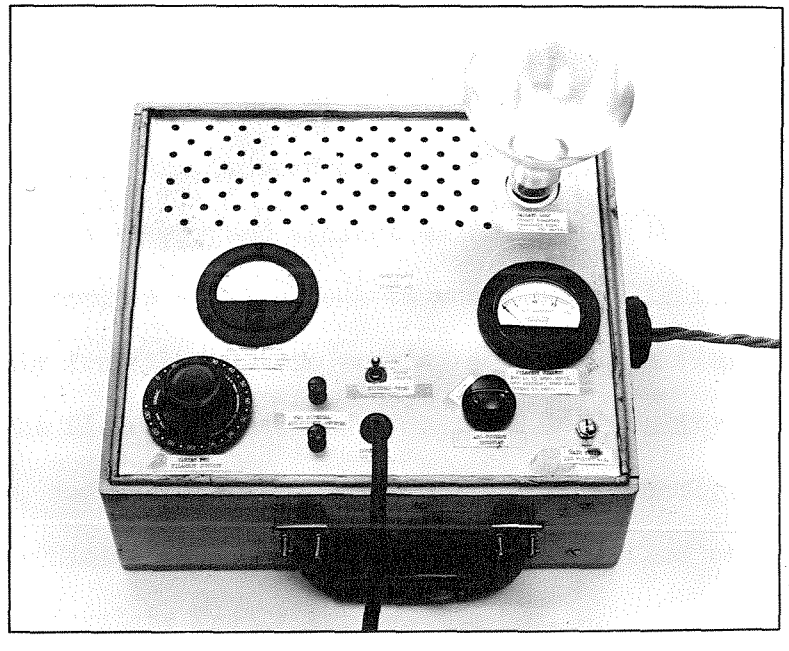

Fig. 54. PORTABLE POWER SUPPLY FOR HYDROGEN ARC.

to that found on the xenon arc spectra; however, in this case more of it was caused by extraneous sources and less of it by scattered hydrogen arc radiation. For exposures substantially longer than 1000 seconds, fogging by extraneous sources such as street lights would have become undesirably important.

(B) HAZE-METER READINGS AT 5500A were obtained using a British Admiralty instrument known as a Loofah. Figure 55 is a photograph of the Loofah used in this experiment, and figure 56 shows its internal construction. The optical system is entirely self-contained, having no light path external to the box.

Light from a 24-volt Siemens projection lamp is formed into an intense diffuse beam, which passes lengthwise through the box. Along the beam a very small part of this light is scattered to various angles by the air through which it passes. As mentioned in Section II, if one assumes absorption negligible compared to scattering (a reasonable assumption for the visible spectrum), then the total attenuation can be related to the amount of light scattered. In this case, scattering is measured by observing the apparent brightness of a certain segment of the beam viewed obliquely at 30° from the forward direction. A light trap or "black hole" provides a suitable background against which to view this field of scattered radiation. A small amount of unscattered light is also extracted directly from the beam to provide a comparison field for visual photometry. The fields are matched by adjusting a density wedge in the comparison arm, and wedge settings are calibrated directly in terms of attenuation coefficient for the air in the box. Baffled vents permit outside air to circulate freely through the box.

Since coefficients measured by the Loofah represent an effective

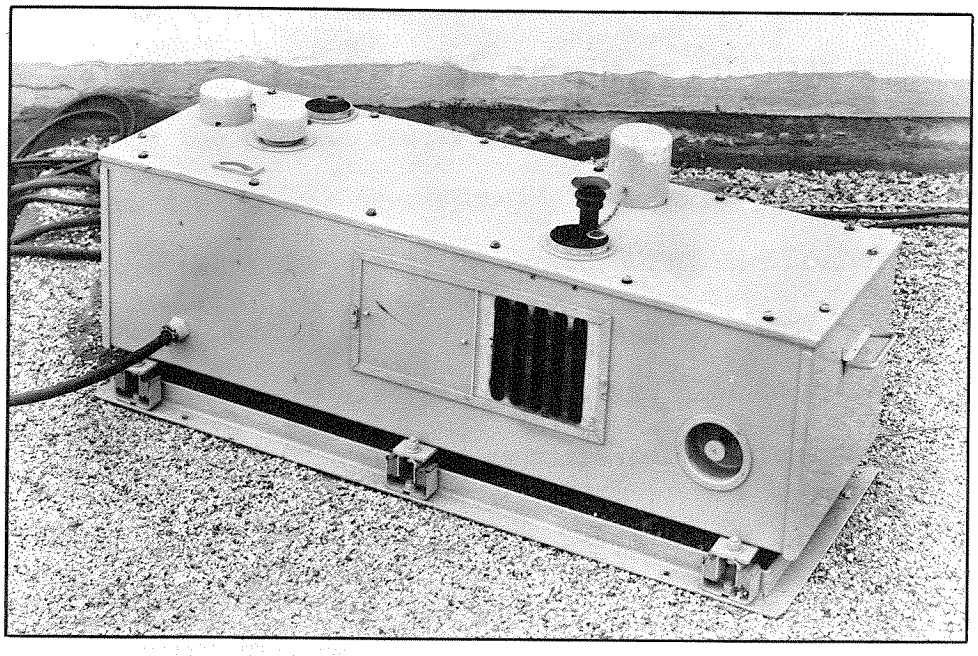

Fig. 55. LOOFAH (BRITISH ADMIRALTY HAZE-METER)

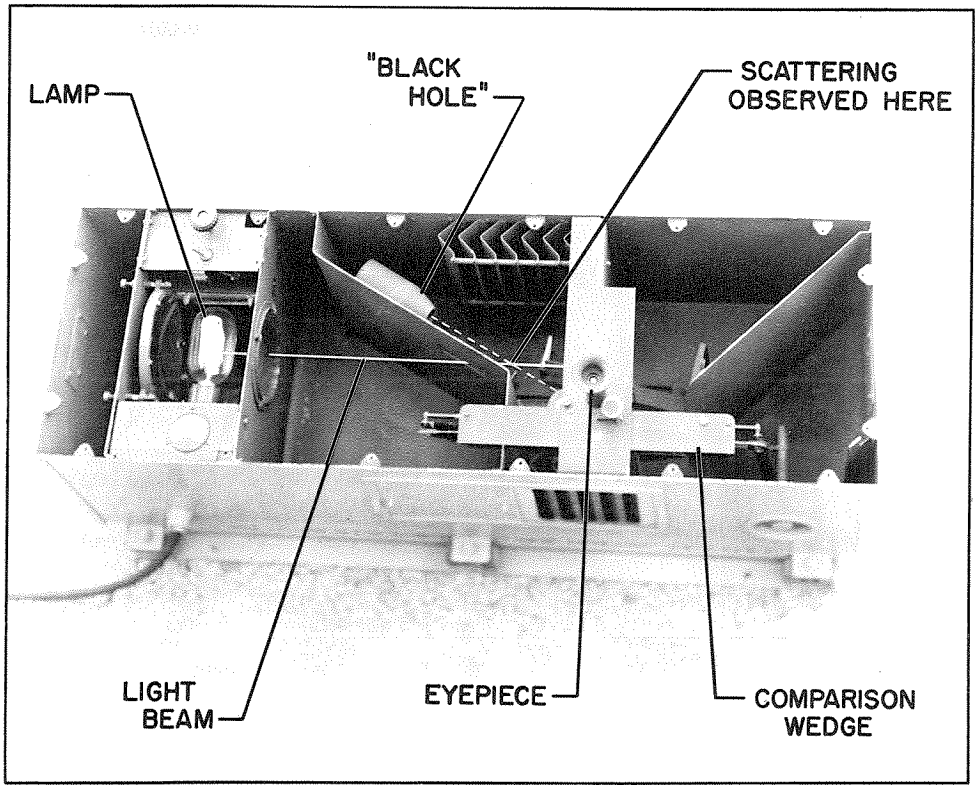

Fig. 56. LOOFAH WITH COVER REMOVED. LENGTH = 43 INCHES.

average for the integrated visible spectrum, we may assign these data to 5500A[10], and then use the Linke-Borne formula to establish approximate values of σ across the visible spectrum. (See Section II.) This visible σ-vs-λ curve should match the corresponding ultraviolet curve both in ordinate and slope where the two join; consequently, the Loofah was a convenient monitoring device for the ultraviolet experiment. Of course, the Loofah coefficients were also put in equation (16) to yield visibility ranges for tagging the air samples whose ultraviolet attenuation curves were measured.

(C) CADMIUM PHOTOCELL DATA AT 2537A provided another useful check on the xenon arc system. This monitoring experiment required no spectrograph or filters; it involved only a mercury vapor light source and a cadmium photocell receiver.

The source was an array of twelve General Electric slim-line germicidal mercury lamps mounted on the penthouse of West Bridge Laboratory as shown in figures 57 and 58. These lamps were 30 inches long and 3/4 inch in diameter; their envelopes were corex glass (which transmits 2537A well), and they contained mercury at a very low pressure. Each lamp consumed 30 watts of input power and emitted about 10 watts in the germicidal region of which over 99% was at 2537A.

A cadmium photocell receiver of the type described by Haynes and Taylor[82] was modified to give greater sensitivity and improved stability. The circuit employed a Victoreen VX-41A electrometer tube and various high resistances up to 10^{10} ohms. Its response extended from about 2100A to 2900A with maximum sensitivity around 2500A. When used in conjunction with the mercury lamp array, this receiver measured monochromatic intensities at 2537A.

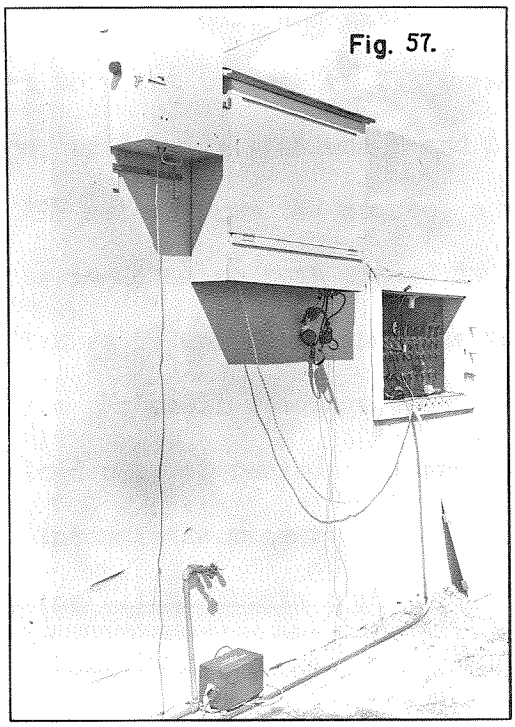

Fig. 57.

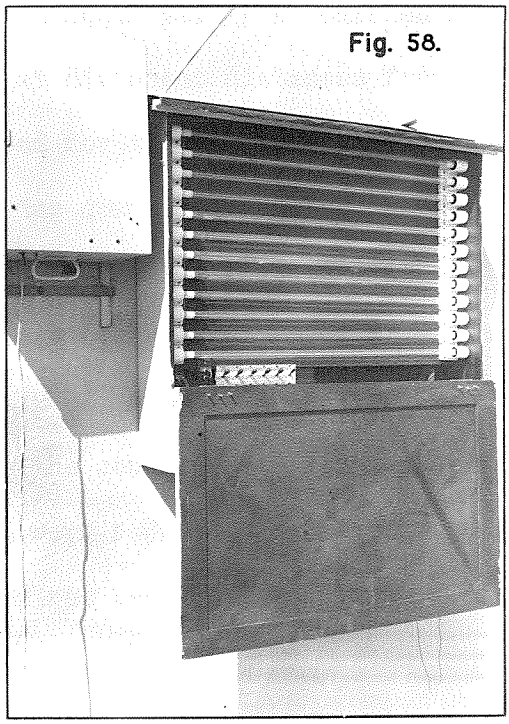

Fig. 58.

GERMICIDAL SLIM-LINE Hg LAMP ARRAY MOUNTED ON WEST BRIDGE LAB.

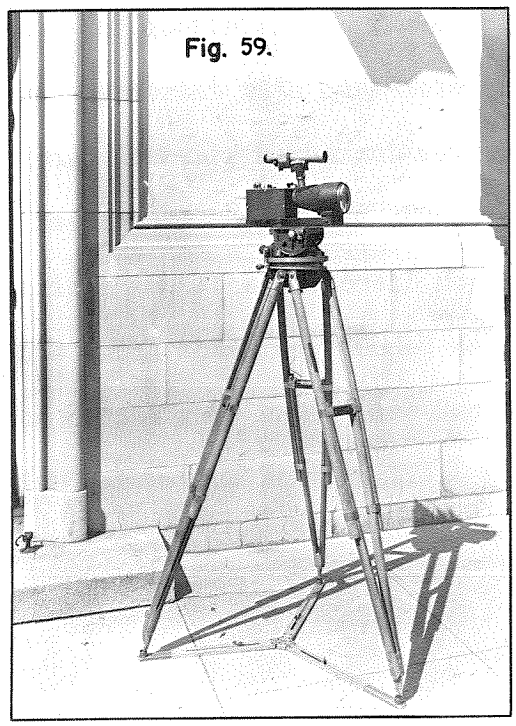

Fig. 59.

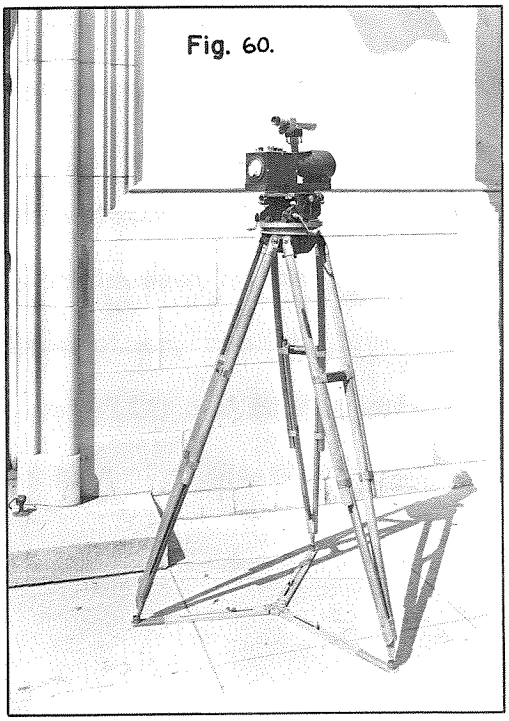

Fig. 60.

CADMIUM PHOTOCELL APPARATUS FOR MEASURING GERMICIDAL RADIATION.

Since the unit was battery operated, it could easily be carried from point to point to measure 2537A radiation at different distances from the lamps; ordinarily stations B and C were used for this purpose. At C, which was 419 meters from the source, a crystalline quartz collecting lens, 4 inches in diameter, was placed in front of the cadmium photocell as shown in figures 59 and 60 to increase the sensitivity by a factor of 11. Since cadmium photocell readings required the help of an assistant, they were obtained only at periodic intervals during the course of this investigation.

Intensities measured by the photocell were reduced very simply by equation (1) to obtain σ at 2537; A dropped out because I was known for two values of x.

All three independent auxiliary experiments which have just been described gave absolute coefficients directly; hence, they were used primarily to calibrate the xenon arc apparatus and to monitor the constancy of that calibration. It was also informative to check them against one another for consistency. The hydrogen arc system was found to be in excellent agreement with haze-meter readings extrapolated by the Linke-Borne formula. However, agreement between hydrogen arc data and cadmium photocell readings at 2537A was somewhat less satisfactory. There is reason to believe that the photocell may have been influenced by two opposite effects which sometimes tended to cancel one another, namely, interference by the Herzberg O_2 bands (see Sections VII and VIII) and Middleton's field-of-view error (see Section II). A further study of these effects is planned[16].

VII. ANALYSIS OF SPECTRA

Spectra produced by both the xenon arc and the hydrogen arc systems were reduced to atmospheric attenuation coefficients by the usual procedures of photographic spectrophotometry. In addition, corrections were applied for photographic fogging due to scattered light, for astigmatic differences introduced by the objective spectrograph, and for spectral dissimilarity of mirror reflectances in the xenon arc system.

Typical sequences of xenon arc spectra are reproduced in figures 61 and 62. Sequences for both the xenon arc and the hydrogen arc are combined in figure 63; it was in this manner that the two systems were compared to derive corrections for mirror reflectances. In all three figures, the long-path spectra (see sequence diagram in figure 65) show the weak Herzberg O_2 bands around 2500A. These bands, shown enlarged in figure 64, have been discussed in Section II (D). They were the only lines or bands found in atmospheric attenuation spectra between 2300A and 4600A.

The spectrograms were analyzed with a modified Leeds and Northrup microdensitometer connected to a Leeds and Northrup Speedomax pen-recorder. Figures 67 and 68 are photographs of this equipment. Modifications to the microdensitometer included the addition of a 100-watt d.c. ribbon filament lamp, a ballast arrangement for accurate regulation of the lamp current, and a device for manipulating neutral filters in the densitometer beam. With these modifications, the usefulness of the instrument was extended from a former range of about 2 density units (100 to 1 transmission ratio) to a new range of 3 units or more (1000 to 1 transmission ratio). Although the response of the equipment was linear with transmission of the photographic emulsion, the recording paper was ruled non-linearly to read directly in density units.

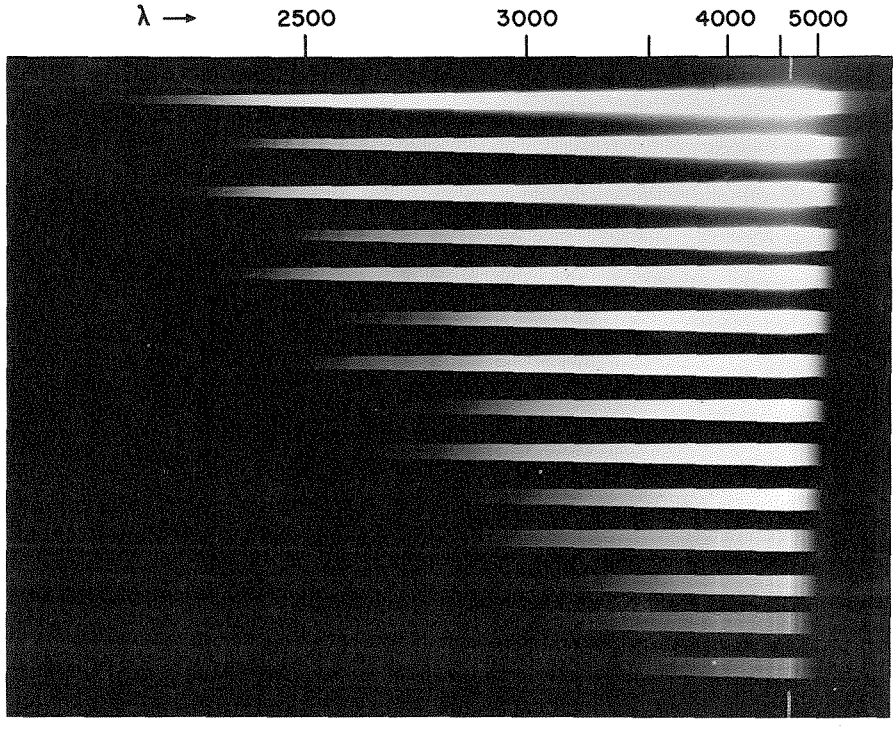

Fig. 61. XENON ARC SPECTRA FOR TYPICAL CLEAR ATMOSPHERE.
DATE = AUGUST 22, 1949. ESTIMATED VISIBILITY = 100 KM.

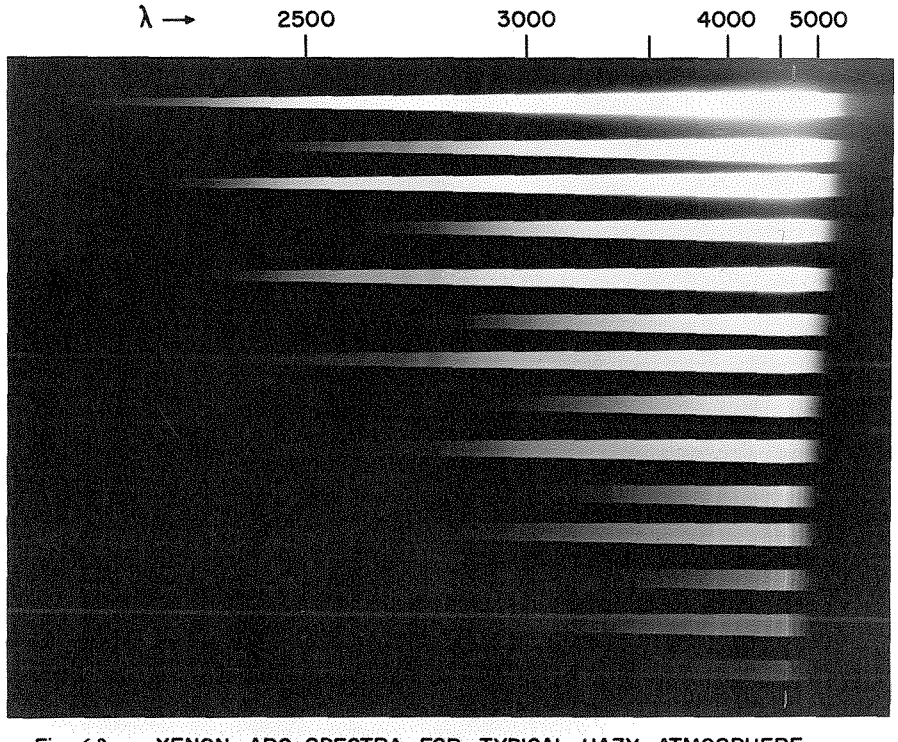

Fig. 62. XENON ARC SPECTRA FOR TYPICAL HAZY ATMOSPHERE.
DATE = JULY 1, 1949. ESTIMATED VISIBILITY = 4 KM.

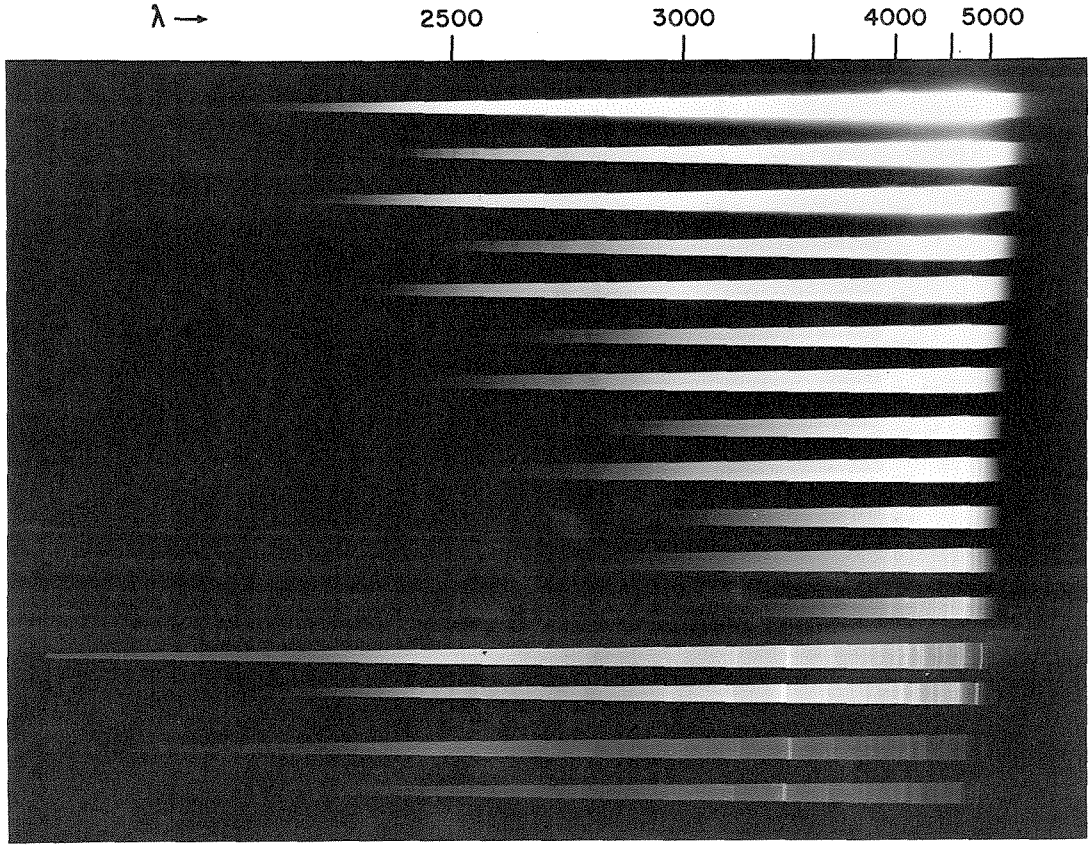

Fig. 63. XENON ARC SPECTRA (UPPER TWELVE) AND HYDROGEN ARC SPECTRA (LOWER FOUR) FOR SEPTEMBER 2, 1949. Fig. 61, Fig. 62, AND THIS ONE ARE ABOUT DOUBLE SIZE.

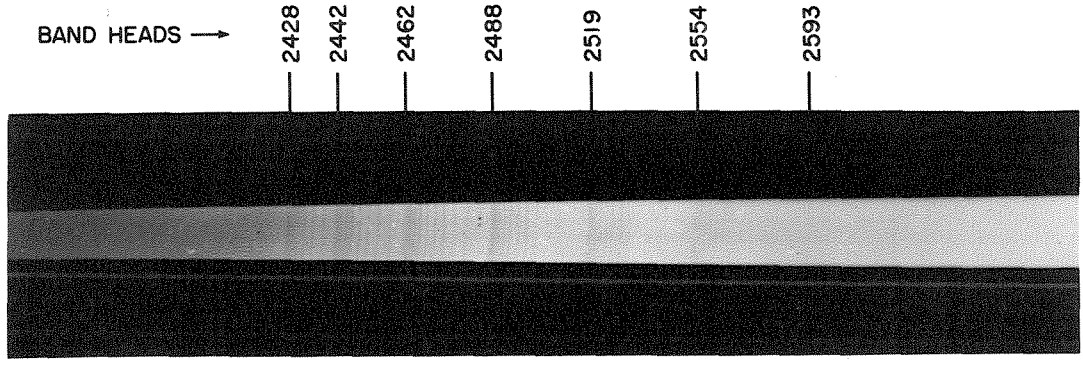

Fig. 64. HERZBERG O_2 BANDS ENLARGED ABOUT TEN TIMES.

Fig. 65. PATTERN OF SPECTROGRAMS MADE WITH THE XENON ARC SYSTEM

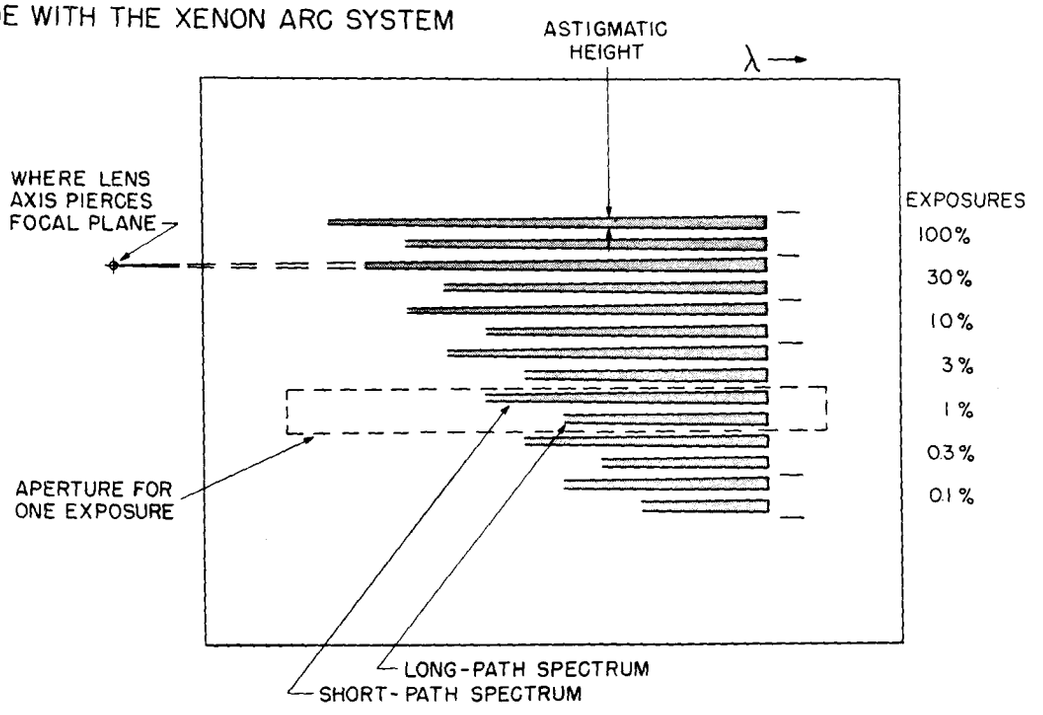

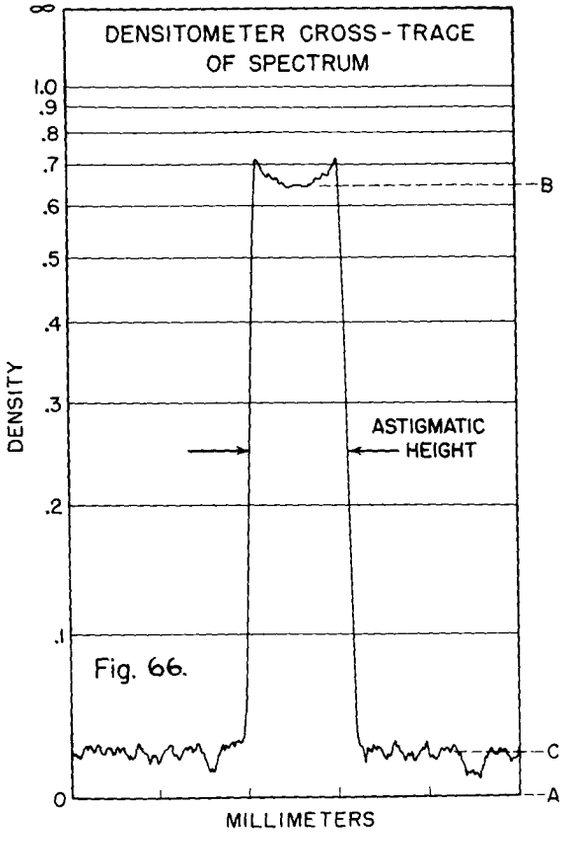

Fig. 66.

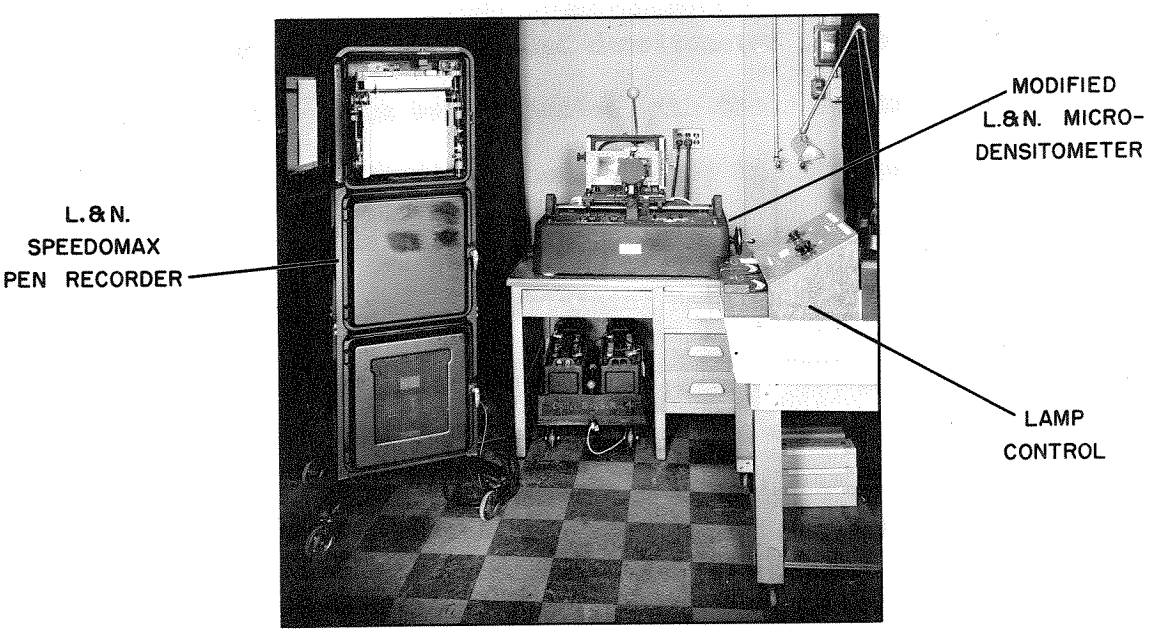

Fig. 67. APPARATUS FOR ANALYZING SPECTRA

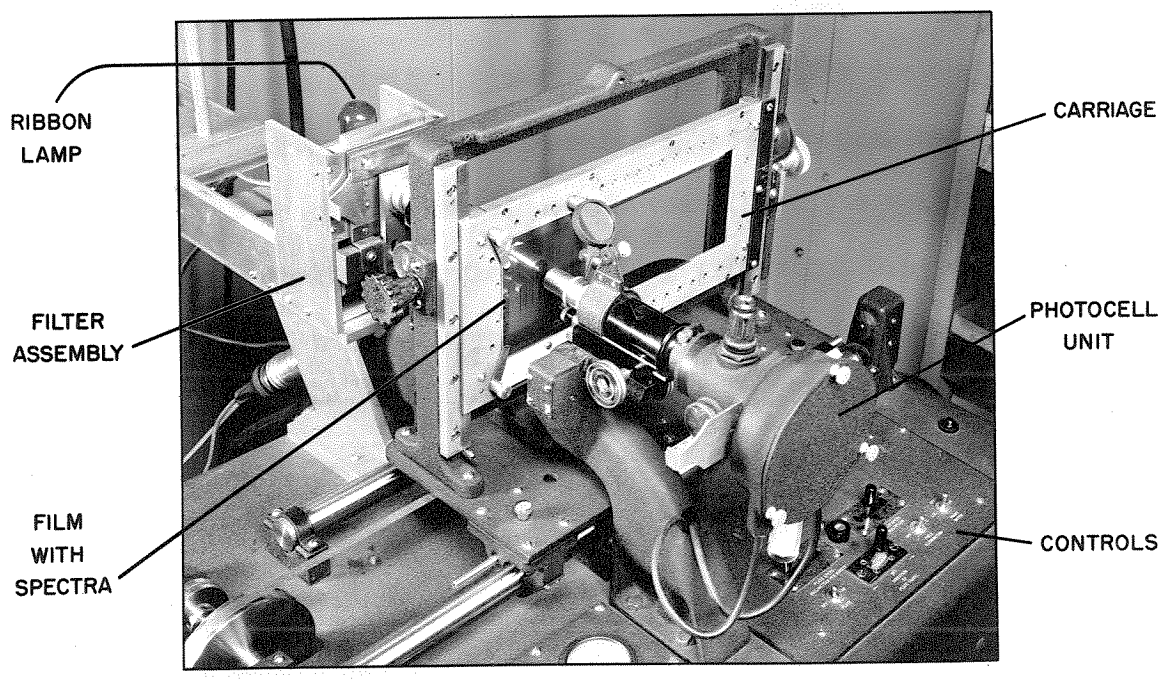

Fig. 68. CLOSE-UP OF MICRODENSITOMETER

Spectrograms on film were sandwiched between lantern-slide coverglasses and were mounted on the microdensitometer plate carriage as shown in figure 68. For obtaining detailed densitometer traces at all wavelengths, some of the films were oriented with their spectra parallel to the travel of the carriage (i.e., horizontal); in this case, the slit image formed on the emulsion by the condensing microscope was ordinarily 0.05 mm by 0.5 mm. However, for obtaining data at a selected group of wavelengths, most of the films were oriented with their spectra vertical; the slit image was then about 0.2 mm square. In either case, densities were always measured at the centers of the astigmatic wedges, because, as seen in figure 66, the average density for any position off center would be slightly different.

H. & D. curves for a typical xenon arc spectrogram on Eastman 103-0 film are shown in figure 69. The relative lateral displacements of these curves for various wavelengths has no particular significance with respect to spectral film sensitivity, because other spectrally dependent quantities are involved. However, this short-coming is of no consequence here, because only the shapes of individual curves affect the analysis. Each curve has a long straight portion extending from about 0.5 to 2.5 in density. The slope of this straight portion, known as the "gamma" of the emulsion, is quite dependent on wavelength in the ultraviolet as indicated by figure 70; the data for 1000-second exposures were obtained from a hydrogen arc sequence.

During development, γ increases approximately according to the exponential law of simple chemical reactions:

$$\gamma = \gamma_\infty(1 - e^{-kt}) \tag{18}$$

where γ_∞ is a limiting value for a particular emulsion, and k is dependent

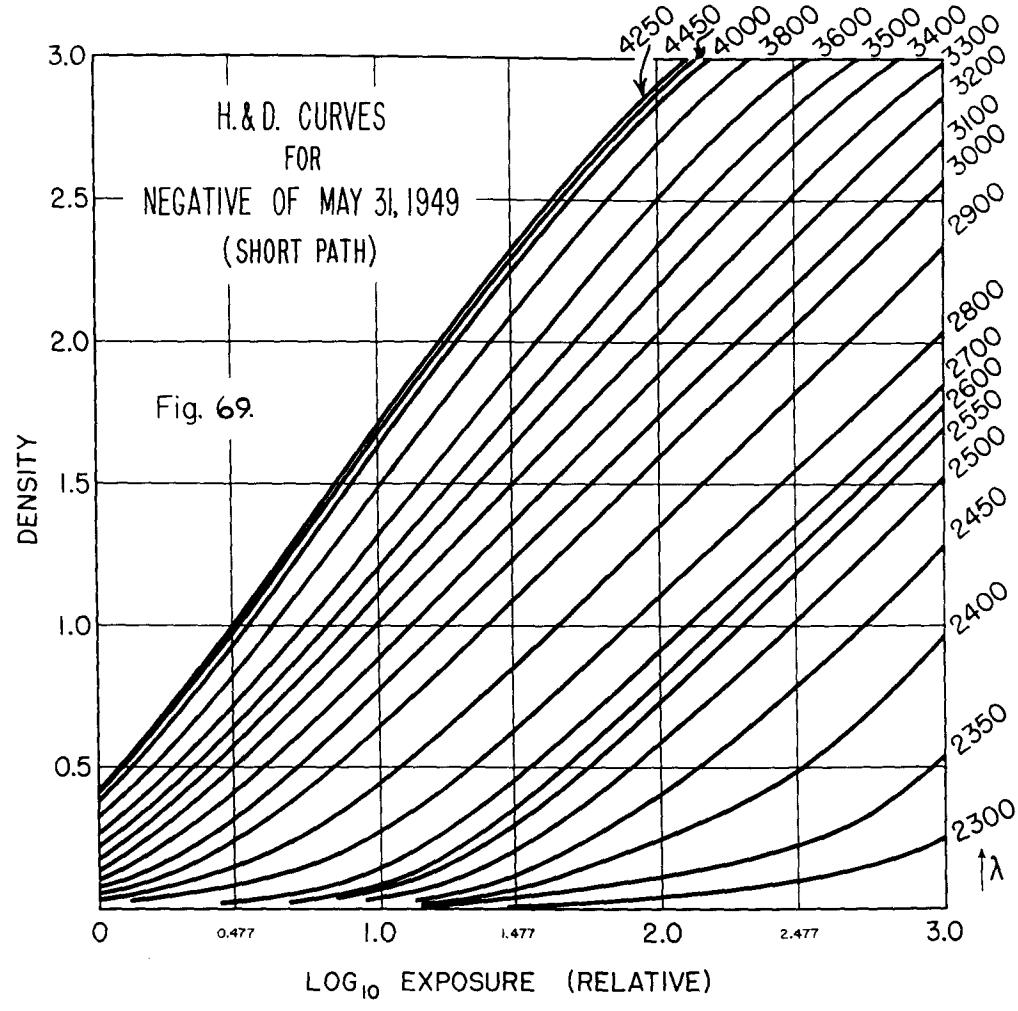
H. & D. CURVES
FOR
NEGATIVE OF MAY 31, 1949
(SHORT PATH)
Fig. 69.
DENSITY
3.0
2.5
2.0
1.5
1.0
0.5
0
0.477
1.0
1.477
2.0
2.477
3.0
LOG10 EXPOSURE (RELATIVE)
4250
4450
4000
3800
3600
3500
3400
3300
3200
3100
3000
2900
2800
2700
2600
2550
2500
2450
2400
2350
2300
λ

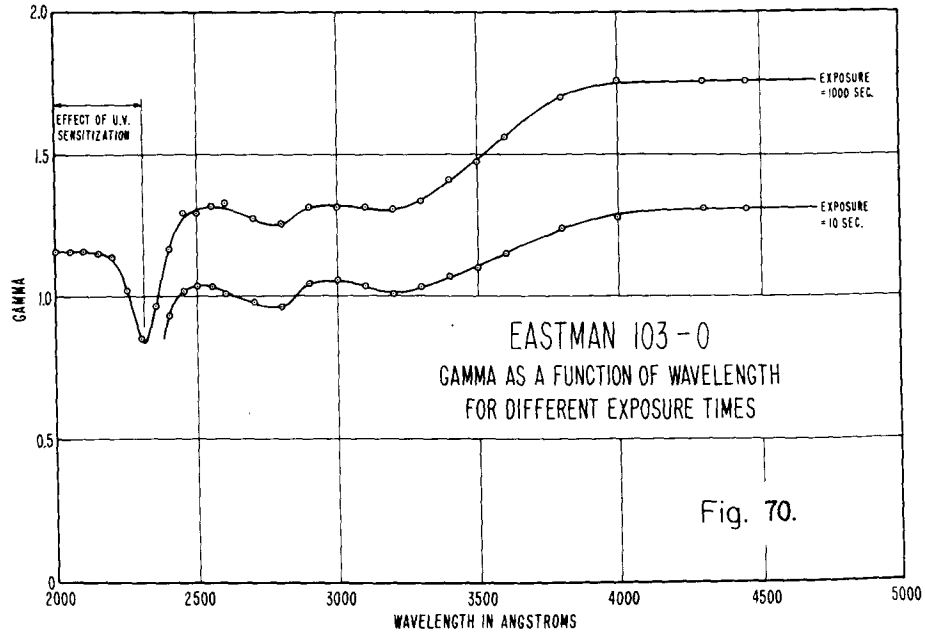
EFFECT OF U.V. SENSITIZATION
EXPOSURE = 1000 SEC.
EXPOSURE = 10 SEC.
EASTMAN 103-0
GAMMA AS A FUNCTION OF WAVELENGTH
FOR DIFFERENT EXPOSURE TIMES
Fig. 70.
GAMMA
2.0
1.5
1.0
0.5
0
2000
2500
3000
3500
4000
4500
5000
WAVELENGTH IN ANGSTROMS

both on the emulsion and the conditions of development[65]. An experiment was conducted to determine how critically γ's for the xenon arc spectra depended upon the duration and temperature of development. It was somewhat surprising to discover that there was practically no such dependence at all for variations from 3.5 to 4.5 minutes and from 66°F to 68°F; however, it was found that the H. & D. curves shifted toward the left at the rate of $\Delta \log E = 0.16$ per minute and $\Delta \log E = 0.04$ per degree Fahrenheit. These results evidently imply that γ has approached γ_∞.

The presence of scattered light was evidenced by a small amount of photographic fog superposed on the more heavily exposed spectra. This fog, which spreads over sizable areas, is not to be confused with turbidity of the emulsion, which causes the spectra to bulge in regions of excessive exposure. Considering simultaneously the spectral distribution of source radiation and the spectral response of the 103-0 film, one may assume that in this experiment most of the fogging was caused by blue light, which can be fairly well represented by an H. & D. curve for 4000A. The margins of each film were protected from scattered light by a close-fitting mask in which it was mounted during exposure. The resulting density within these shielded areas was adopted as the reference zero above which all other densities on the film were measured. In figure 66, "A" represents this zero level, "B" is the spectrum density, and "C" is the fog background.

It was found, however, that fog densities did not correspond to scattered light exposures proportional to the spectrum exposures neighboring them; that is, instead of following the spectrum exposure sequence (100%, 30%, 10%, 3%, 1%, 0.3%, and 0.1%), the corresponding relative scattered light sequence was: 100%, 51%, 33%, 16%, 7%, 3%, and 1%. The difference may be explained by supposing that while each frame of the

spectrogram was exposed, the neighboring frames received a little light scattered inside the spectrograph. Adopting this hypothesis, one can show with a little algebra that about 50% of the scattered light fell in the frame being exposed, while 12% fell in the neighboring frame on each side, 9% in the next frame, and so on.

Stray light from extraneous sources was found to be entirely negligible for 10-second exposures; even with the xenon arc operating and illuminating the field of view, there was no measurable darkening produced on the film when the path-folding mirrors (M_3 and M_4) remained covered. For 1000-second exposures, faint fogging due to street lights began to appear; the maximum resulting density was around 0.08.

Actually we care little where the scattered light originated; the more important problem is to correct for its influence on spectrum densities. Figure 71 shows how this can be done, and the reasoning behind it is simple. Using an H. & D. curve for 4000A, let E_s and E_f be the exposures corresponding to measured spectrum and fog densities, respectively. Then, if reciprocity failure is not too serious, the spectrum density which would have been produced in the absence of fog corresponds to an exposure equal to $E_s - E_f$. Attention is invited to the numerical example in the figure. Even though H. & D. curves for various wavelengths apply to the spectrum itself, the correct curve for computing fog corrections is always the one fitting scattered light.

Since about six thousand spectrum densities required fog corrections in the present investigation, it was found expedient to plot the correction curves shown in figure 72 rather than to reckon each correction individually by figure 71.

Some investigators have incorrectly made fog corrections simply by

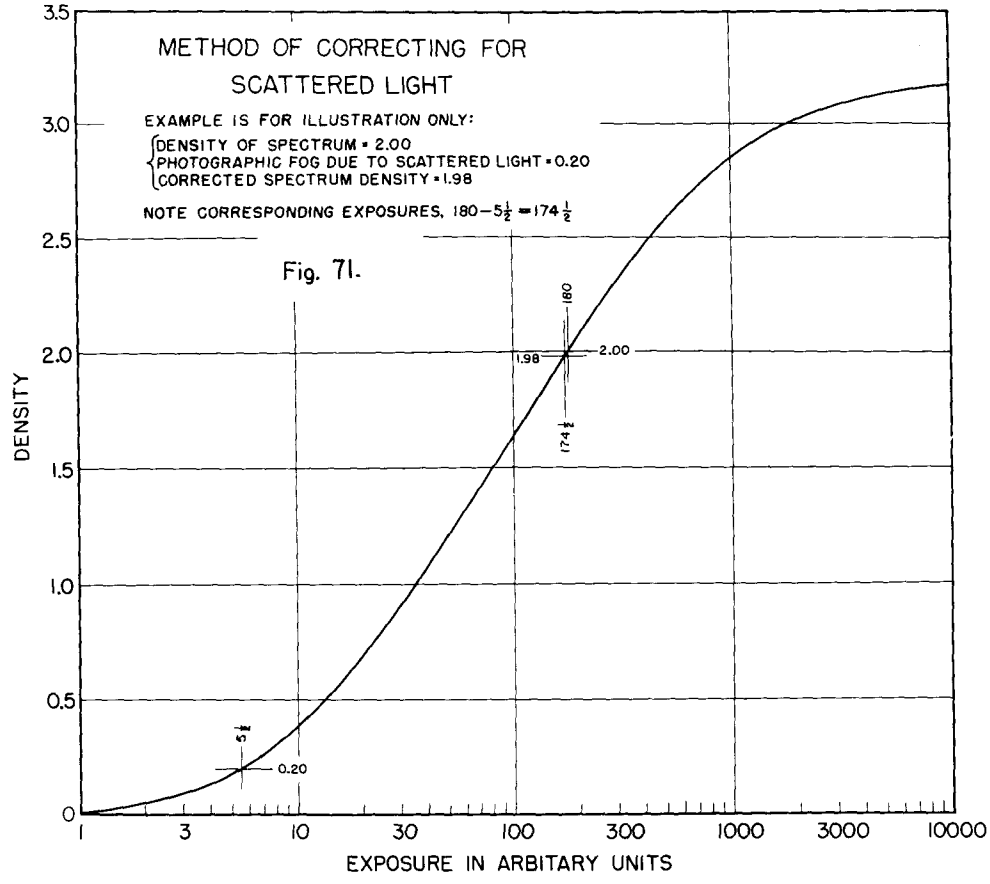
METHOD OF CORRECTING FOR
SCATTERED LIGHT
EXAMPLE IS FOR ILLUSTRATION ONLY:
DENSITY OF SPECTRUM = 2.00
PHOTOGRAPHIC FOG DUE TO SCATTERED LIGHT = 0.20
CORRECTED SPECTRUM DENSITY = 1.98
NOTE CORRESPONDING EXPOSURES, 180 − 5½ = 174½
DENSITY
EXPOSURE IN ARBITARY UNITS
0.20
1.98
2.00
180
174½
5½

Fig. 71.

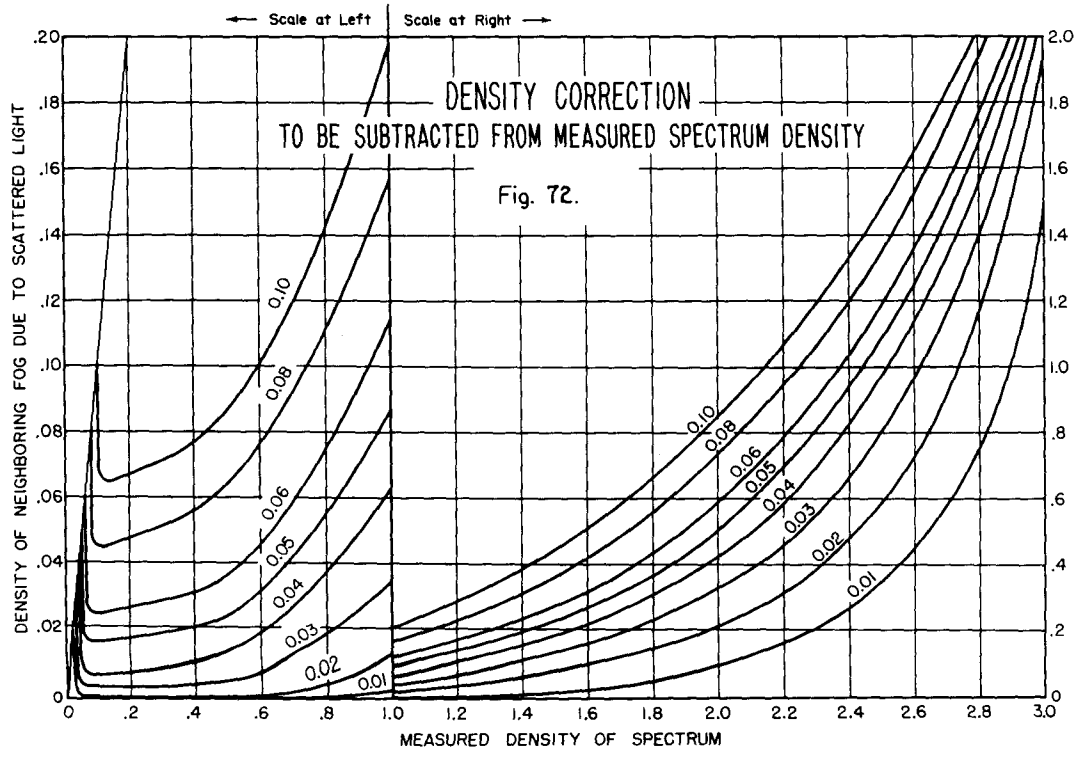
Scale at Left
Scale at Right
DENSITY CORRECTION
TO BE SUBTRACTED FROM MEASURED SPECTRUM DENSITY
DENSITY OF NEIGHBORING FOG DUE TO SCATTERED LIGHT
MEASURED DENSITY OF SPECTRUM
0.10
0.08
0.06
0.05
0.04
0.03
0.02
0.01

Fig. 72.

subtracting the fog density from the image density. It is startling to realize what large errors such a procedure can introduce; for example, if instead of using figure 71, we had merely subtracted 0.20 from 2.00 to obtain a "corrected" spectrum density of 1.80, we would have been ten times as far off as to have neglected fog altogether.

The experimental verification of fog corrections by the method of figures 71 and 72 was excellent. Parts of three films were intentionally fogged in an area where natural fogging was otherwise negligible; densities just inside and just outside the boundary of the fogged area were measured, leading to the data in Table IV. Although this test was not performed in precisely the same way that natural fogging occurs inside the spectrograph, it is unlikely that there should be much difference in the result.

Table IV

Density of fogged image	0.56	1.41	2.20
Density of neighboring fog	0.04	0.27	0.54
Correction by figure 72	-0.06	-0.07	-0.04
Predicted image without fog	0.50	1.34	2.16
Actual image without fog	0.51	1.34	2.16

After the density data from each spectrogram had been corrected for scattered light fog using figure 72, two families of H. & D. curves, each like figure 69, were plotted on two sheets of graph paper, one for short-path data and the other for long-path data. Members of the long-path family were individually congruent to corresponding members of the short-path family, but they were laterally displaced by various amounts depending on wavelength. These displacements, $\Delta \log E$, were determined by superposing the two sheets of graph paper over an illuminated glass table.

At each wavelength, $\Delta \log E$ is related to the ratio of intensities incident upon the film by

$$\Delta \log E = \log \frac{E_S}{E_L} = \log \frac{I_S}{I_L} \tag{19}$$

where subscripts S and L denote short-path and long-path spectra. It now remains to translate this information into attenuation coefficients.

Since the spectrograph viewed two sources (or source images) at different distances simultaneously, it could not focus their spectra both in exactly the same plane; therefore, the film was located at a compromise position between the two planes of individually sharp focus. As a result, astigmatic heights of short-path and long-path spectra were different[83]. Figure 73 is a plot of astigmatic heights of the xenon arc spectra measured with a Mann comparator; on account of emulsion turbidity, these measurements were limited to regions where the density was 0.8 or less.

Astigmatic height ratios are given in figure 74 for both the xenon-arc system and the hydrogen-arc system. The ratio of intensities in equation (19) must be multiplied by the height ratio for each wavelength to obtain the ratio of intensities incident upon the spectrograph aperture.

Let ρ represent the ratio of long-path to short-path intensity incident upon the spectrograph aperture, and let ρ_o be the ratio which would exist in a vacuum; then at each wavelength

$$\rho = \rho_o e^{-\sigma(x_L - x_S)} \tag{20}$$

Solving (20) for the attenuation coefficient, we get

$$\sigma = \frac{\ln \rho_o - \ln \rho}{x_L - x_S} = 2.303 \frac{\log \rho_o - \log \rho}{x_L - x_S}. \tag{21}$$

For the hydrogen-arc system, $x_L - x_S = 0.340$ km and $\rho_o = 1.08$, giving

$$\sigma = 0.23 - 6.78 \log \rho \ \text{km}^{-1}. \tag{22}$$

Actually by geometry alone, $\rho_o = 0.0108$, but exposures were chosen to

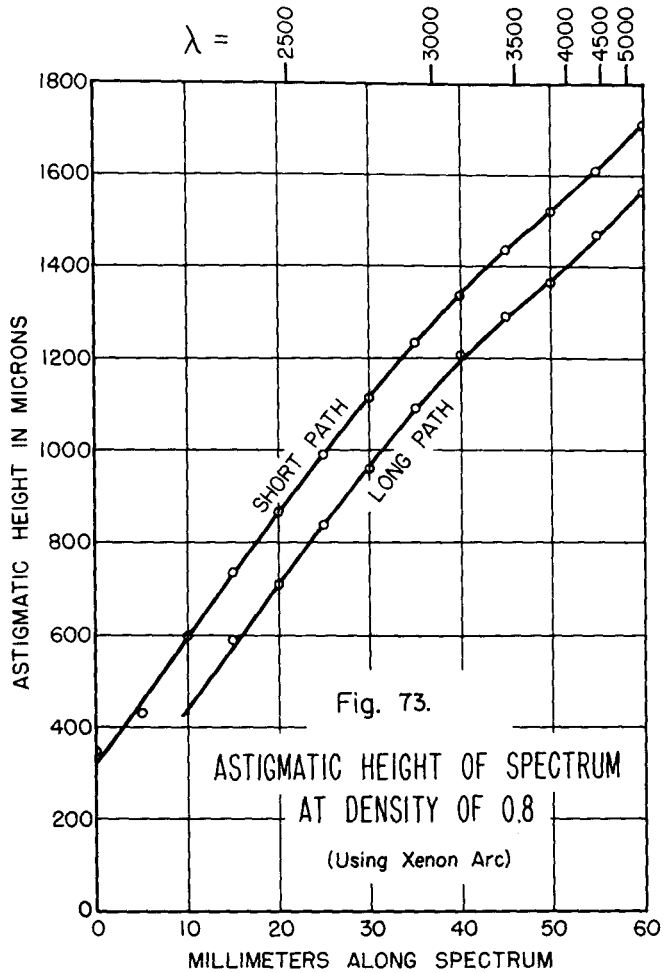

Fig. 73.

ASTIGMATIC HEIGHT OF SPECTRUM AT DENSITY OF 0.8

(Using Xenon Arc)

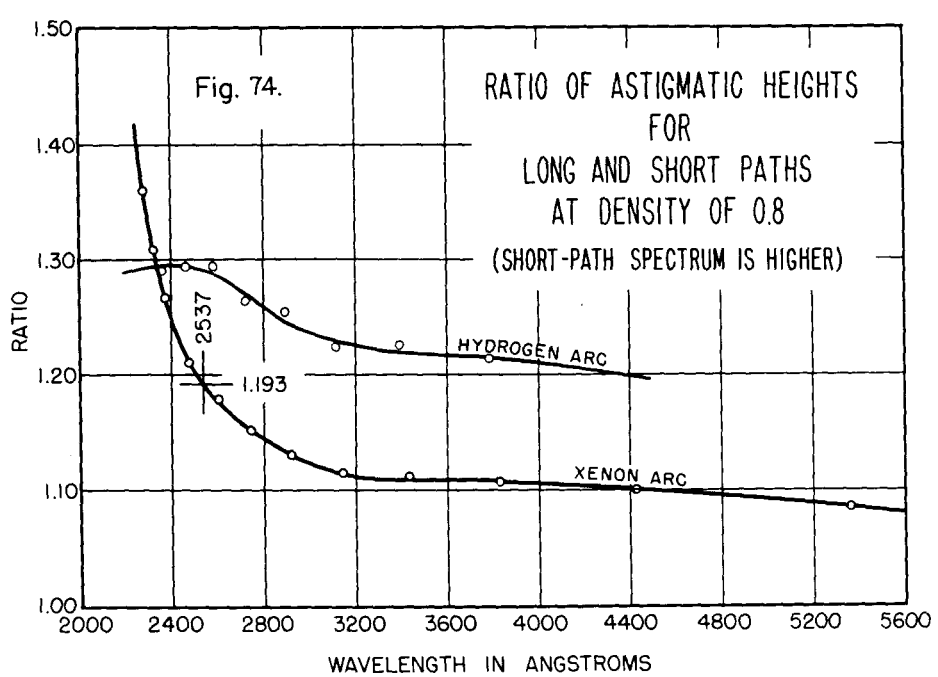

Fig. 74.

RATIO OF ASTIGMATIC HEIGHTS FOR LONG AND SHORT PATHS AT DENSITY OF 0.8

(SHORT-PATH SPECTRUM IS HIGHER)

introduce a factor of 100.

For the xenon-arc system, $x_L - x_S = 0.680$ km, giving

$$\sigma = 3.39 \ (\log \rho_o - \log \rho) \ \text{km}^{-1}, \qquad (23)$$

where ρ_o is a function of wavelength because of the spectral dissimilarity of mirror reflectances.

Equation (22) was sufficient to reduce hydrogen arc data (after fog and astigmatic corrections) to absolute spectral attenuation coefficients, but for xenon-arc data it was necessary to determine ρ_o as a function of wavelength empirically before equation (23) could be applied.

The principal aim of conducting the hydrogen-arc experiment described in Section VI was to determine the vacuum intensity ratio ρ_o of the xenon-arc system at all wavelengths in the spectral region of interest. The Loofah and the cadmium photocell also were of value in monitoring changes of ρ_o with time.

From March 19 to September 20, 1949, the four mirrors of the xenon arc system were used with their original coatings, which included a silicon-monoxide layer. The corresponding vacuum intensity ratio differed considerably from its pure geometrical value (about 1.3) and was also found to have quite a marked dependence on wavelength as shown by figure 75. Although this dependence was somewhat inconvenient, it did not especially affect the accuracy of the experiment.

On September 21, 1949, the mirrors were re-aluminized and the silicon monoxide layer was omitted; at the same time the xenon lamp was moved so as to increase the size of its enlarged image in M_1. The resulting vacuum intensity ratio agreed fairly well with its geometrical value (about 6) and had relatively little wavelength dependence above 3000A as shown by figure 76. Since these uncoated surfaces weathered nearly as well as the previous

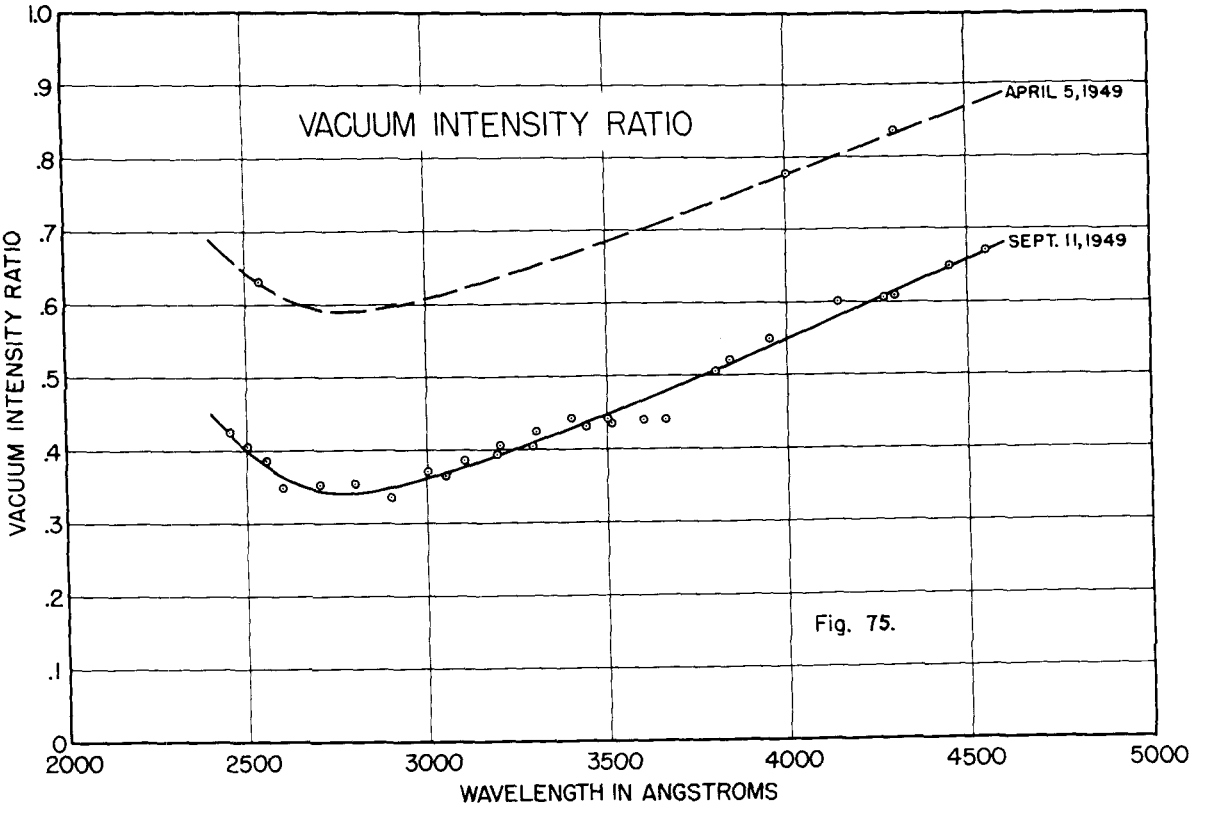
VACUUM INTENSITY RATIO
APRIL 5, 1949
SEPT. 11, 1949
VACUUM INTENSITY RATIO
WAVELENGTH IN ANGSTROMS
1.0
.9
.8
.7
.6
.5
.4
.3
.2
.1
0
2000
2500
3000
3500
4000
4500
5000

Fig. 75.

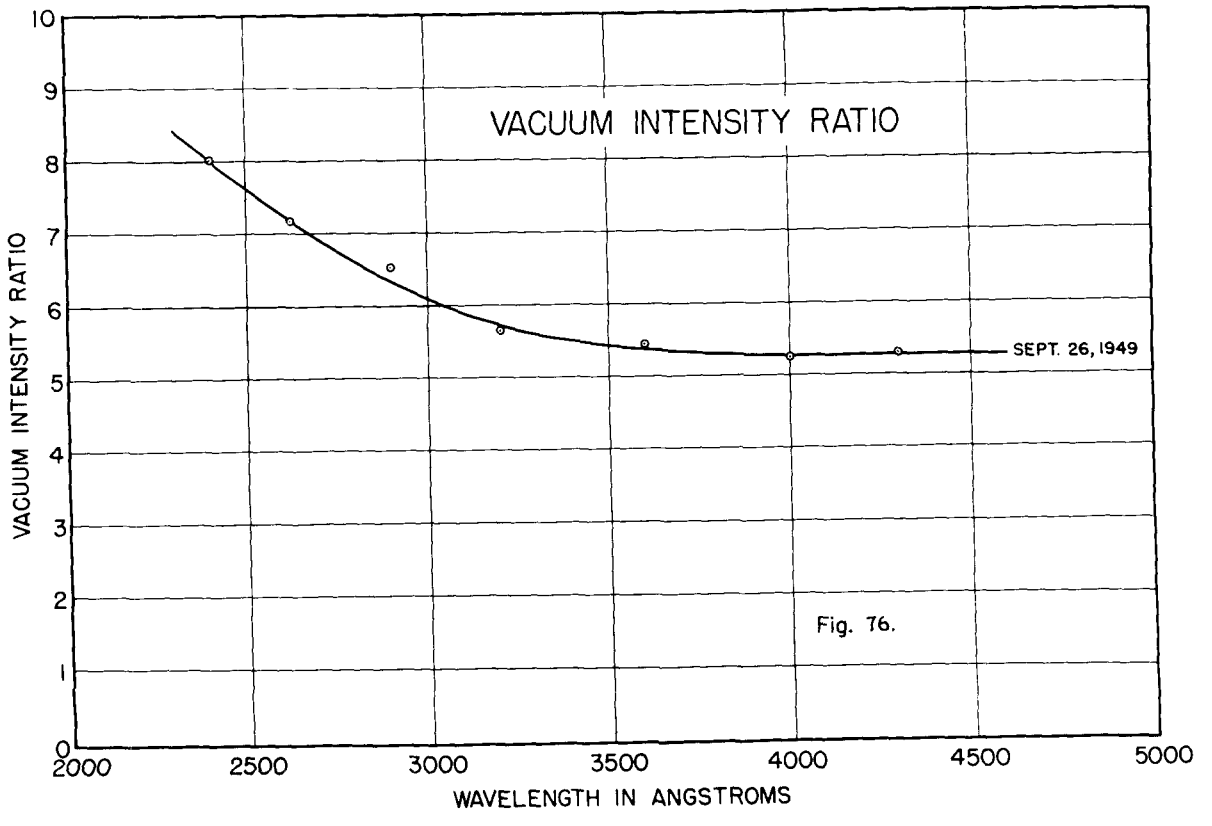
VACUUM INTENSITY RATIO
SEPT. 26, 1949
VACUUM INTENSITY RATIO
WAVELENGTH IN ANGSTROMS
10
9
8
7
6
5
4
3
2
1
0
2000
2500
3000
3500
4000
4500
5000

Fig. 76.

set, it was concluded that silicon monoxide coatings were of doubtful merit for ultraviolet work.

Loofah data extrapolated by equation (11), the Linke-Borne formula, showed that the vacuum intensity ratio around 4000A was changing slowly with time; presumably this was caused by dissimilar aging of the several mirror surfaces. Though a little less accurate, cadmium photocell readings showed a corresponding drift in ρ_o at 2537A, as indicated by figure 77. The possible sub-dependence of these photocell ρ_o data on the magnitude of σ at 2537A may have been caused by Middleton's field-of-view effect[19].

Figure 78 is a sort of chronological interpolation of figure 75 based upon the indication of all available data that the time dependence was more-or-less linear. Values of ρ_o obtained from figure 78 were used in equation (23) to compute final values of σ for various wavelengths.

Briefly in review, the process for extracting attenuation coefficients from the spectra was as follows: first, densities were measured with the microdensitometer. Next, they were corrected for scattered light fog using figure 72 and then plotted in the form of H. & D. curves. The lateral displacements, $\Delta \log E$, between long-path and short-path curves were determined graphically. These data were then corrected for the ratio of astigmatic heights using figure 74 and finally (in the case of xenon-arc data) for the vacuum intensity ratio of the apparatus using figure 78. In practice it was found expedient to perform the last two steps simultaneously using figure 79.

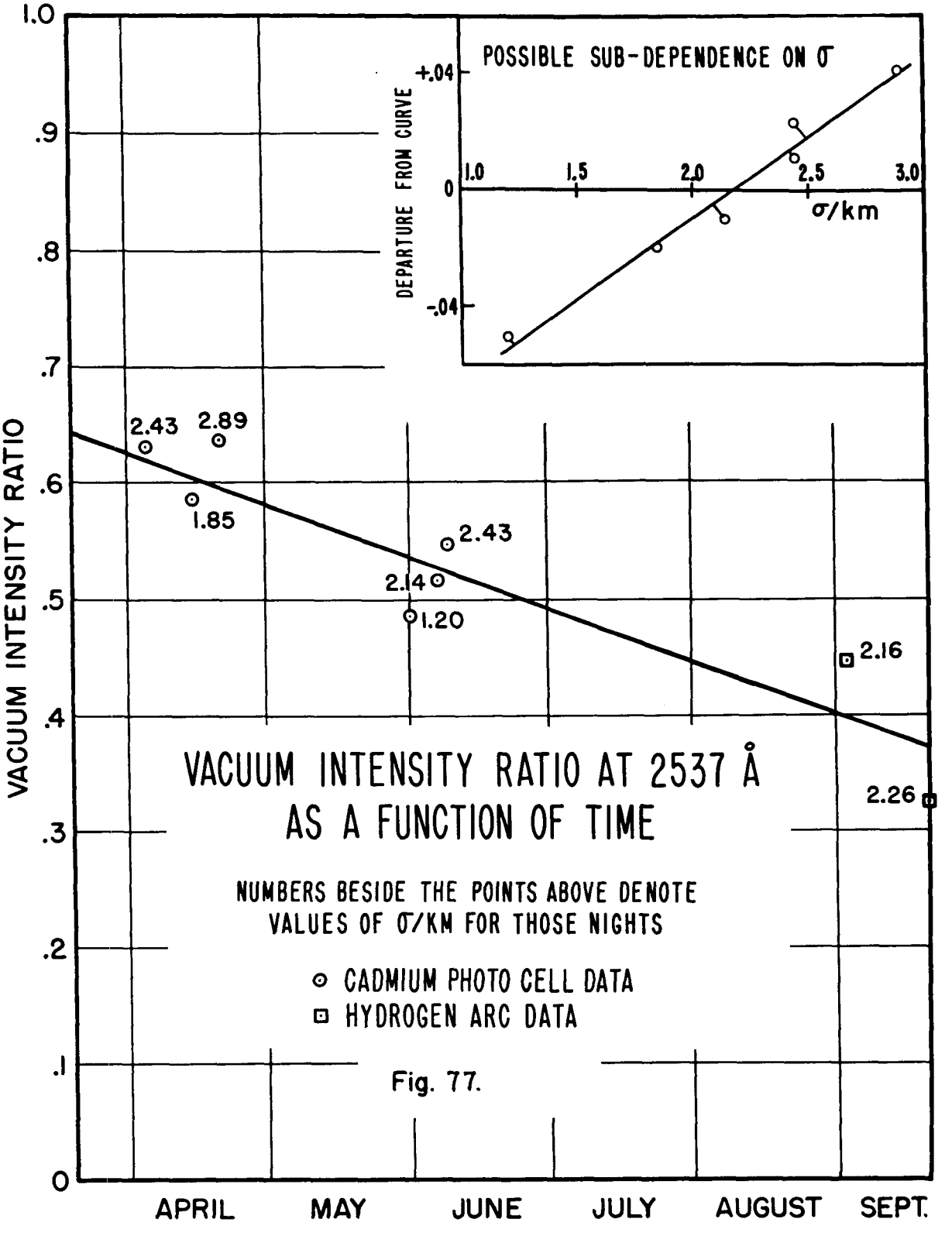

VACUUM INTENSITY RATIO AT 2537 Å
AS A FUNCTION OF TIME

NUMBERS BESIDE THE POINTS ABOVE DENOTE
VALUES OF σ/KM FOR THOSE NIGHTS

⊙ CADMIUM PHOTO CELL DATA
⊡ HYDROGEN ARC DATA

Fig. 77.

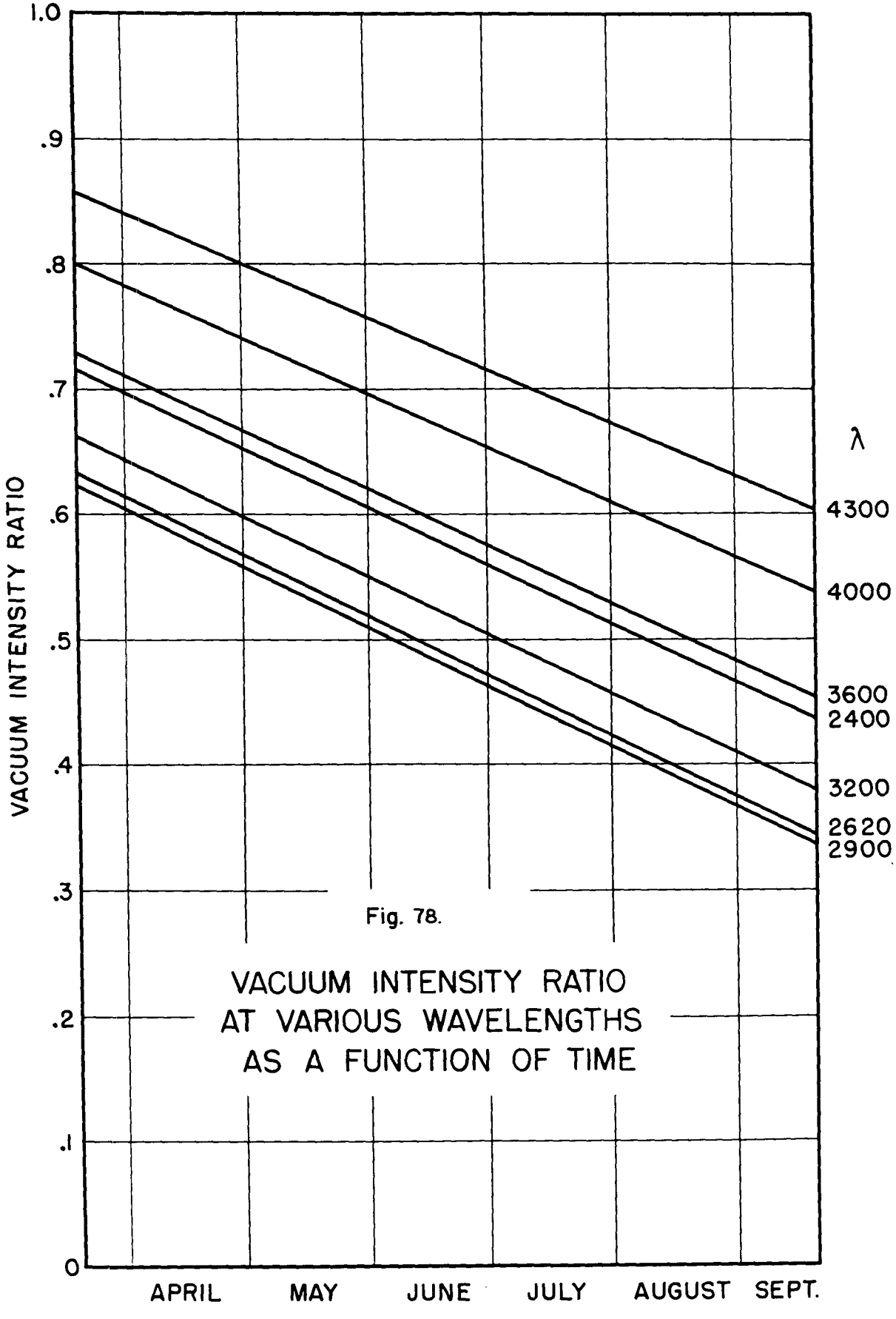

Fig. 78.

VACUUM INTENSITY RATIO
AT VARIOUS WAVELENGTHS
AS A FUNCTION OF TIME

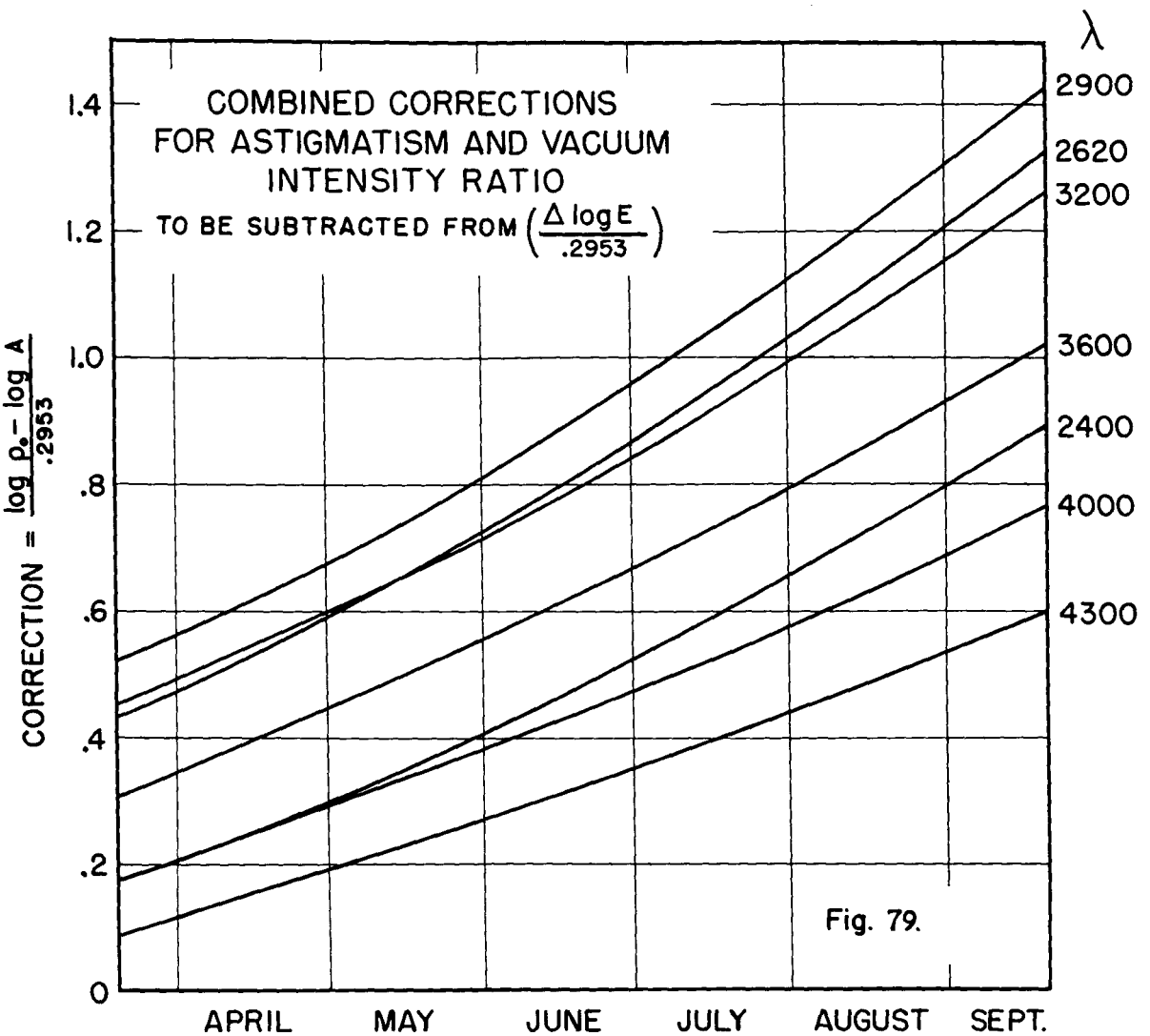
COMBINED CORRECTIONS
FOR ASTIGMATISM AND VACUUM
INTENSITY RATIO
TO BE SUBTRACTED FROM $\left(\frac{\Delta \log E}{.2953}\right)$
CORRECTION = $\frac{\log \rho_o - \log A}{.2953}$
1.4
1.2
1.0
.8
.6
.4
.2
0
APRIL
MAY
JUNE
JULY
AUGUST
SEPT.
λ
2900
2620
3200
3600
2400
4000
4300

Fig. 79.

VIII. ATTENUATION DATA

Using the procedure of analysis outlined in the preceding section, ultraviolet attenuation coefficients in km^{-1} were plotted against wavelengths in Angstroms for 78 representative nights from among the 125 on which spectra were photographed. Six of these nights were studied in detail, while the remaining 72 were reduced to the minimum number of points required to define the attenuation curves reasonably well. Since none of the spectra showed any discrete absorptions except for the Herzberg O_2 bands, all of the curves are known to be smooth from 2300A to 2420A and from 2600A to 4600A. For convenience, they have also been drawn smooth through the Herzberg region (2420A to about 2600A) by selecting data between the bands; thus obtaining the curve which would exist if the bands were actually absent.

Attenuation curves for the six nights studied in detail are plotted in figure 80; they represent typical visibility conditions and they possess typical shapes and features. Over most of the spectral region plotted, σ's are correct in absolute value to ± 0.05 or less; the relative accuracy of neighboring points may be somewhat better than that. Errors in wavelength measurement (the order of an Angstrom) are entirely negligible. Note that two curves can have equal σ's at one wavelength but be quite different at another. Note also that, while no two curves are shaped exactly alike, there is a tendency for some of the same bumps to recur.

The wavelengths and relative strengths of absorption lines in the Herzberg O_2 bands as measured by the present experiment are given in Table V; band heads are denoted by asterisks (*). It is likely that many of these "lines" are actually superpositions of several. Figure 81 is a densitometer trace of some of these bands. In order to include them mean-

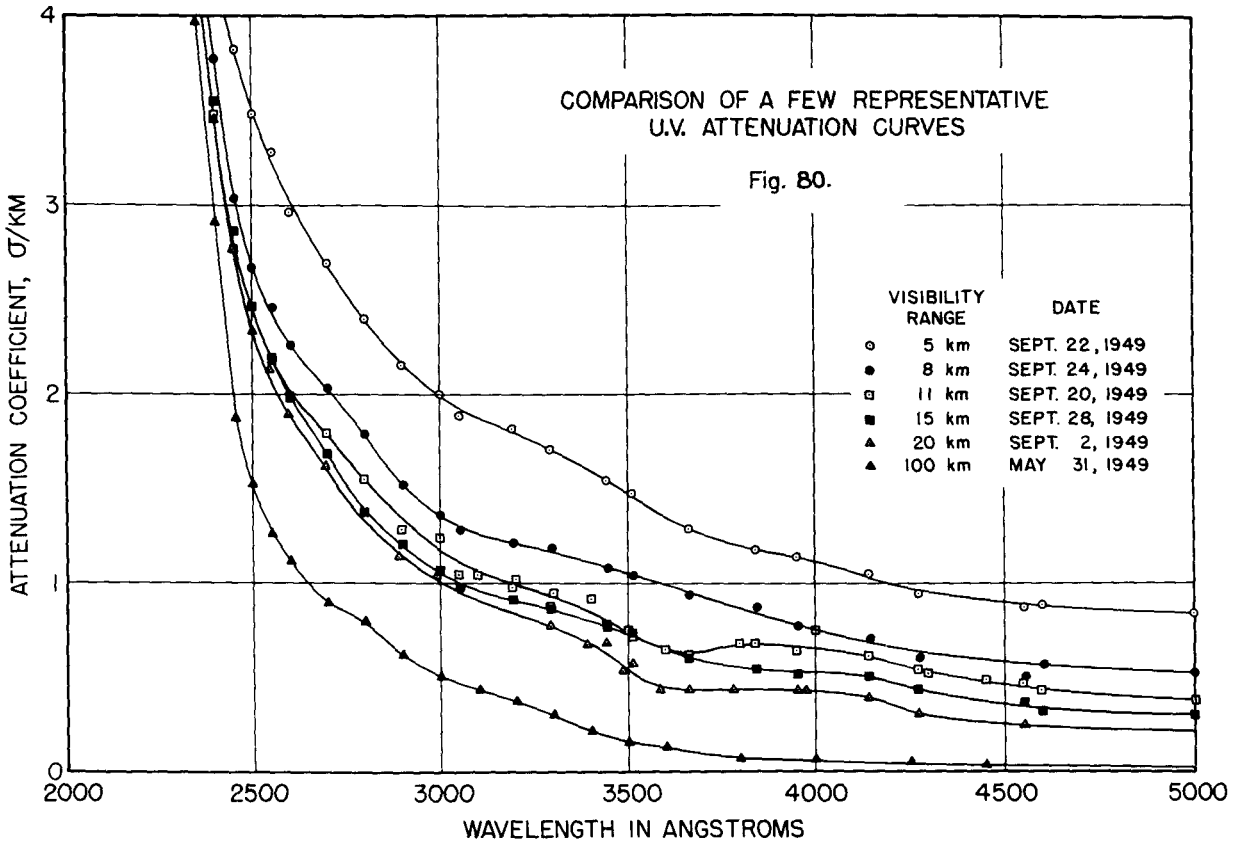
COMPARISON OF A FEW REPRESENTATIVE
U.V. ATTENUATION CURVES
Fig. 80.
VISIBILITY RANGE
DATE
5 km SEPT. 22, 1949
8 km SEPT. 24, 1949
11 km SEPT. 20, 1949
15 km SEPT. 28, 1949
20 km SEPT. 2, 1949
100 km MAY 31, 1949
ATTENUATION COEFFICIENT, σ/KM
WAVELENGTH IN ANGSTROMS
0
1
2
3
4
2000
2500
3000
3500
4000
4500
5000

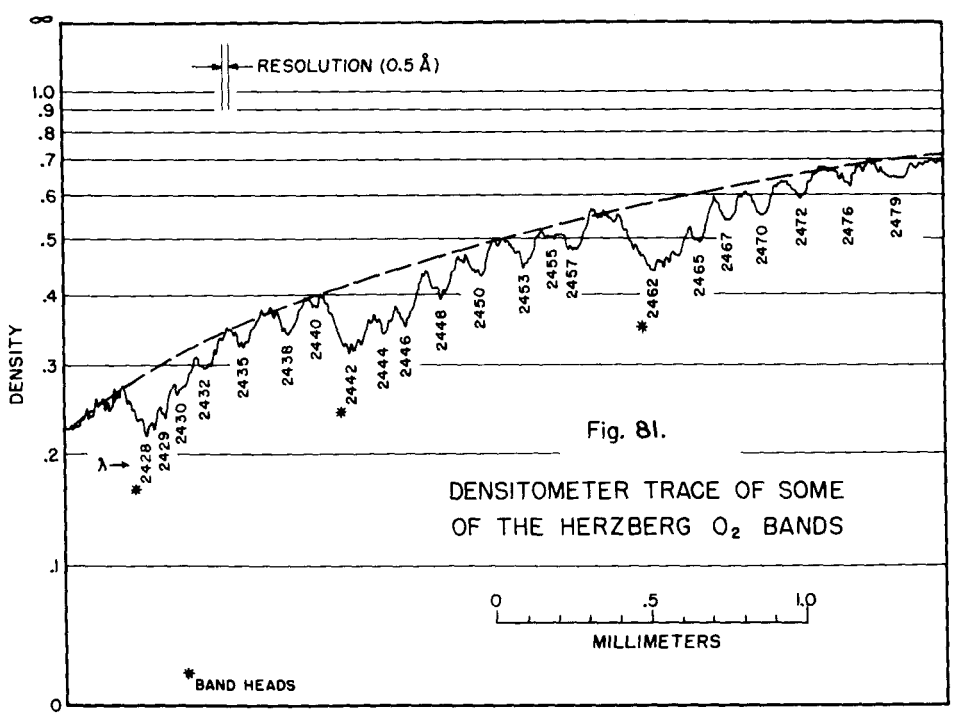
RESOLUTION (0.5 Å)
DENSITY
1.0
.9
.8
.7
.6
.5
.4
.3
.2
.1
0
λ→
*2428
2429
2430
2432
2435
2438
2440
*2442
2444
2446
2448
2450
2453
2455
2457
*2462
2465
2467
2470
2472
2476
2479
Fig. 81.
DENSITOMETER TRACE OF SOME
OF THE HERZBERG O_2 BANDS
0
.5
1.0
MILLIMETERS
*BAND HEADS

ingfully on an attenuation curve, it would be necessary to photograph them at many times the present resolution and over a shorter path, say around 100 meters. Under those circumstances, it might also be interesting to compute f-values for the "forbidden" transitions they represent.

Table V

*2421	4	*2488	16	*2593	5
2422	1	2490	11	2597	3
		2491	10	2599	4
*2428	7	2493	9	2602	3
2429	6	2496	9	2604	3
2430	4	2499	10		
2432	3	2502	6	*2638	5
2435	3	2506	4		
2438	4	2509	5	*2684	2
2440	1	2513	2		
		2516	1		
*2442	9				
2444	9	*2519	12		
2446	9	2522	7		
2448	6	2524	5		
2450	5	2526	6		
2453	5	2529	6		
2455	2	2532	4		
2457	6				
		*2554	7		
*2462	13	2557	5		
2465	11	2559	5		
2467	7	2561	6		
2470	8	2563	4		
2472	6	2566	2		
2476	4	2569	2		
2479	5	2573	2		
2484	5	2577	2		
		2580	1		

For comparison with the attenuation curves in figure 80, the contribution due to molecular diffusion, discussed in Section II(A), is plotted on the same scale in figure 82. Also shown for comparison is Mme. Vassy's data (12) for exceptionally clear air at high elevations (figure 83); it is quite similar to the author's curve for May 31, 1949, except for the general neighborhood of 3000A where her data show greater transparency than

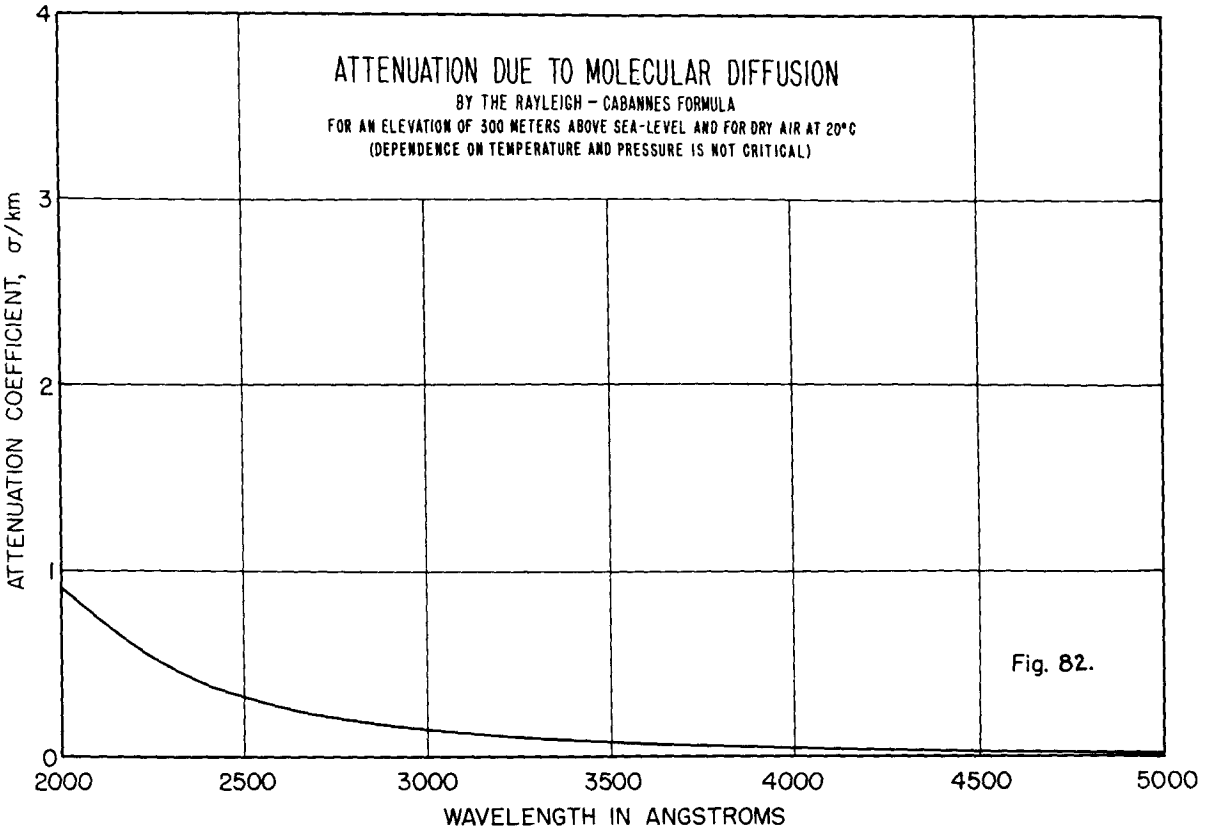
ATTENUATION DUE TO MOLECULAR DIFFUSION
BY THE RAYLEIGH – CABANNES FORMULA
FOR AN ELEVATION OF 300 METERS ABOVE SEA-LEVEL AND FOR DRY AIR AT 20°C
(DEPENDENCE ON TEMPERATURE AND PRESSURE IS NOT CRITICAL)
ATTENUATION COEFFICIENT, σ/km
0
1
2
3
4
2000
2500
3000
3500
4000
4500
5000
WAVELENGTH IN ANGSTROMS

Fig. 82.

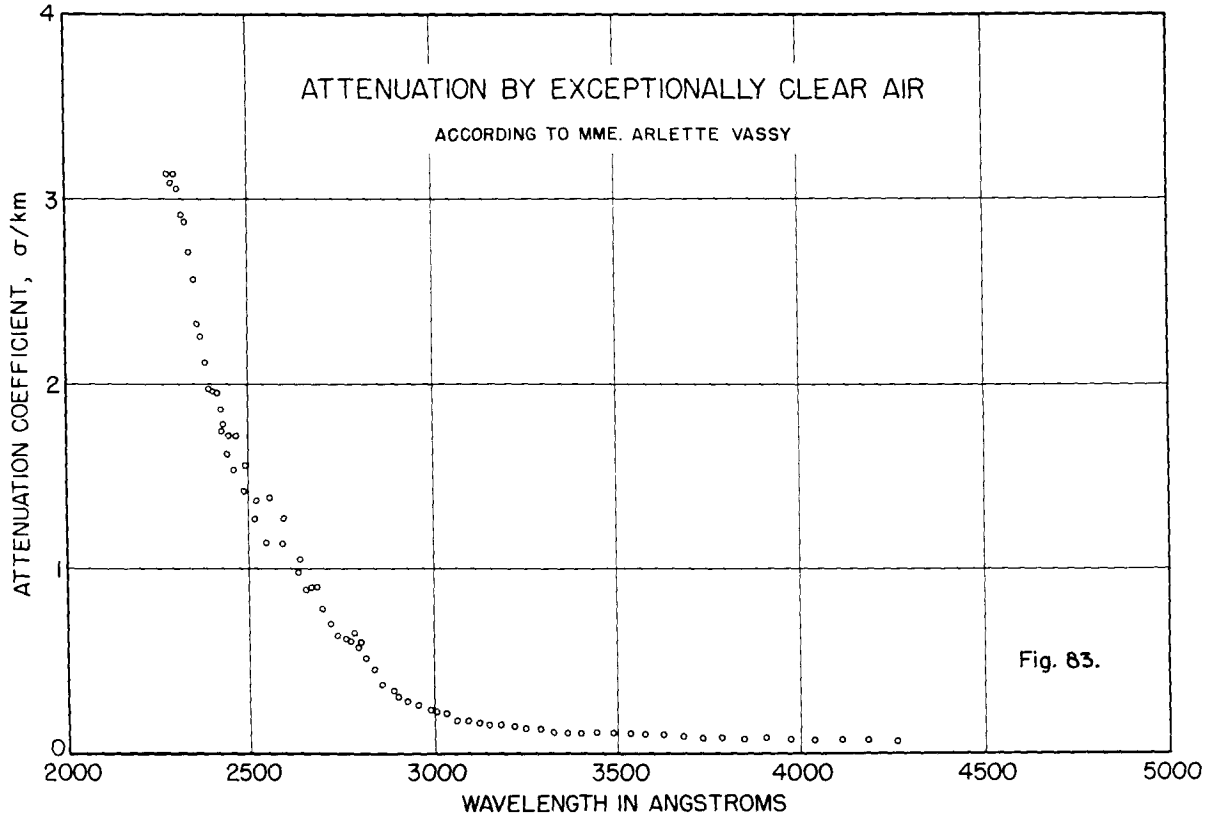
ATTENUATION BY EXCEPTIONALLY CLEAR AIR
ACCORDING TO MME. ARLETTE VASSY
ATTENUATION COEFFICIENT, σ/km
0
1
2
3
4
2000
2500
3000
3500
4000
4500
5000
WAVELENGTH IN ANGSTROMS

Fig. 83.

observed in Pasadena.

On the following ten pages are ultraviolet attenuation curves for 78 nights including the six of figure 80. They are adequately identified by date; hence, figure numbers have been omitted. Each is plotted separately to avoid the confusion that would result by grouping them randomly. Wavelengths of the points are in all cases: 2400, 2620, 2900, 3200, 3600, 4000, and 4300 Angstroms. An additional point appears at 5500A for dates when the Loofah was available for use in Pasadena; the corresponding visibility ranges were obtained by equation (16). When the Loofah was not available, visibilities had to be estimated by extrapolation and by direct observation of air conditions. Note that curves for the first 45 nights are consecutive; they represent part of a continuous run that lasted 74 nights.

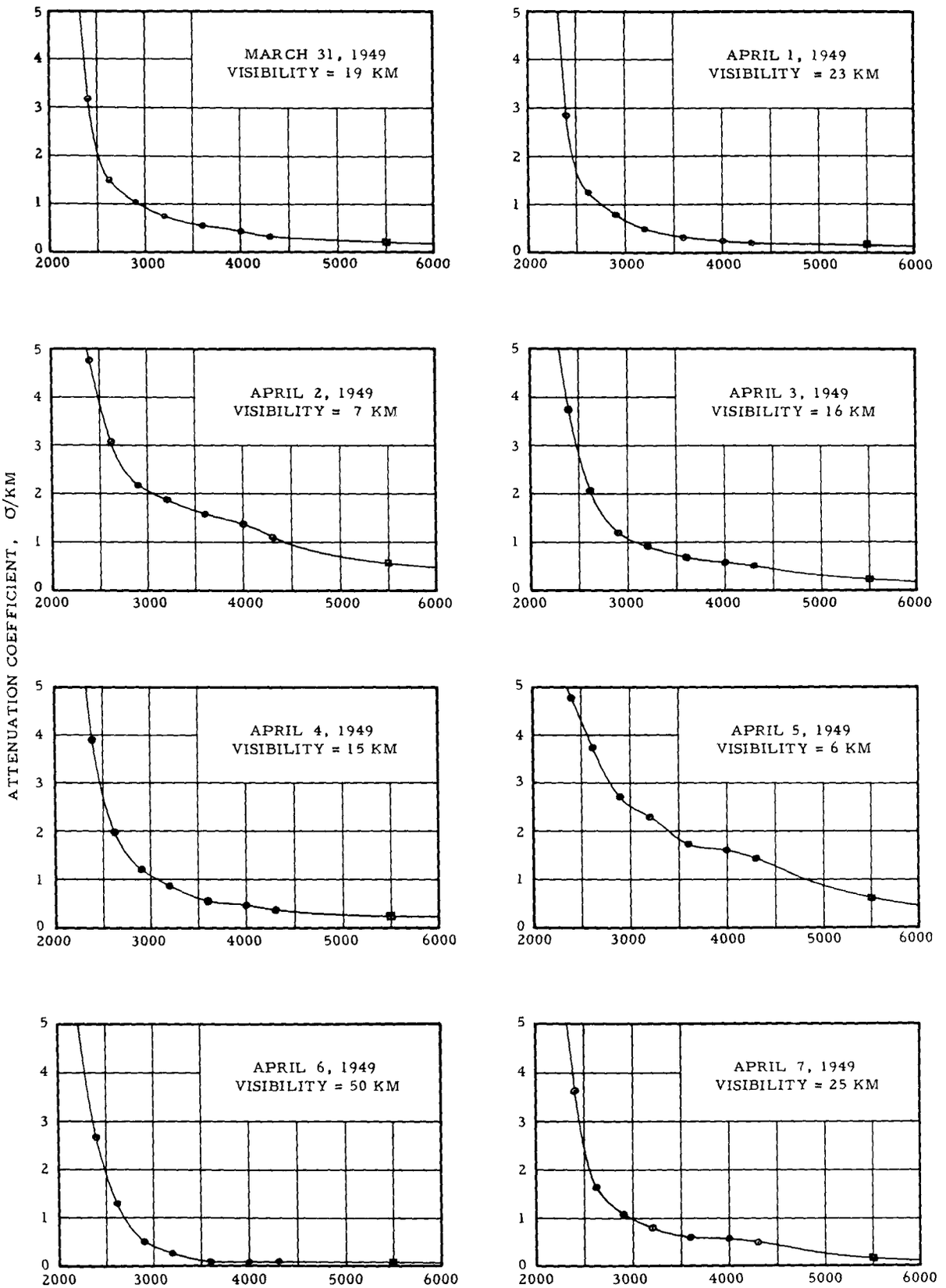
MARCH 31, 1949
VISIBILITY = 19 KM
APRIL 1, 1949
VISIBILITY = 23 KM
APRIL 2, 1949
VISIBILITY = 7 KM
APRIL 3, 1949
VISIBILITY = 16 KM
APRIL 4, 1949
VISIBILITY = 15 KM
APRIL 5, 1949
VISIBILITY = 6 KM
APRIL 6, 1949
VISIBILITY = 50 KM
APRIL 7, 1949
VISIBILITY = 25 KM
ATTENUATION COEFFICIENT, Ø/KM
WAVELENGTH IN ANGSTROMS

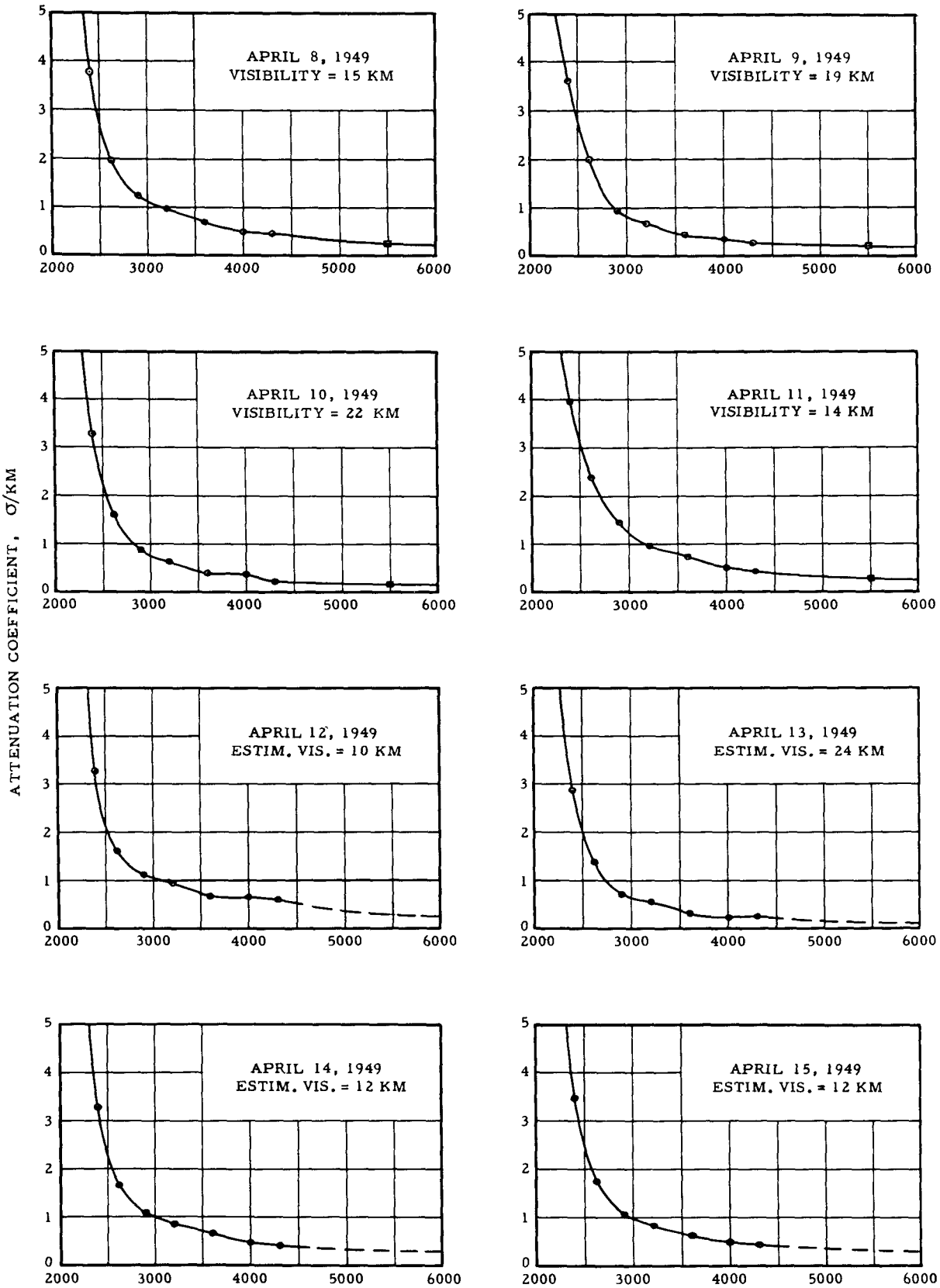
APRIL 8, 1949
VISIBILITY = 15 KM
APRIL 9, 1949
VISIBILITY = 19 KM
APRIL 10, 1949
VISIBILITY = 22 KM
APRIL 11, 1949
VISIBILITY = 14 KM
APRIL 12, 1949
ESTIM. VIS. = 10 KM
APRIL 13, 1949
ESTIM. VIS. = 24 KM
APRIL 14, 1949
ESTIM. VIS. = 12 KM
APRIL 15, 1949
ESTIM. VIS. = 12 KM
ATTENUATION COEFFICIENT, σ/KM
WAVELENGTH IN ANGSTROMS

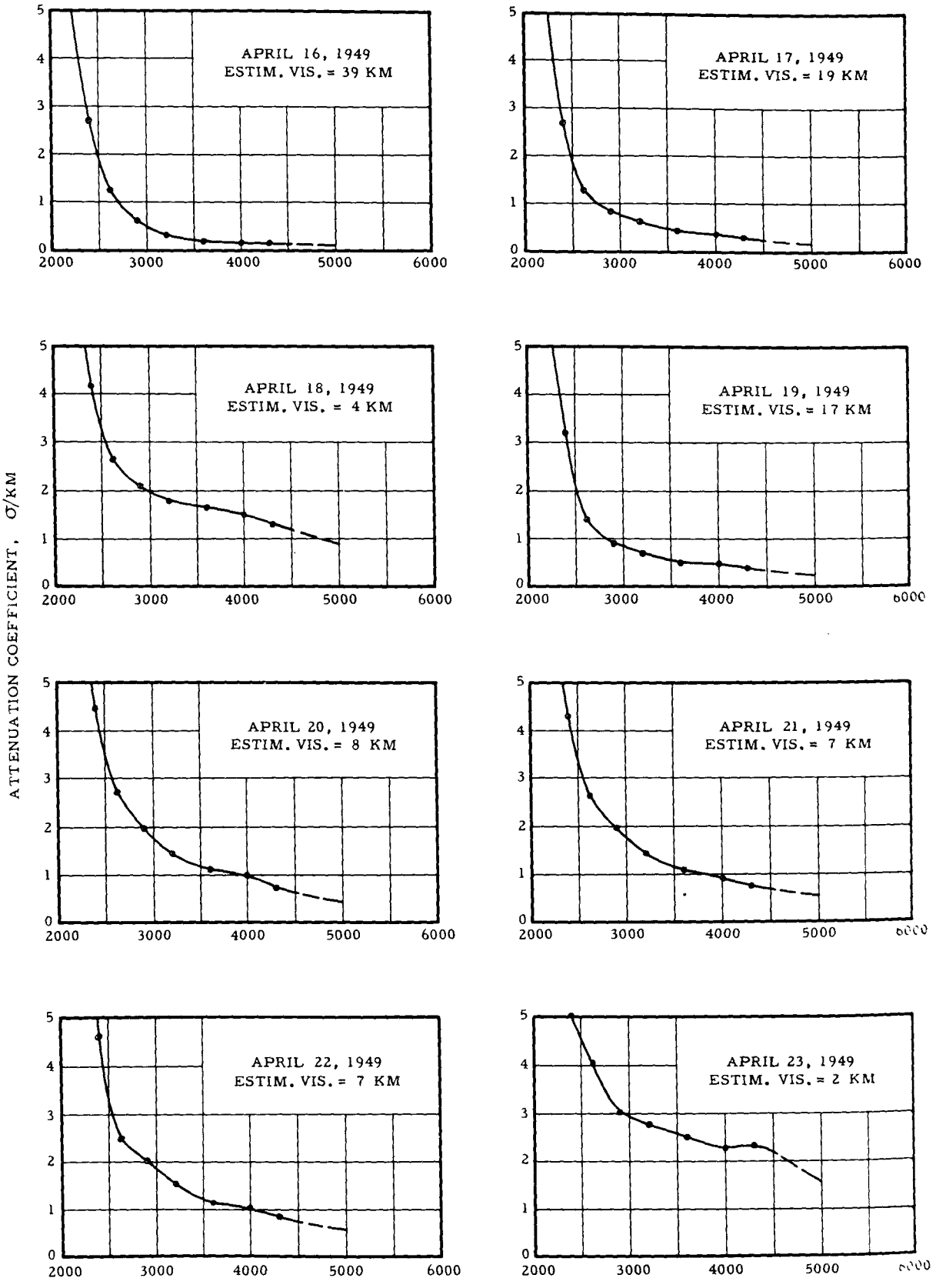
APRIL 16, 1949
ESTIM. VIS. = 39 KM
APRIL 17, 1949
ESTIM. VIS. = 19 KM
APRIL 18, 1949
ESTIM. VIS. = 4 KM
APRIL 19, 1949
ESTIM. VIS. = 17 KM
APRIL 20, 1949
ESTIM. VIS. = 8 KM
APRIL 21, 1949
ESTIM. VIS. = 7 KM
APRIL 22, 1949
ESTIM. VIS. = 7 KM
APRIL 23, 1949
ESTIM. VIS. = 2 KM
ATTENUATION COEFFICIENT, σ/KM
WAVELENGTH IN ANGSTROMS

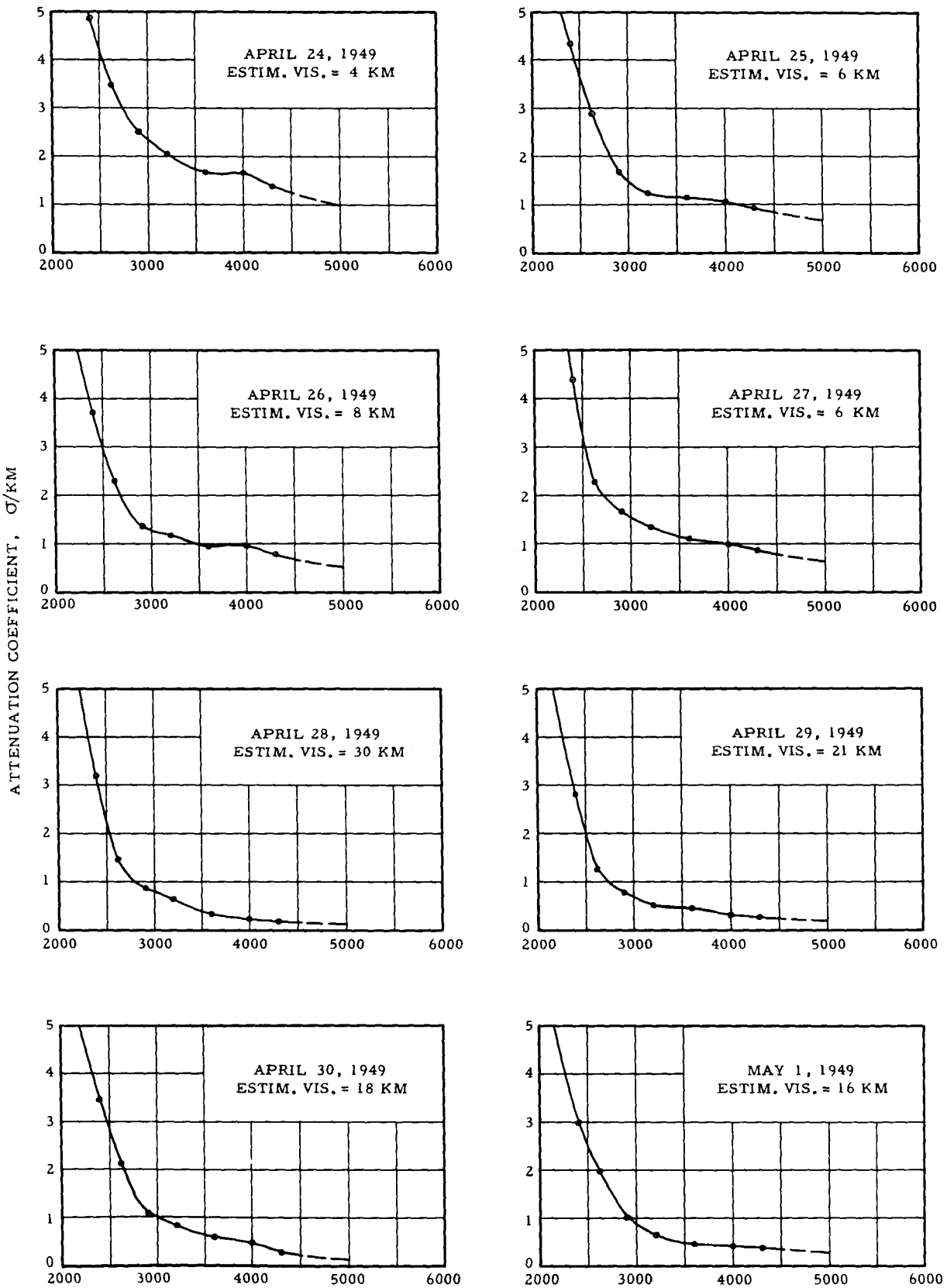
APRIL 24, 1949
ESTIM. VIS. = 4 KM
APRIL 25, 1949
ESTIM. VIS. = 6 KM
APRIL 26, 1949
ESTIM. VIS. = 8 KM
APRIL 27, 1949
ESTIM. VIS. = 6 KM
APRIL 28, 1949
ESTIM. VIS. = 30 KM
APRIL 29, 1949
ESTIM. VIS. = 21 KM
APRIL 30, 1949
ESTIM. VIS. = 18 KM
MAY 1, 1949
ESTIM. VIS. = 16 KM
ATTENUATION COEFFICIENT, σ/KM
WAVELENGTH IN ANGSTROMS
0
1
2
3
4
5
2000
3000
4000
5000
6000

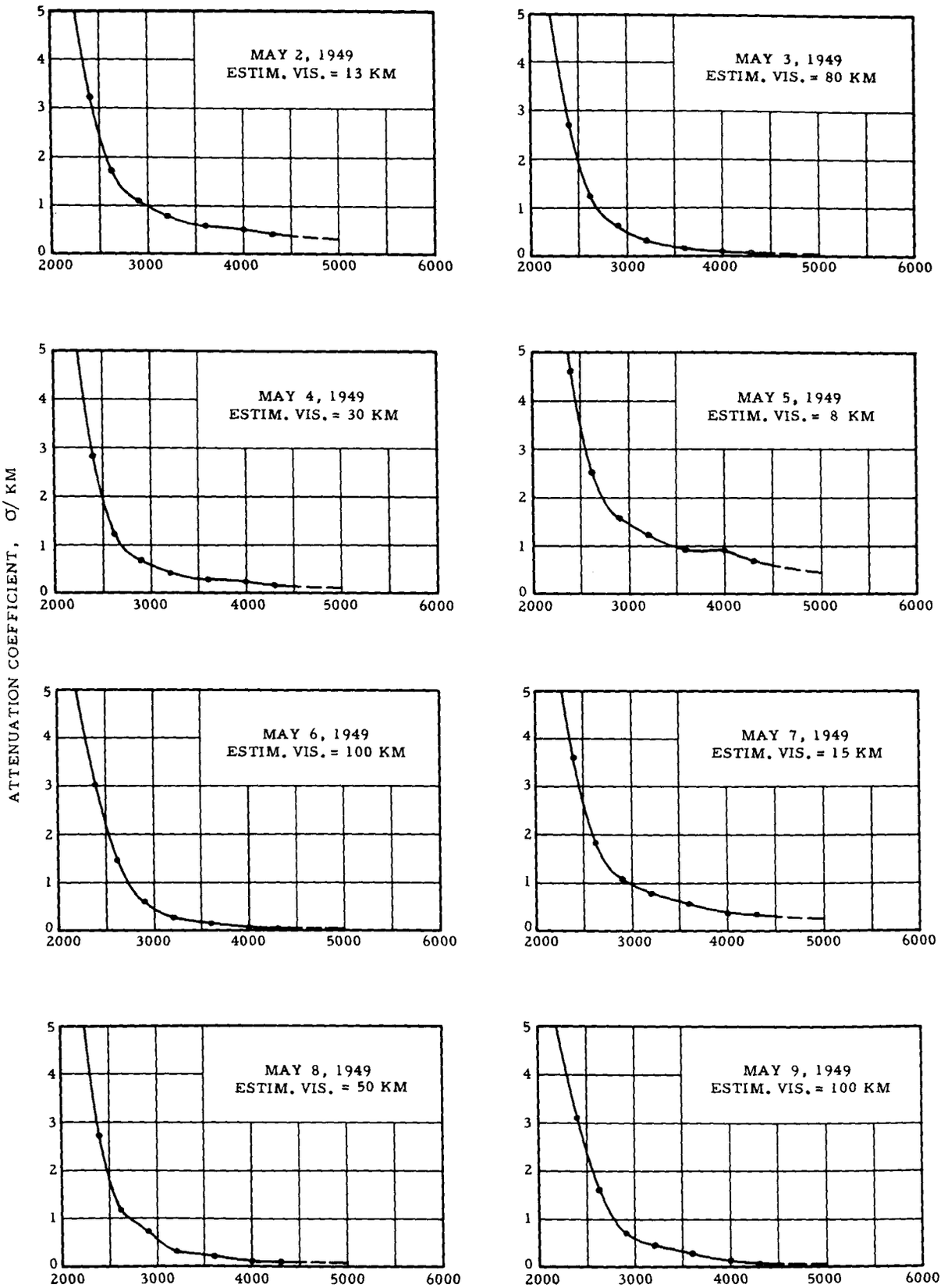
MAY 2, 1949
ESTIM. VIS. = 13 KM
MAY 3, 1949
ESTIM. VIS. = 80 KM
MAY 4, 1949
ESTIM. VIS. = 30 KM
MAY 5, 1949
ESTIM. VIS. = 8 KM
MAY 6, 1949
ESTIM. VIS. = 100 KM
MAY 7, 1949
ESTIM. VIS. = 15 KM
MAY 8, 1949
ESTIM. VIS. = 50 KM
MAY 9, 1949
ESTIM. VIS. = 100 KM
ATTENUATION COEFFICIENT, σ/ KM
WAVELENGTH IN ANGSTROMS

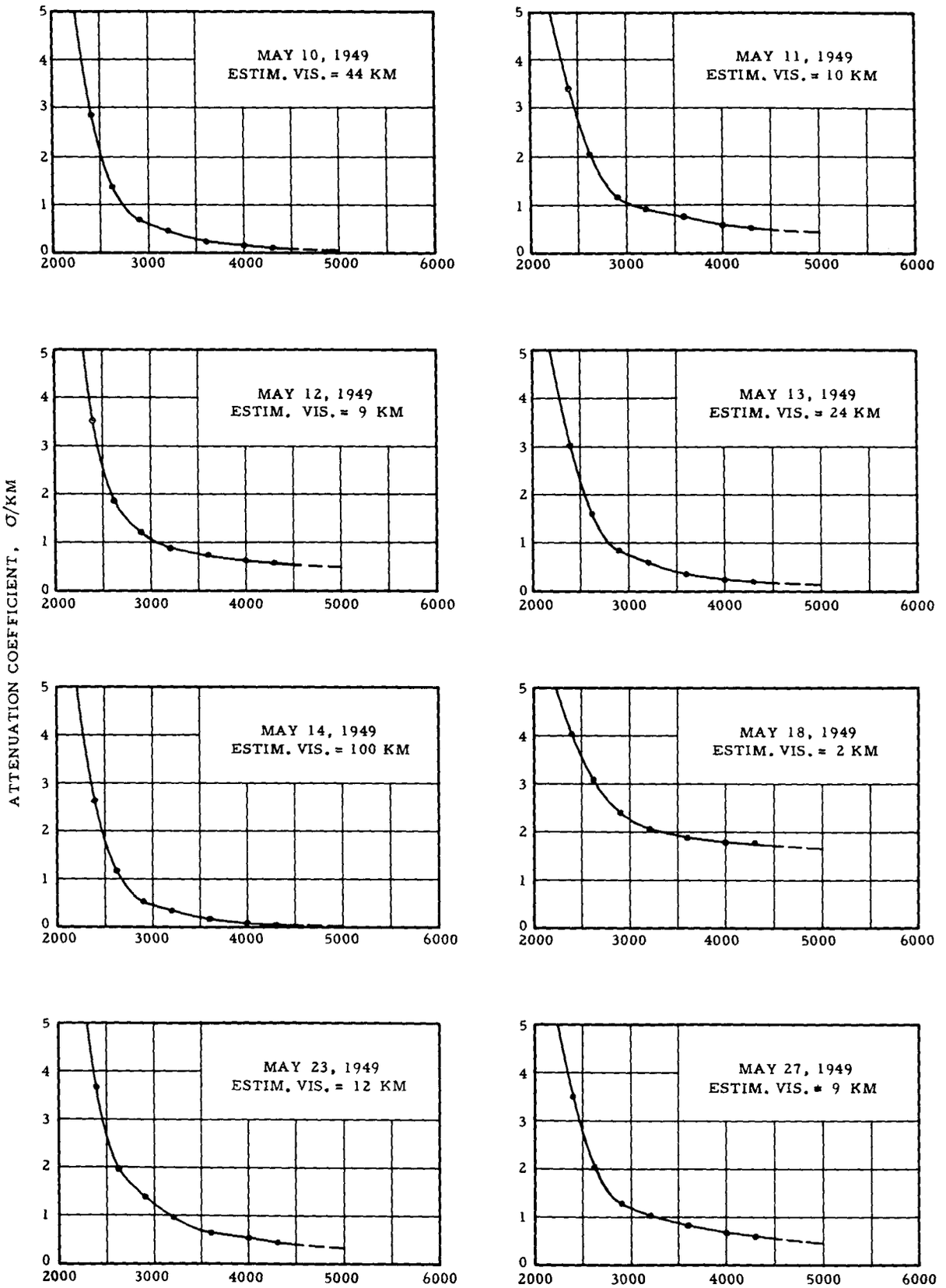
MAY 10, 1949
ESTIM. VIS. = 44 KM
MAY 11, 1949
ESTIM. VIS. = 10 KM
MAY 12, 1949
ESTIM. VIS. = 9 KM
MAY 13, 1949
ESTIM. VIS. = 24 KM
MAY 14, 1949
ESTIM. VIS. = 100 KM
MAY 18, 1949
ESTIM. VIS. = 2 KM
MAY 23, 1949
ESTIM. VIS. = 12 KM
MAY 27, 1949
ESTIM. VIS. = 9 KM
ATTENUATION COEFFICIENT, σ/KM
WAVELENGTH IN ANGSTROMS

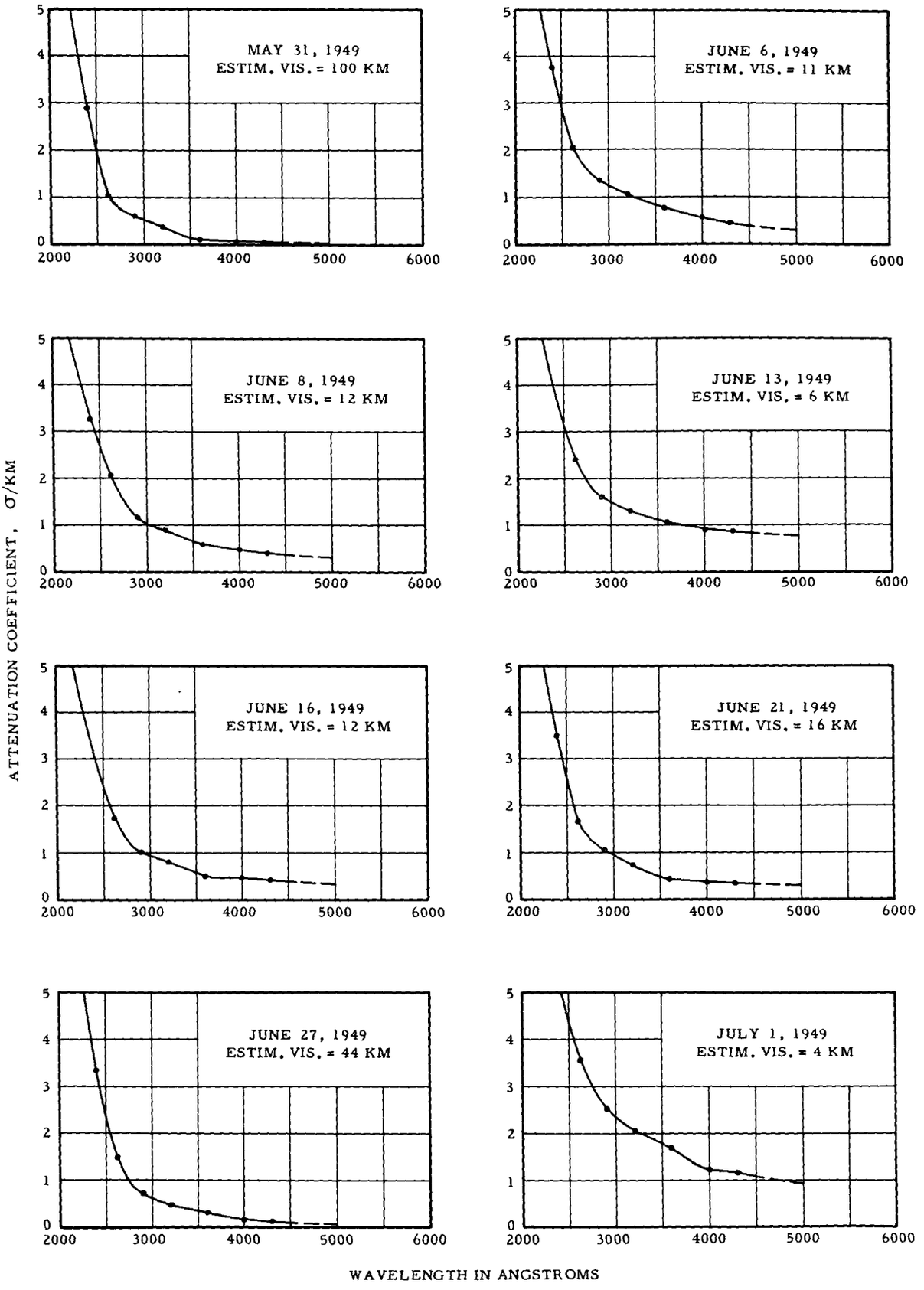
MAY 31, 1949
ESTIM. VIS. = 100 KM
JUNE 6, 1949
ESTIM. VIS. = 11 KM
JUNE 8, 1949
ESTIM. VIS. = 12 KM
JUNE 13, 1949
ESTIM. VIS. = 6 KM
JUNE 16, 1949
ESTIM. VIS. = 12 KM
JUNE 21, 1949
ESTIM. VIS. = 16 KM
JUNE 27, 1949
ESTIM. VIS. = 44 KM
JULY 1, 1949
ESTIM. VIS. = 4 KM
ATTENUATION COEFFICIENT, σ/KM
WAVELENGTH IN ANGSTROMS

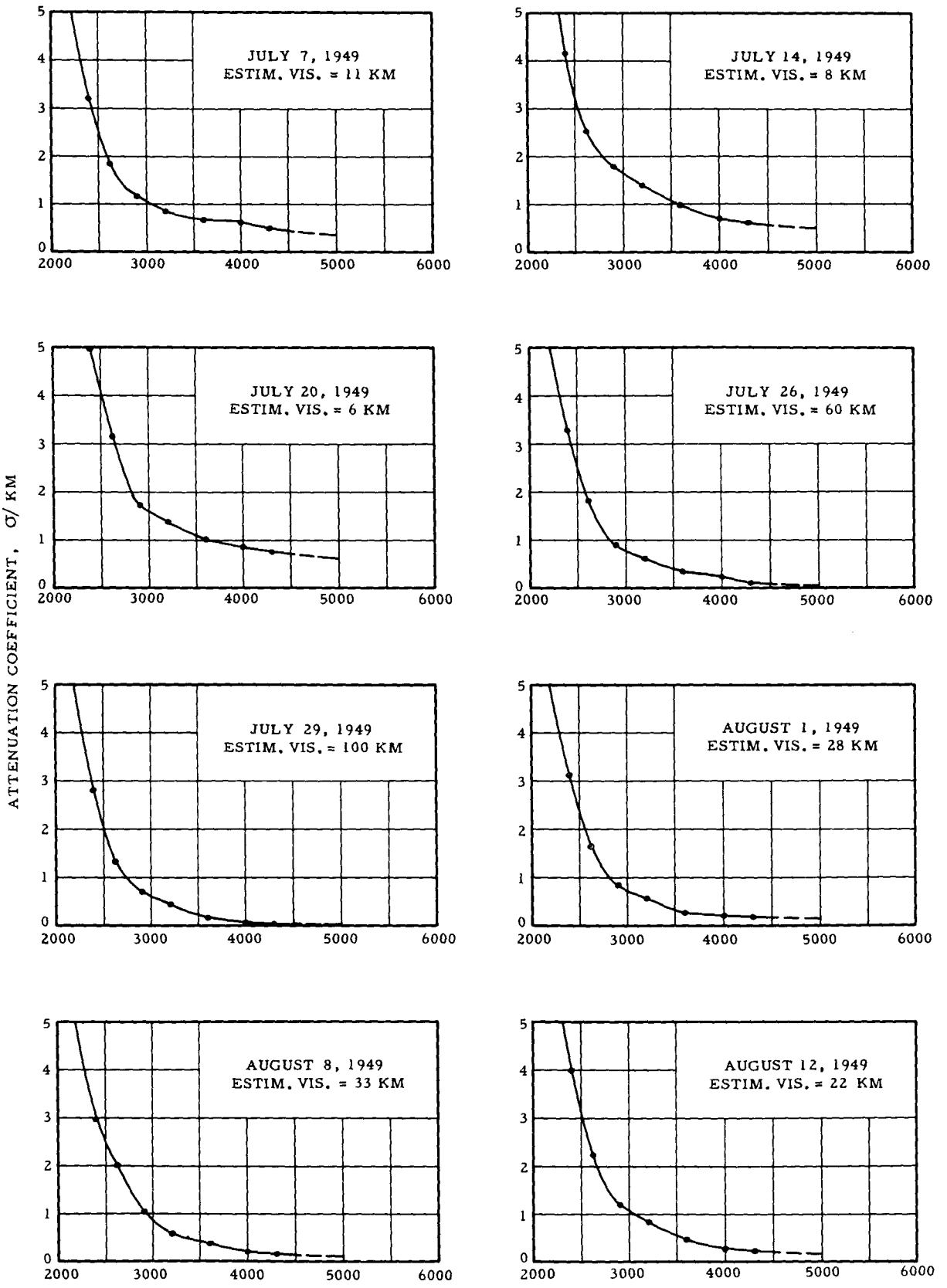
JULY 7, 1949
ESTIM. VIS. = 11 KM
JULY 14, 1949
ESTIM. VIS. = 8 KM
JULY 20, 1949
ESTIM. VIS. = 6 KM
JULY 26, 1949
ESTIM. VIS. = 60 KM
JULY 29, 1949
ESTIM. VIS. = 100 KM
AUGUST 1, 1949
ESTIM. VIS. = 28 KM
AUGUST 8, 1949
ESTIM. VIS. = 33 KM
AUGUST 12, 1949
ESTIM. VIS. = 22 KM
ATTENUATION COEFFICIENT, σ/ KM
WAVELENGTH IN ANGSTROMS

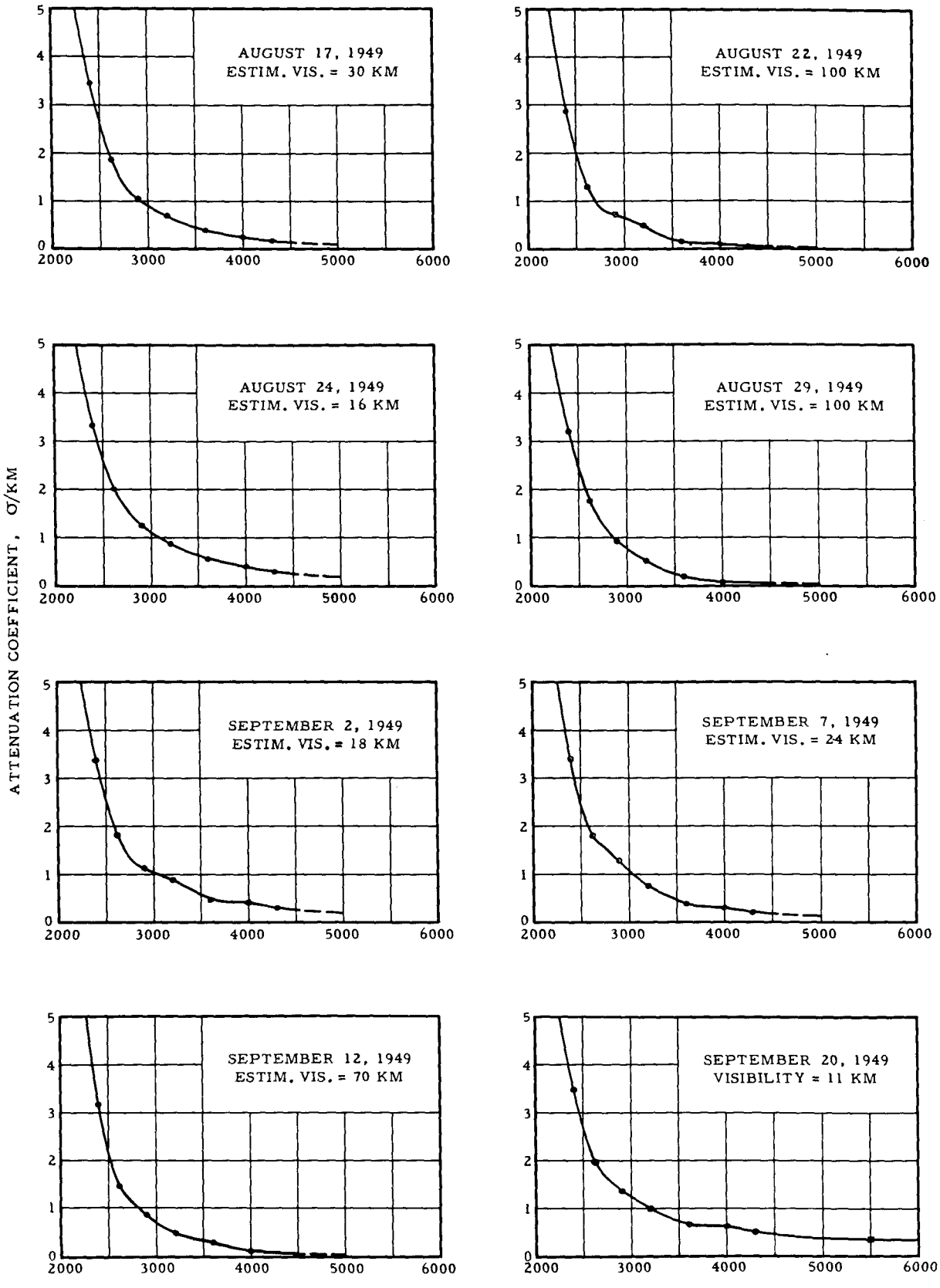
AUGUST 17, 1949
ESTIM. VIS. = 30 KM
AUGUST 22, 1949
ESTIM. VIS. = 100 KM
AUGUST 24, 1949
ESTIM. VIS. = 16 KM
AUGUST 29, 1949
ESTIM. VIS. = 100 KM
SEPTEMBER 2, 1949
ESTIM. VIS. = 18 KM
SEPTEMBER 7, 1949
ESTIM. VIS. = 24 KM
SEPTEMBER 12, 1949
ESTIM. VIS. = 70 KM
SEPTEMBER 20, 1949
VISIBILITY = 11 KM
ATTENUATION COEFFICIENT, σ/KM
WAVELENGTH IN ANGSTROMS

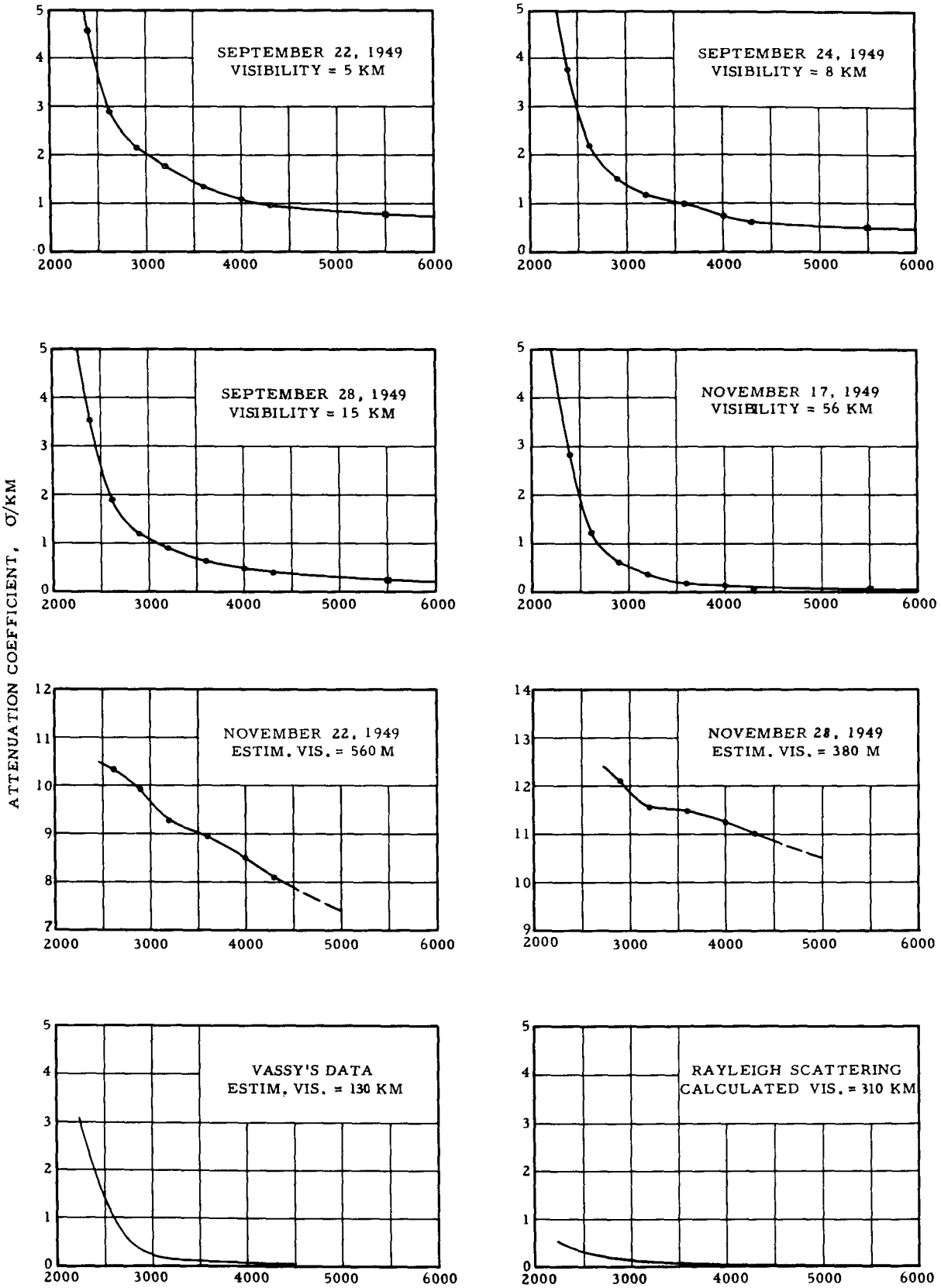
SEPTEMBER 22, 1949
VISIBILITY = 5 KM
SEPTEMBER 24, 1949
VISIBILITY = 8 KM
SEPTEMBER 28, 1949
VISIBILITY = 15 KM
NOVEMBER 17, 1949
VISIBILITY = 56 KM
NOVEMBER 22, 1949
ESTIM. VIS. = 560 M
NOVEMBER 28, 1949
ESTIM. VIS. = 380 M
VASSY'S DATA
ESTIM. VIS. = 130 KM
RAYLEIGH SCATTERING
CALCULATED VIS. = 310 KM
ATTENUATION COEFFICIENT, σ/KM
WAVELENGTH IN ANGSTROMS

IX. INTERPRETATION OF DATA

Various people acquainted with this investigation have expressed interest in several related topics to which they believe the attenuation coefficients presented in the preceding section ought to be applied. Some would like to see average curves for various visibilities; some want an ultraviolet attenuation formula; others seek correlations with meteorological variables; still others believe that the curve shapes should be analyzed variously for particle diameters, for detection of industrial pollutants (smog), or for measurement of ozone concentrations. Some of these wishes have been overly optimistic; the measured data do not in all cases lend themselves well to the treatments involved.

Since empirical attenuation curves have all sorts of shapes under otherwise similar circumstances, any attempt to select a family of representative curves for various visibilities or to devise a formula for the same thing is necessarily based on rather arbitrary criteria. Nevertheless, such an attempt was made and the results are presented here for whatever value they may have.

The first step toward selecting a representative family of attenuation curves was to examine the correlation between σ's at various wavelengths. When σ for some particular wavelength was plotted against $\bar{\sigma}$ for 5500A, a scatter of points was obtained, one point for each spectrogram analyzed. In figure 84, coefficients at each of seven ultraviolet wavelengths have been separately plotted in that manner against $\bar{\sigma}$. Originally, points for all 78 nights were used, but to avoid confusion and to insure maximum accuracy, only those points associated with Loofah readings have been included in the figure; that is, those based on extrapolated data at 5500A have been omitted.

Fig. 84a.

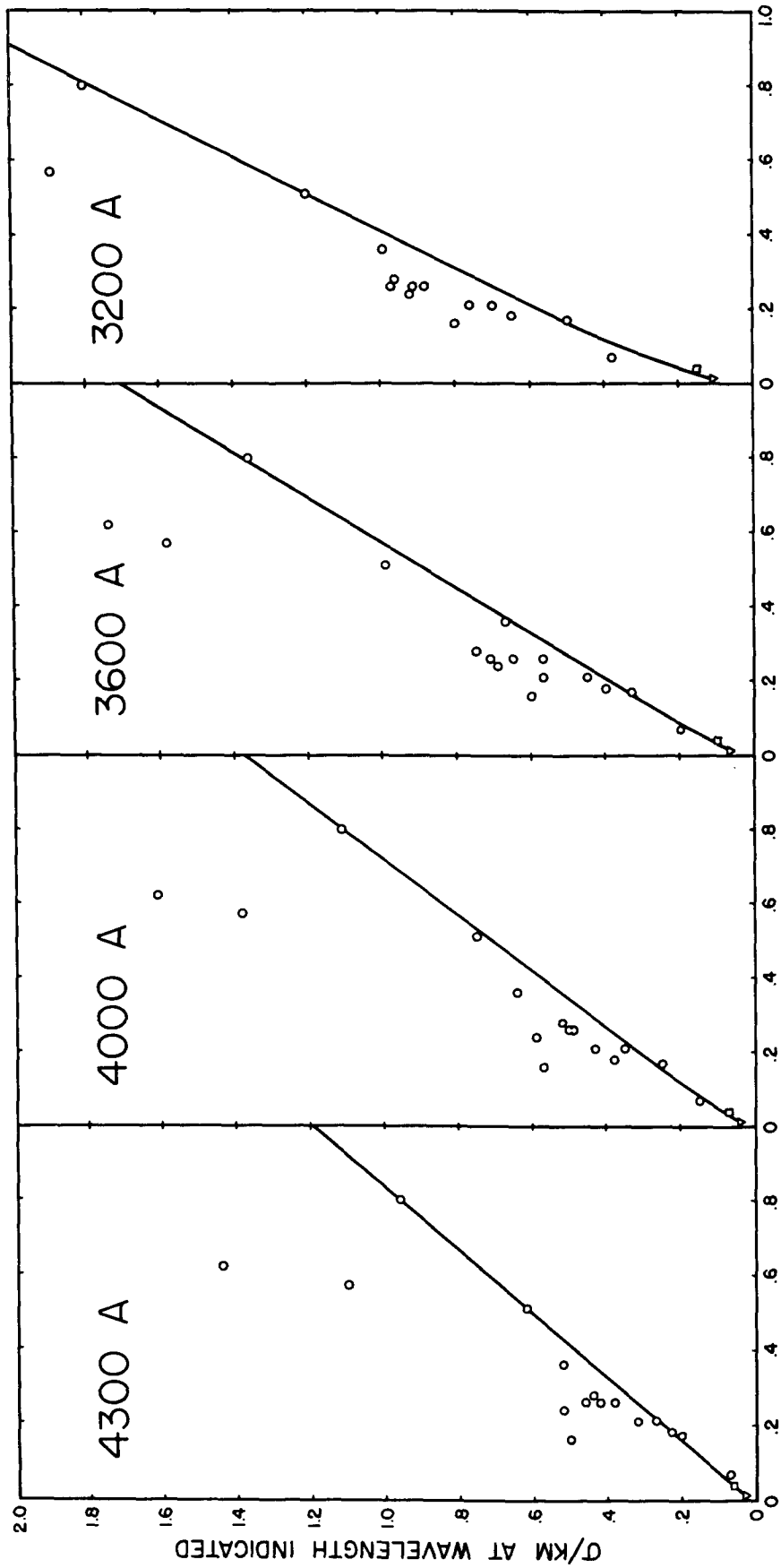

Continued on next page.

U.V. ATTENUATION COMPARED TO VISIBLE ATTENUATION

The curves represent "clean air" conditions. They are approximately straight for $0.1 < \sigma_{5500} < 1.0$.

○ Data from the present experiment.
□ Vassy's results at Mont-Ventoux.
▽ Rayleigh scattering.

Fig. 84 b.

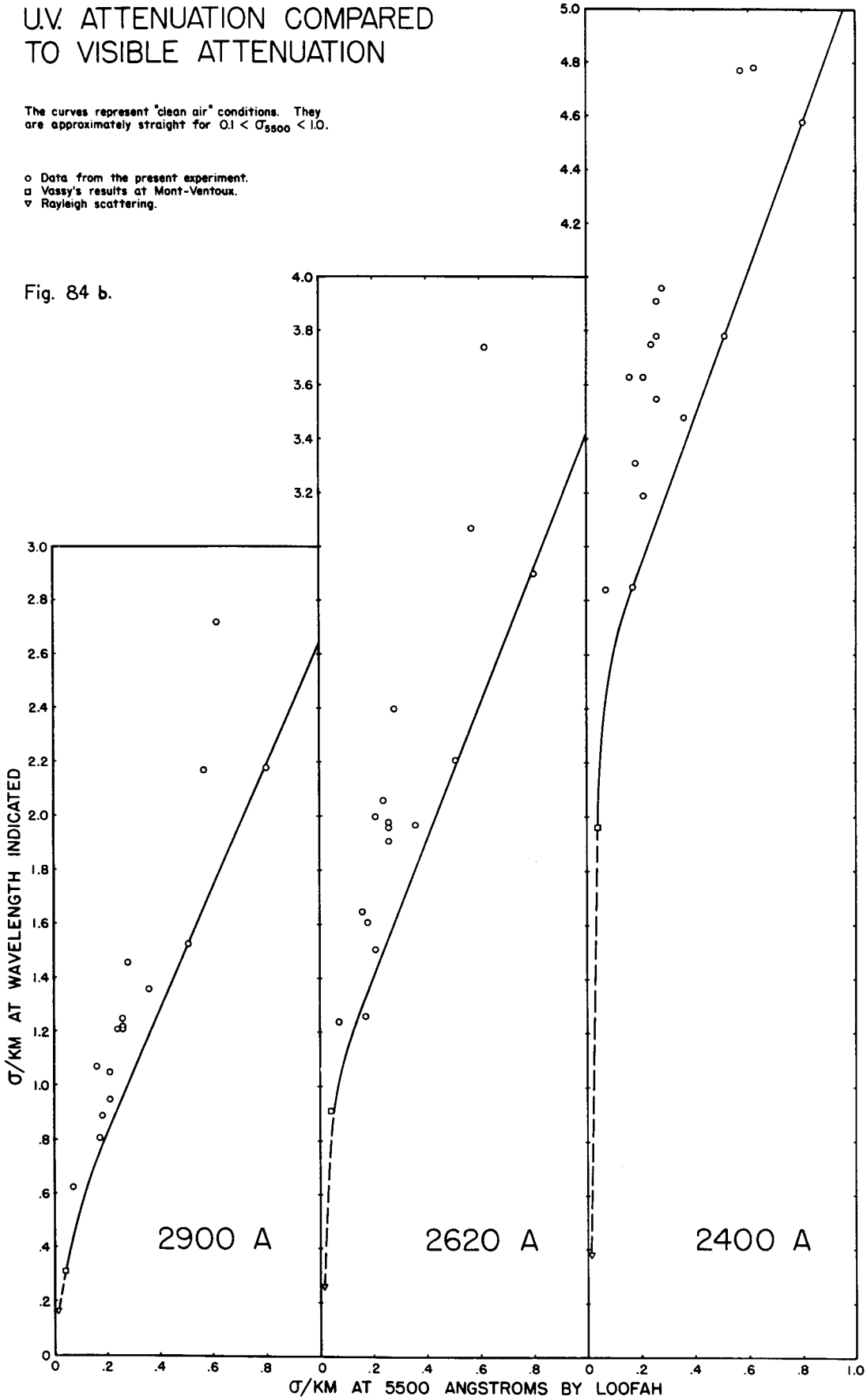

In each of these seven plots, the scatter of points was found to have a rather definite lower boundary, and an envelope drawn along it was found to pass through or near points associated with nights when the air was believed to be comparatively free of pollutants, such as just after a rain or during a mountain breeze. We must distinguish carefully here between clear air and clean air; the former implies good visibility, while the latter applies to any natural unpolluted condition including fog.

In the main, points lying substantially above the envelope represented somewhat smoggy conditions or at least stagnant city air, implying that smog tends to introduce more pronounced attenuation in the ultraviolet than in the visible. It was also interesting to find two or three isolated nights whose points (not shown in figure 84) fell substantially below the envelope and to discover that they represented conditions when the air was filled with abnormally large particles, such as rain or falling mist; as one might expect, such an atmosphere tends to be spectrally more neutral than average.

The "clean air" envelope for each ultraviolet wavelength appears to be fairly straight for $0.1 < \bar{\sigma} < 1.0$, corresponding to visibilities from 40 km down to 4 km. This straight portion can be represented by

$$\sigma = m\bar{\sigma} + \sigma_o , \tag{24}$$

where the ordinate intercept σ_o and the slope m depend on wavelength as shown in figures 85 and 86, respectively. It was found empirically that σ_o can be expressed very well by

$$\sigma_o = \left(\frac{a}{\lambda - \lambda_o}\right)^n = \left(\frac{793}{\lambda - 1800}\right)^{3.115} \approx \left(\frac{800}{\lambda - 1800}\right)^3 . \tag{25}$$

From figure 86, we see that m is a remarkably linear function of wavelength for $2400\text{A} < \lambda < 4000\text{A}$ and is given by

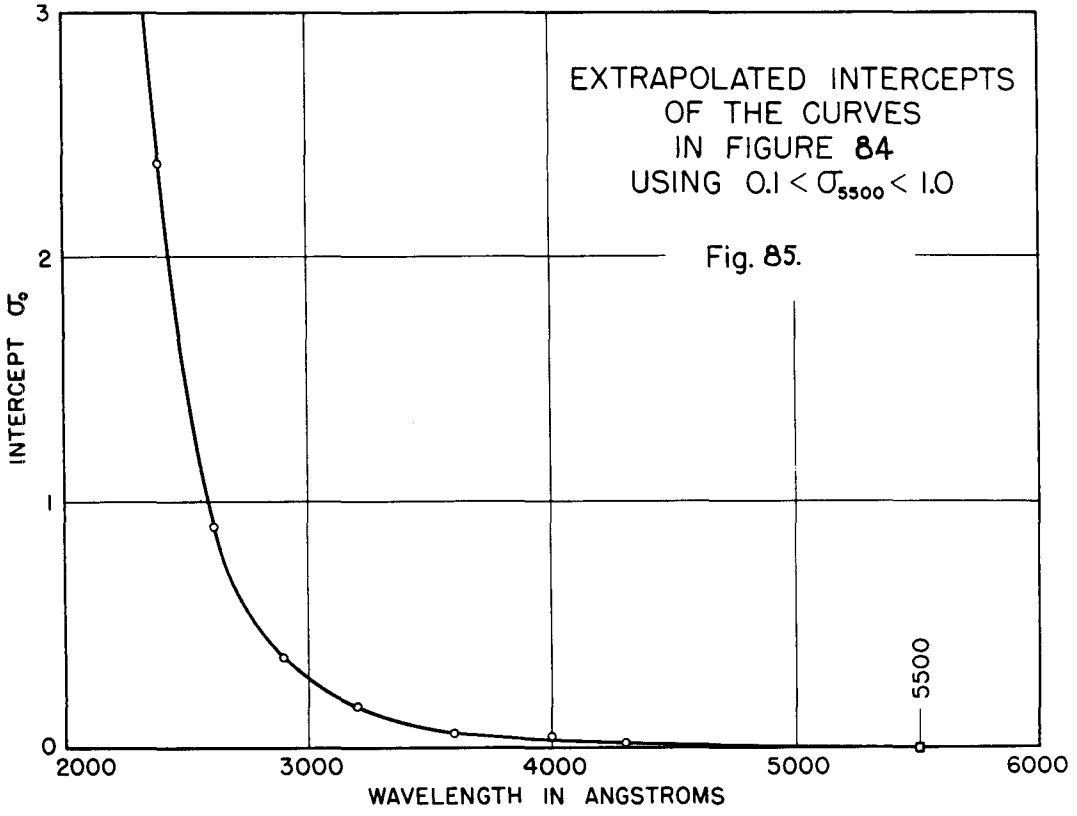
EXTRAPOLATED INTERCEPTS
OF THE CURVES
IN FIGURE 84
USING 0.1 < σ5500 < 1.0
INTERCEPT σo
3
2
1
0
2000
3000
4000
5000
6000
5500
WAVELENGTH IN ANGSTROMS

Fig. 85.

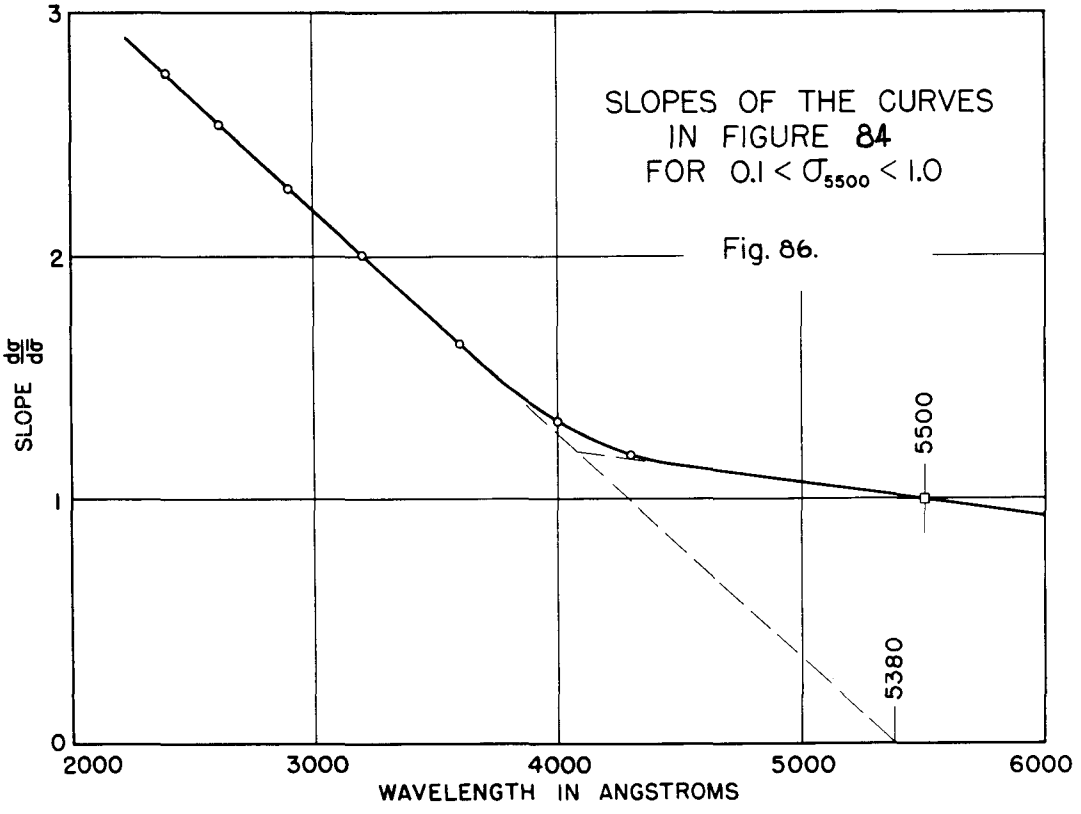
SLOPES OF THE CURVES
IN FIGURE 84
FOR 0.1 < σ5500 < 1.0
SLOPE dσ/dσ
3
2
1
0
2000
3000
4000
5000
6000
5500
5380
WAVELENGTH IN ANGSTROMS

Fig. 86.

$$m = b(\lambda_1 - \lambda) = 0.00092\ (5380 - \lambda). \qquad (26)$$

Substituting (25) and (26) into (24), and using (16) for converting $\bar{\sigma}$ to visibility range v, we obtain finally

$$\sigma = \frac{c(\lambda_1 - \lambda)}{v} + \left(\frac{a}{\lambda - \lambda_o}\right)^n \qquad (27)$$

If λ is in Angstroms, v is in kilometers, and σ is in inverse kilometers, then

$$\begin{aligned} c &= 0.0036\ A^{-1} \\ \lambda_1 &= 5380A \\ a &= 800A \cdot km^{-1/3} \\ \lambda_o &= 1800A \\ n &= 3 \end{aligned}$$

It should be emphasized that equation (27) is intended only for 4 km $< v <$ 40 km and for 2400A $< \lambda <$ 4000A. There is a possibility that it might also fit wavelengths a little below 2400A and visibilities somewhat less than 4 km.

Figure 87 is a family of attenuation curves for clean air, based in the ultraviolet region on equation (27) and in the visible region on equation (11). The two regions thus determined are seen to join perfectly. The same family of curves are drawn on a log-log scale in figure 88, where the slopes indicate how the power of λ fitting these coefficients depends on wavelength and visibility. For illustration, the exponents of λ at 3600A have been plotted against corresponding $\bar{\sigma}$'s in figure 89.

Data for "dense" atmospheres ($\bar{\sigma} > 1.0$, or visibilities less than 4 km) were rather scanty in the present experiment. Exceptionally heavy fogs which occurred on November 22 and 28, 1949, were unfortunately accompanied by considerable air pollution. Nevertheless, since values of σ were at least several times greater on those two occasions than at other times when the degree of pollution was similar, it is reasonable to believe that

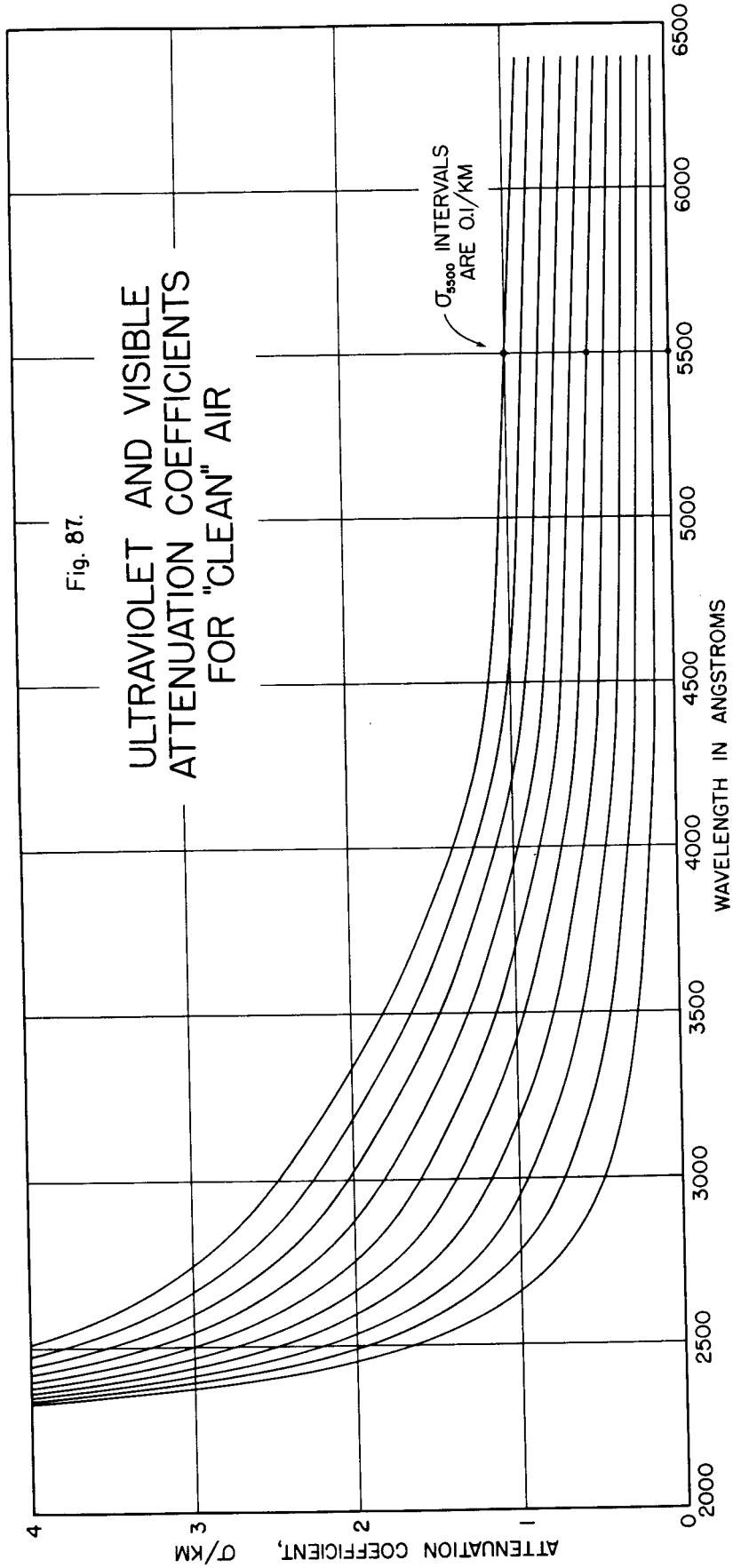
ULTRAVIOLET AND VISIBLE
ATTENUATION COEFFICIENTS
FOR "CLEAN" AIR
σ_{5500} INTERVALS
ARE 0.1/KM
ATTENUATION COEFFICIENT, σ/KM
WAVELENGTH IN ANGSTROMS
0
1
2
3
4
2000
2500
3000
3500
4000
4500
5000
5500
6000
6500

Fig. 87.

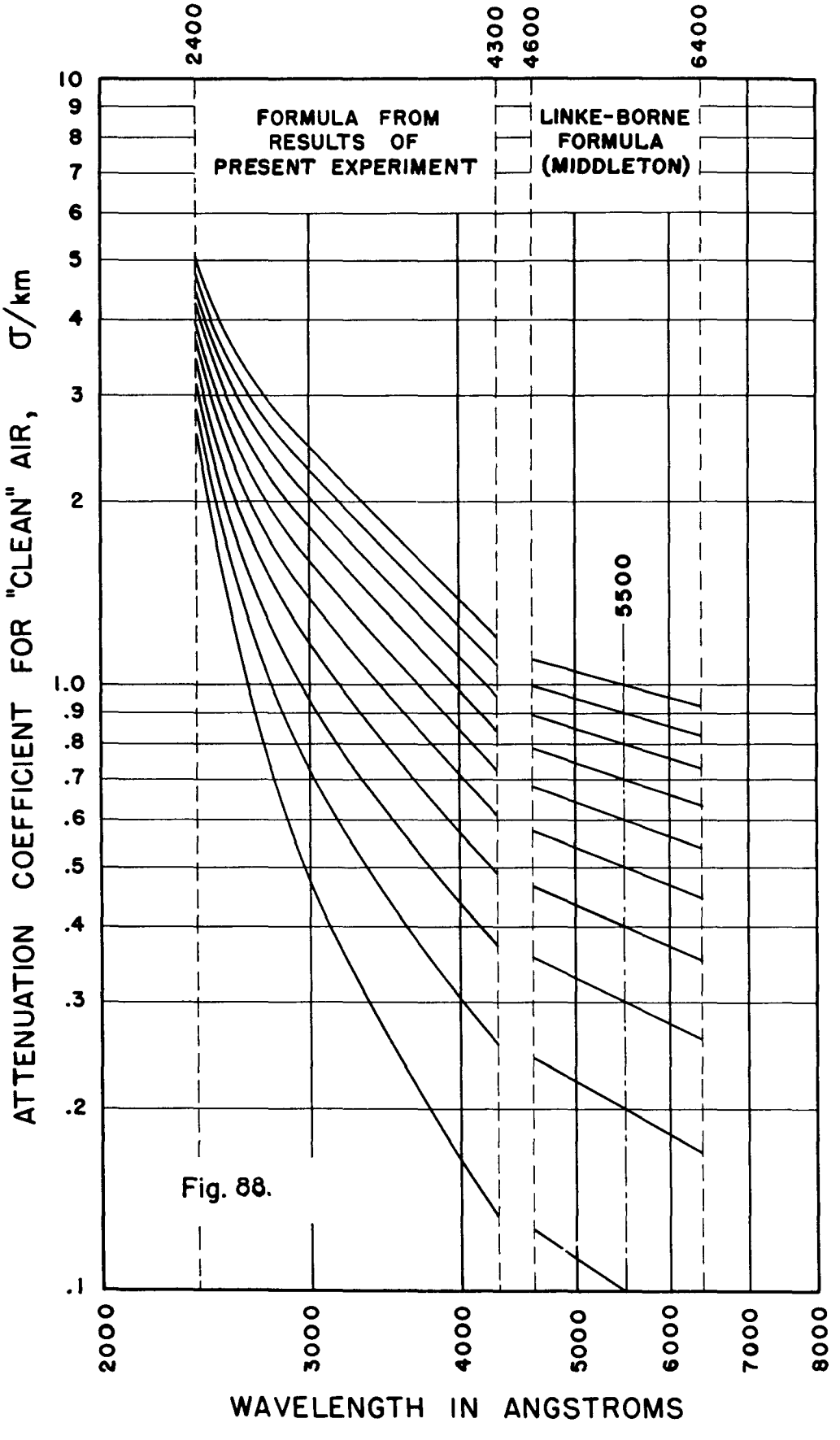
2400
4300
4600
6400
FORMULA FROM RESULTS OF PRESENT EXPERIMENT
LINKE-BORNE FORMULA (MIDDLETON)
5500
10
9
8
7
6
5
4
3
2
1.0
.9
.8
.7
.6
.5
.4
.3
.2
.1
ATTENUATION COEFFICIENT FOR "CLEAN" AIR, σ/km
2000
3000
4000
5000
6000
7000
8000
WAVELENGTH IN ANGSTROMS

Fig. 88.

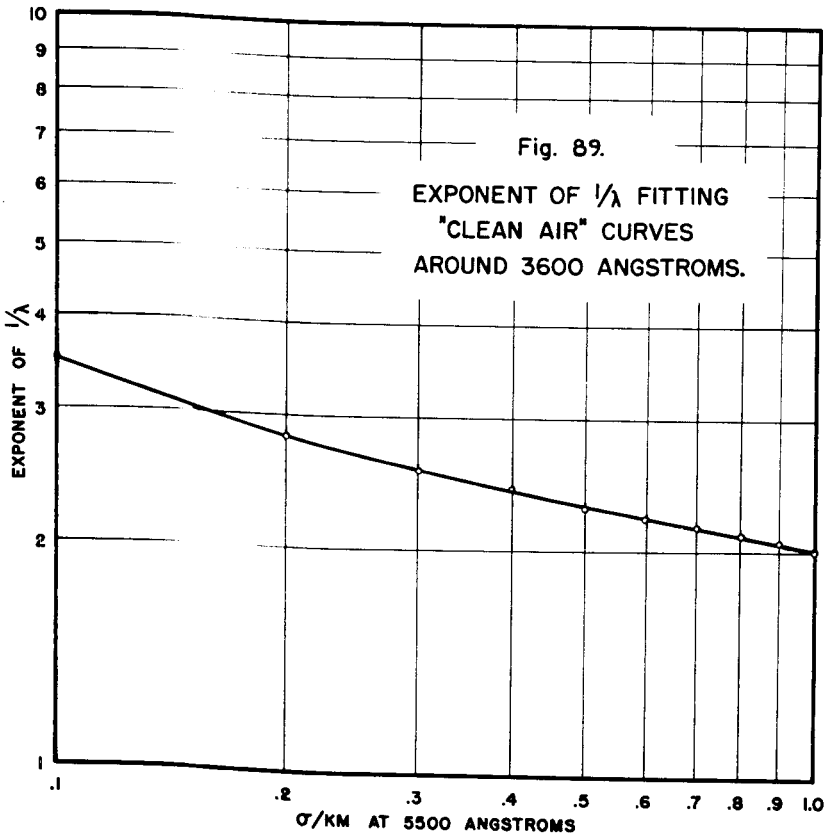

Fig. 89.

EXPONENT OF $1/\lambda$ FITTING "CLEAN AIR" CURVES AROUND 3600 ANGSTROMS.

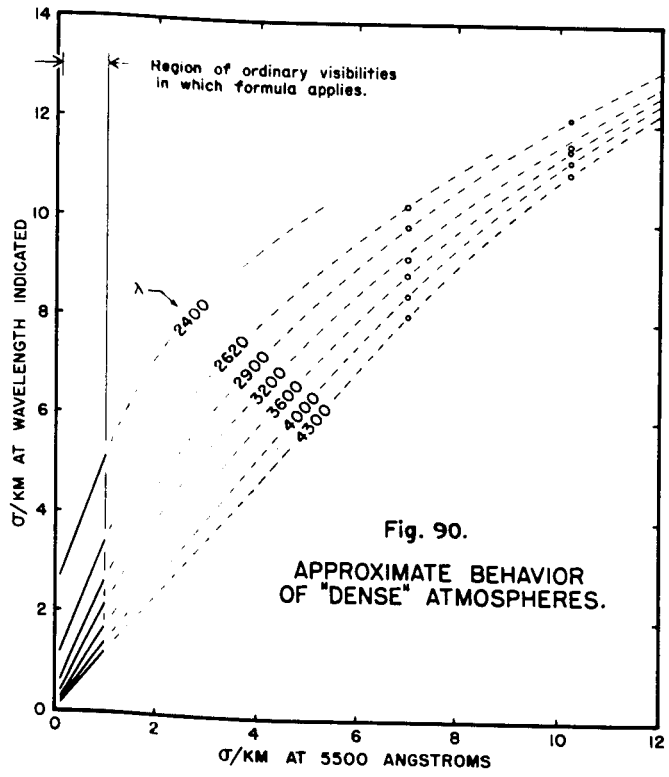

Fig. 90.

APPROXIMATE BEHAVIOR OF "DENSE" ATMOSPHERES.

attenuation was due largely to scattering by natural fog nuclei, and that pollutants introduced a lesser fraction of the total attenuation than they ordinarily would. There still remains, however, the objection that the size distribution of the fog nuclei is apt to be influenced during condensation by the amount of non-gaseous material present; viz, smoke and dust particles; consequently, it is not possible to judge how closely the attenuation data for November 22 and 28 should approximate that which would be found for "clean" fog.

In spite of the foregoing limitation, these data are still quite informative and are shown in figure 90. It has already been pointed out that ultraviolet σ values for clean air always lie below σ values for polluted air having the same $\bar{\sigma}$ (same visibility); hence, σ's for November 22 and 28 place an upper limit on the "clean" air envelopes when extrapolated to $\bar{\sigma} > 1.0$. We find that they cannot continue as diverging straight lines indefinitely but must all bend in the direction of decreasing slopes and must tend partially to converge again as conditions approach that of comparatively opaque "white" fog.

Going back now to the original attenuation data, let us consider finally the feasibility of analyzing curve shapes to study particle sizes, smog contributions, and ozone concentrations. We are faced at the start with the problem of distinguishing between the effects of these three possibilities, and the available means for doing so are rather poor.

It has been found in several previous researches, such as that of Stratton and Houghton[34], that scattering by air-borne particles or droplets can introduce humps in the spectral attenuation curve if certain particle sizes predominate in abundance. Assuming that some of the observed humps may have been produced in that manner, one would expect them

to appear at different places in the spectrum under various weather conditions; that is, there is no reason to suppose that particular sizes would be consistently favored under all conditions.

As mentioned in Section VIII, none of the spectra showed any discrete gas absorptions except for the Herzberg O_2 bands; moreover, broad humps which may be caused by gases are too slight for details of their shapes to be observed. Consequently, the identification of gas absorptions must depend solely upon the fact that their humps necessarily reappear at the same places in the spectrum instead of varying in position as those associated with particle scattering do.

Two or three possible recurrent humps were observed in attenuation curves obtained from the present experiment, but only one manifested itself with any definiteness. This particular hump, which is centered somewhere a little above 4000A, can be seen to a greater or lesser degree in about half of the curves presented in Section VIII; see especially the curves for September 2 and September 20 in figure 80. It was likely caused by NO_2, whose detrimental effects as a smog constituent have been cogently emphasized by Mills[84].

The detection of ozone in this experiment was not at all definite. The presence of miscellaneous humps, presumably caused by particle scattering, made it impossible on most attenuation curves to distinguish any characteristic absorption which might be identified as ozone. Moreover, if one applies the method of Fabry and Buisson[43] to data for air which is not exceptionally clear, the Rayleigh curve does not join the measured curve tangentially around 3300A as it should but crosses it at a substantial angle instead; clearly, no meaningful ozone data can be measured under such circumstances. A more sensible procedure might be to subtract

clean-air curves instead of a Rayleigh curve, but the problem is still fraught with too much uncertainty to justify its pursuit here.

In addition to a fair selection of attenuation data for various conditions, the present investigation yielded one other useful result. It showed that except for the region of the Herzberg O_2 bands, the attenuation of air is a smooth (sometimes wavy) function of wavelength down to 2300A and can validly be measured using sources emitting line radiation. This conclusion automatically lends more weight to the data of previous investigators who have used line sources.

LIST OF REFERENCES

1. Schaeffer, Proc. Am. Acad. Arts and Sc. 57, 365 (1922).

2. Dawson, Granath, and Hulburt, Phys. Rev. 34, 136 (1929).

3. Granath and Hulburt, Phys. Rev. 34, 140 (1929).

4. Link and Hugon, Comptes Rendus 190, 810 (1930).

5. Buisson, Jausseran, and Rouard, Comptes Rendus 190, 808 (1930); 194, 1477 (1934).

6. Gotz and Maier-Leibnitz, Zeits. fur Geophys. 9, 253 (1933).

7. J. Duclaux, Jour. de Phys. 6, 323 and 401 (1935).

8. W.E.K.Middleton, "Visibility in Meteorology", Second Edition, Univ. of Toronto Press (1941).

9. Stiles, Bennett, and Green, "Visibility of Light Signals with Special Reference to Aviation Lights", British Air Ministry, Aeronautical Research Committee, Reports and Memoranda No. 1793 (1937).

10. E.O.Hulburt, Naval Research Laboratory, Washington 20, D.C. Verbal communication.

11. A. Vassy and E. Vassy, Jour. de Phys. 10, 75, 403, and 459 (1939).

12. A. Vassy, Thesis, Univ. of Paris (1941).

13. B. Koch, Optik 5, 258 (1949).

14. H. Dessens, Ann. de Geophys. 1, 157 (1944); 2, 68 (1946).

15. J. Strong, "The Infrared Atmospheric Transmission Problem," O.N.R. report under contract No. N5-ori-166,T.O.5. (1948).

16. L. Dunkelman et al, Optics Division, Naval Research Lab., Washington 20, D.C. Research is now in progress.

17. Smithsonian Physical Tables, Eighth Edition (1933). See Tables 444(b), 767, and 775.

18. Intern. Crit. Tables, First Edition (1930). See vol. V, p. 268; vol. VII, p. 2, 5.

19. W.E.K.Middleton, J. Opt. Soc. Am. 39, 576 (1949).

20. Lord Rayleigh, Phil. Mag. 41, 107 (1871) et seq. Also in "Collected Works" vol. 1, art. 8.

21. L. King, Proc. Royal Soc. A88, 83 (1913).

22. C.G.Abbot, Astrophys. Jour. 34, 197 (1911).

23. M. v.Smoluchowski, Ann. der Phys. 25, 205 (1908).

24. A. Einstein, Ann. der Phys. 33, 1275 (1910).

25. J. Cabannes, "La Diffusion Moleculaire de la Lumiere", Presses Universitaires, Paris (1929).

26. Martin and Lehrman, J. Phys. Chem. 26, 75 (1922).

27. M. Born, "Optik", J. Springer, Berlin (1933).

28. Dawson and Hulburt, J. Opt. Soc. Am. 31, 554 (1941).

29. R. Tousey and E.O.Hulburt, J. Opt. Soc. Am. 37, 78 (1947).

30. H. Dessens, Ann. de Geophys. 2, 276 and 343 (1946); 3, 68 (1947).

31. H. Houghton, Phys. Rev. 38, 152 (1931).

32. D. Nukiyama and A. Kobayasi, Tokyo Univ. Aeronaut. Research Inst., Report No. 82 (1932).

33. G. Mie, Ann. der Phys. 25, 377 (1908).

34. J. Stratton and H. Houghton, Phys. Rev. 38, 159 (1931).

35. H.C. van de Hulst, Thesis, Univ. of Utrecht (1946).

36. Houghton and Chalker, J. Opt. Soc. Am. 39, 955 (1949).

37. F. Linke and H. v.dem Borne, Gerl. Beitr. zur Geophys. 37, 49 (1932).

38. O.R.Wulf, J. Opt. Soc. Am. 25, 231 (1935).

39. O.R.Wulf and L.S.Deming, Terr. Mag. 41, 299 and 375 (1936); 42, 195 (1937); 43, 283 (1938).

40. F.W.P.Gotz, Ergeb. der Kosm. Phys., Band I (1931); Band III (1938).

41. Reichsamt fur Wetterdienst, Luftwaffe. Arbeitskreis Meteorologie. "Vortrage und Diskussionen der Sondertagung 'Ozon'", Tharandt (1944).

42. E.O.Hulburt, J. Opt. Soc. Am. 37, 405 (1947).

43. C. Fabry and H. Buisson, Comptes Rendus 192, 457 (1931).

44. Gotz and Ladenburg, Naturwis. 19, 373 (1931).

45. Gotz, Schein, and Stoll, Gerl. Beitr. zur Geophys. 45, 237 (1935).

46. D. Chalonge and E. Vassy, Jour. de Phys. 5, 309 (1934).

47. R. Auer, Gerl. Beitr. zur Geophys. 54, 137 (1939).

48. Ny Tsi-Ze and Choong Shin-Piaw, Comptes Rendus 195, 309 (1932); 196, 916 (1933).

49. Granath, Phys. Rev. 34, 1045 (1929).

50. G. Herzberg, Naturwis. 20, 577 (1932).

51. O.R.Wulf, Proc. Nat. Acad. Sci. 14, 609 (1928).

52. D. Chalonge and E. Vassy, Comptes Rendus 198, 1318 (1934).

53. L. Herman, Thesis, Univ. of Paris (1939).

54. Bonhoeffer and Hartek, "Grundlagen der Photochemie", Steinkopff, Dresden (1933).

55. G. Herzberg, "Molecular Spectra and Molecular Structure", Prentice-Hall, N.Y. (1939).

56. Pearse and Gaydon, "The Identification of Molecular Spectra", Chapman-Hall, London (1941).

57. Sponer, Rev. Mod. Phys. 13, 75 (1941).

58. E.H.Melvin and O.R.Wulf, Jour. of Chem. Phys. 3, 755 (1935).

59. E.J.Jones and O.R.Wulf, Jour. of Chem. Phys. 5, 873 (1937).

60. E.O.Hulburt, J. Opt. Soc. Am. 31, 467 (1941).

61. K. Bullrich, Optik 2, 301 (1947).

62. H. Koschmieder, Naturwis. 26, 521 (1938).

63. Coleman, Morris, and Rosenberger, J. Opt. Soc. Am. 39, 515 (1949).

64. W.E.K.Middleton, J. Opt. Soc. Am. 27, 112 (1937).

65. "Photographic Plates for Scientific and Technical Use", Sixth Edition, Eastman Kodak Company (1948).

66. C.E.K.Mees, "The Theory of the Photographic Process", MacMillan, N.Y. (1942).

67. T.H.James and G.C.Huggins, "Fundamentals of Photographic Theory", Wiley, N.Y. (1948).

68. W.A.Baum and L. Dunkelman, J. Opt. Soc. Am. 39, 1055(A) (1949).

69. P. Schulz, Zeits. fur Naturfor. 2a, 583 (1947).

70. P. Schulz, Ann. der Phys. 6, 95 and 107 (1947).

71. P. Schulz, Reichsberichte fur Physik 1, 147 (1945).

72. G.R.Harrison, J. Opt. Soc. Am. 18, 492 (1929).

73. H.G.MacPherson, J. Opt. Soc. Am. 30, 189 (1940).

74. Allen and Franklin, J. Opt. Soc. Am. 29, 453 (1939).

75. Matz and Merrill, J. Opt. Soc. Am. 39, 635(A) (1949).

76. G. Hass and N. Scott, J. Opt. Soc. Am. 39, 179 (1949).

77. J. Strong, "Procedures in Experimental Physics", Prentice-Hall, N.Y. (1946).

78. D. Chalonge and E. Vassy, Revue d'Optique 13, 113 (1934).

79. Riggs, Mueller, Graham, and Mote, J. Opt. Soc. Am. 37, 415 (1947).

80. E.O.Lawrence and N.E.Edlefson, Rev. Sc. Instr. 1, 45 (1930).

81. Kistiakowsky, Rev. Sc. Instr. 2, 549 (1931).

82. Taylor and Haynes, G.E.Rev. 50, 27 (1947).

83. Hardy and Perrin, "The Principles of Optics", McGraw-Hill, N.Y. (1932). See page 100.

84. C.A.Mills, Science 111, 67 (1950).